UNIVERSITÄT KAISERSLAUTERN

HS

UNIVERSITÄT KAISERSLAUTERN

Lehrstuhl für hochfrequente

Signalübertragung und -verarbeitung

- Grundlagen der Elektrotechnik -

Diplomarbeit

Investigations of interference cancellation schemes for a TD-CDMA mobile radio system

April 2000

Betreuer: Prof. Dr. -Ing. habil. P. W. Baier

Dipl. -Ing. Martin Weckerle

Verfasser: Juan José Catany Hernández

Murillo 9, 2

07013 Palma de Mallorca

España

I hereby assure that I did not use other aid than the ones mentioned within the text to write this thesis.

Kaiserslautern, 12 April 2000
Juan José Catany Hernández

Acknowledgements

The author wishes to thank his family and his friends, for all the support which he has received from them. Furthermore, to the Spanish Electrotechnik group, for their help to realize the thesis, as well as for the good moments he spend with them. Also the author wishes to thank for the chance given by Ignasi Furió of the Universitat de les Illes Balears and the Research Group for RF Communications, Universität Kaiserslautern, headed by the Prof. P. W. Baier to realize this thesis. Finally the author very specially wishes to thank Martin Weckerle for all the help to realize this thesis.

El autor desea dar las gracias a su familia y amigos por todo el apoyo que ha recibido. Además desea agradecer a todo el grupo de telecos españoles, la ayuda prestada en la realización del proyecto, así como los buenos momentos pasados con ellos. El autor quiere dar las gracias a Ignasi Furió de la Univertat de les Illes Balears y al Research Group for RF Communications Univesität Kaiserslautern, encabezado por el Prof P. W. Baier, por la oportunidad brindada para realizar este proyecto. Finalmente el autor desea dar las gracias muy especialmente a Martin Weckerle por toda la ayuda prestada para realizar este proyecto de final de carrera.

Kaiserslautern, 12 April 2000

Contents

1 Introduction

1.1 Overview

With a surging increase in demand for personal wireless radio communications within the 80ies and 90iess, there is a growing need for technological innovations to satisfy these demands. Future technology must be able to allow users to share common resources efficiently. It involves the frequency spectrum, computing facilities, databases, or storage facilities. As with mobile cellular telephony, the driving forces behind this demand includes the mobility and flexibility that this technology provides. In contrast to wired communicatons, future personal communication networks will allow users the connection to a multitude of resources while enjoying the freedom of mobility [YL98].

In cellular mobile radio, the early systems as, C-Netz in Germany, the Total Access Communications System (TACS) in Great Britain, Italy and Spain, the Nordic Mobile Telephone (NMT) in Scandinavia and the Advanced Mobile Phone Service (AMPS) in the United States of America apply analog technology. They are also called first generation systems [PGH95]. Second generation systems are based on digital technology and have now been introduced into all major markets of the world [PGH95]. There are 4 cellular mobile radio standarts:

- Global System of Mobile communications (GSM) Developed in Europe [Rec88], [MoP92],
- IS-54 developed in USA [PGH95],
- IS-95 developed in USA [SaG91],
- PDC developed in Japan [Lor93].[PGH95].

In order to clarify which technical requirements are necessary to improve the performance of mobile radio systems compared to the ones which are state of the art, the features of cellular mobile radio systems will be discussed from a technical point of

view. The following considerations focus on the air interface and omit e.g. network aspects, source encoding methods and security aspects [JCN95]. Although the air interface constitutes only a minor portion of the total expense necessary to establish a mobile radio system [Kit94], its design is decisive for a third generation mobile radio system [Bai94] and [BKN94]. For characterizing mobile radio systems from a technical point of view, the radio transmission structure will be considered.

The general structure of a multiple access system is shown in Fig. 1.1. A number K of active users transmit data symbols over a common transmission channel to a $K_a$antenna array. In the uplink of a mobile radio system, the K transmitters represent K mobile stations, which are in general in different locations. The receiver represents the base station (BS). The number K of active users transmit data symbols over a common channel to an antenna array may vary with time. Each of the K active users

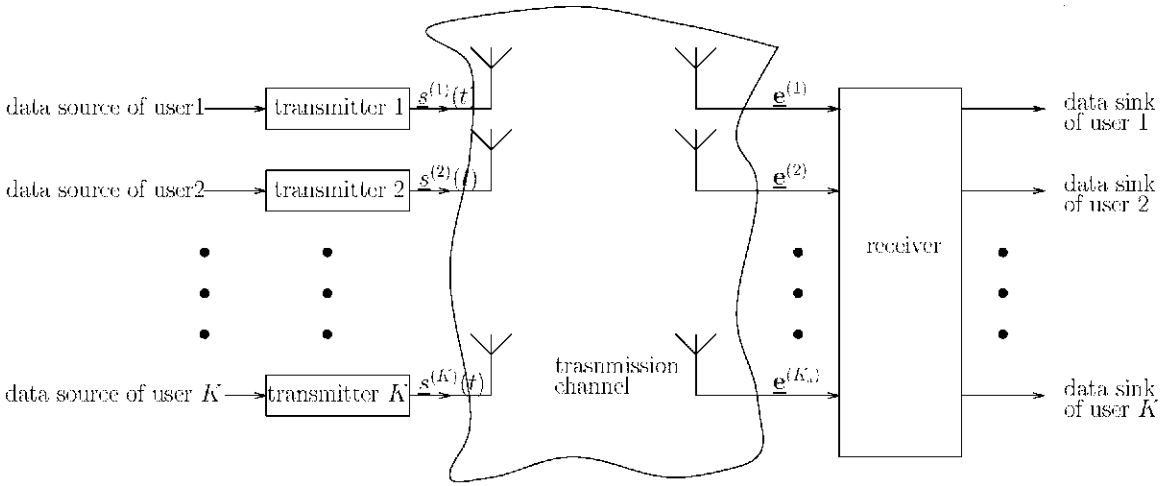

Figure 1.1. General structure of a multiple access system.

transmits a signal $\underline{s}^{(k)}(t)$ which is digitally modulated by the data symbols generated by the data source of user k, $k = 1...K$. After transmission over the channel, which leads to distortion and disturbances of the transmitted signals $\underline{s}^{(k)}(t)$,$k = 1...K$, the compound signals $\underline{\mathbf{e}}^{(k_a)}, k_a = 1...K_a$ appears at the receiver [ARY95]. The compound signals $\underline{\mathbf{e}}^{(k_a)}$ are the superpositions of the K distorted and distributed transmitted signals. Due to the distortions and disturbances, it is impossible to perfectly recover the data symbols transmitted by the K users at the receiver [Pro89]. At the receiver

the compound signals $\underline{\mathbf{e}}^{(k_a)}$ has to be processed by a separation algorithm in order to determine estimates of the data symbols transmitted by each of the K users. The estimates of the data symbols transmitted by user k are delivered to the data link of user k, $k = 1...K$ [Kl96].

1.2 Multiple access schemes

The three principal types of multiple access schemes are Frequency Division Multiple Access (FDMA), Time Division Multiple Access (TDMA) and Code Division Multiple Access (CDMA).

FDMA systems allocate a frequency band to a channel for the duration of the connection, it is not simple to share an FDMA channel among multiple users or accommodate

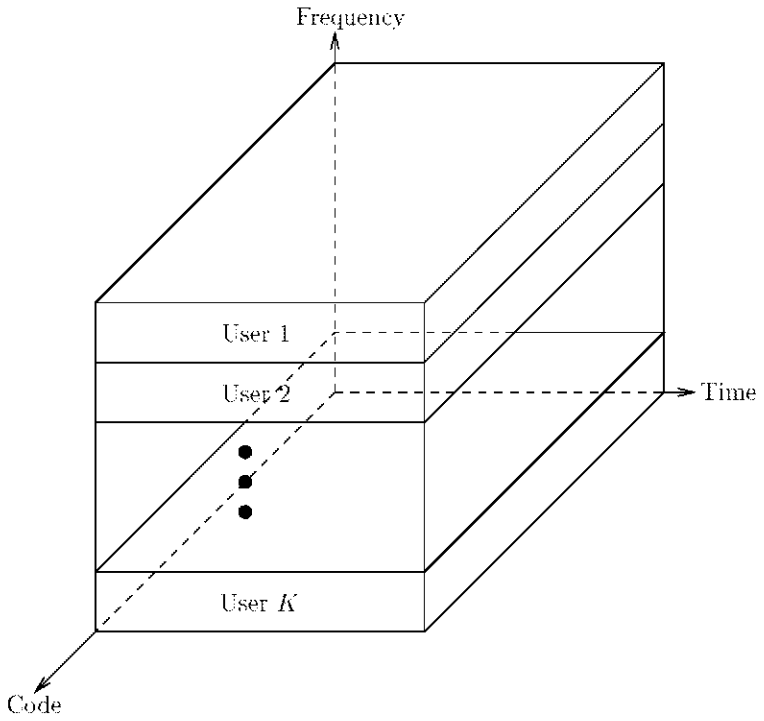

Figure 1.2. FDMA.

variable bandwidth signals. A fundamental result from communications theory is that the signals from multiple users may share a transmission medium if their signals can

be made orthogonal [Pro89]. In FDMA systems, the signals are made orthogonal by separating channels into distinct frequency bands. The channels may alternatively be separated by making them mutually orthogonal based on some other characteristic, such as the time slot occupied by the channel, an underlying signal property, or even spatial position. FDMA is often used in combination of other multiple access schemes.Therefore to exploit the benefits of digital modulation, FDMA is not the best choice [LR98].

In TDMA, see Fig. 1.3, the channels are made orthogonal by separating them in time, with all users using the same frequency band. A TDMA time slot can be assigned to each user. Each user transmit at a very high data rate during the brief time slot. For instance, if there are N_s time slots, each having a duration if T_s seconds, then each user, producing data at some data rate R_d, must store data for $N_s T_s$ seconds and transmit at a data rate $N_s R_d$ during a T_s second time slot. High data rate users may

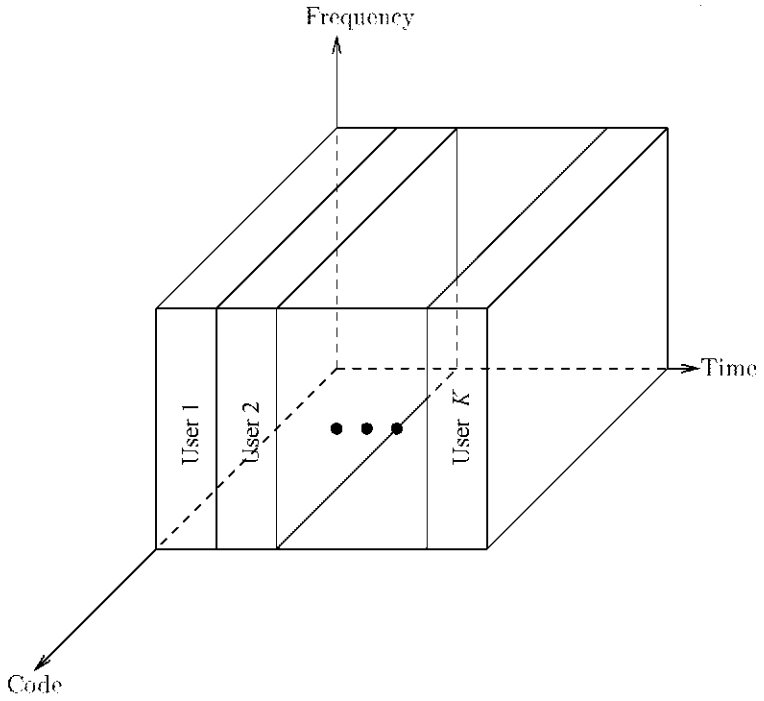

Figure 1.3. TDMA.

be accommodated by assigning more than one time slot to a user. For instance, if M time slots are assigned to a user, then the data rate can be increased to MR_d bits per

second at the expense of allowing fewer users on the system [LR98].

Alternatively, in a Direct Sequence CDMA (DS-CDMA) system, see Fig. 1.4, all users transmit in the same frequency band at the same time. Different channels are distinguished by assigning a different underlying pseudo-noise (PN) sequence to each channel. The bandwidth of the PN-sequence is much larger than the bandwidth of the data sequence transmitted by the user [LR98].

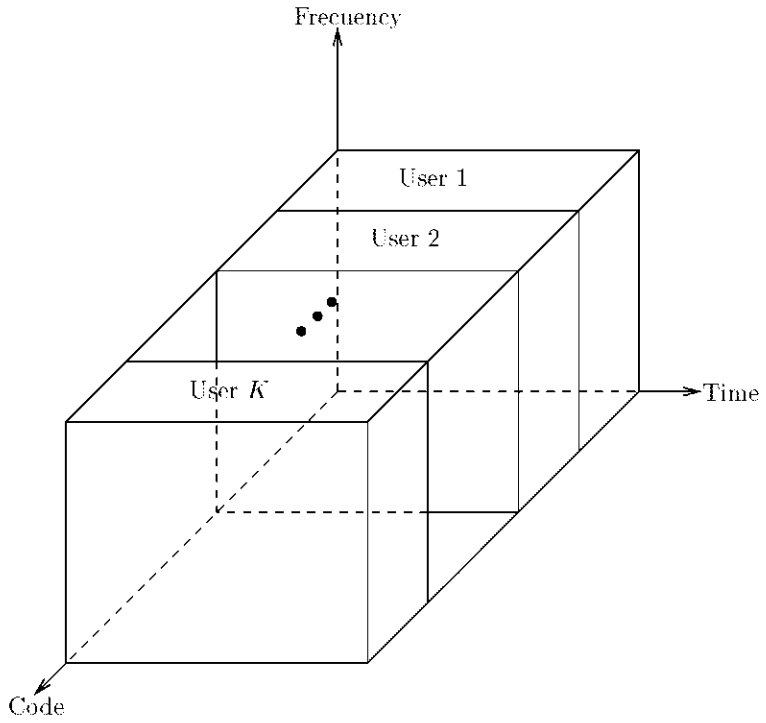

Figure 1.4. CDMA.

1.3 Key terms and concepts in wireless communications

In the following a brief glossary of key terms is given, which are used in this document:

Smart antennas : Smart antenna systems are formed by an array of multiple antennas and coordinated transceivers and advanced digital signal processing algorithms. Instead of having a single fixed beam pattern from a traditional antenna, the smart an-

tenna can effectively generate multiple beam patterns, each of which is pointed towards a particular user. Such beam patterns can also adapt to follow any mobile user, see adaptive antennas. On the receive side, such a feature, i.e., spatially selective receive, can greatly increase the receive sensivity, minimize the co-channel interference from co-channel users at different locations leading to higher capacity. It can also effectively incorporate multipath components to combat multipath fading. On the transmission side, intelligent spatial selective beamforming transmit can reduce the interference to other co-channel users and leading to higher capacity and dramatically reduce the output power requirement [ITU98].

Adaptive antenna : Smart antennas are often called adaptive antennas if an array of antennas is able to change its antenna pattern dynamically in order to maximize the signal-to-noise ratio. Adaptive array antennas can adjust their pattern to track portable users. Adaptative antennas are used to enhance received signal power in the uplink and may also be used for beam forming in the downlink to suppress interference [LR98].

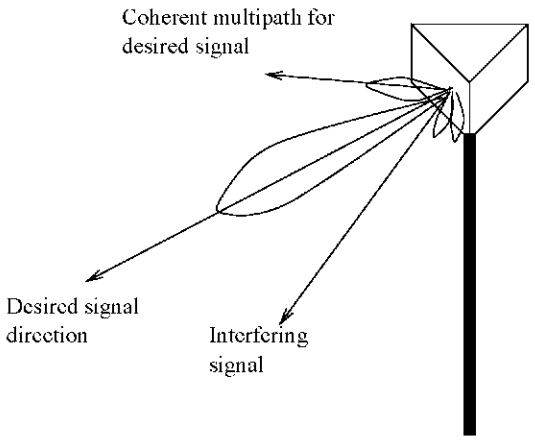

Figure 1.5. Adaptive antenna.

Switched Beam Antennas : Switched Beam Antennas use a number of fixed beams at an antenna site. The receiver selects the beam that provides the greatest signal enhancement and interference reduction. Switched beam systems may not offer the degree of performance improvement offered by adaptive systems, but they are often

much less complex and are easier to retro-fit to existing wireless technologies [LR98].
Macrocells : Large cells, covering several kilometers with each BS [LR98].

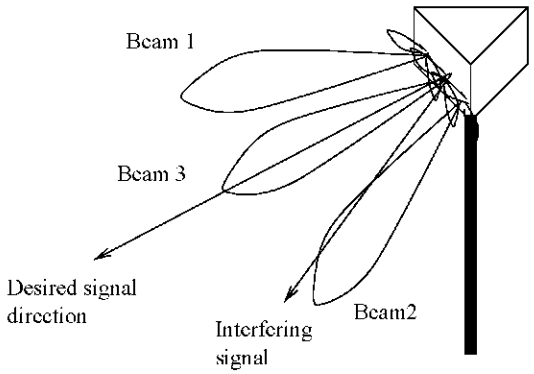

Figure 1.6. Switched Beam System. Beam 3 is selected here for the desired signal.

Microcells : Smaller cells, used to provide increased capacity with cell spacing of few hundred meters to a kilometer [LR98].

Picocells : Very smart cells, used to provide extremely high capacity indoors and in high traffic pedestrian areas [LR98].

Low Tier Systems : wireless systems using picocells and microcells to provide low power service to pedestrian users indoors and in pedestrian areas. Typically, low tier system, such as Digital European Cordless Telephone (DECT) and Personal Access Communications System (PACS), are not as well suited for high vehicle speeds as High Tier systems, and are more susceptible to multipath. However, low tier systems are usually to suport higher voice quality. Because low tier systems do not have to contend with high time delay spread, BSs and subscriber units can be less expensive, and now power requeriments allow very long battery life. Low Tier systems excel at covering high density areas, but are less in rural, low density and high speed environments [LR98].

High Tier Systems : High Tier Systems use macrocells, such as IS-95 and GSM, use a variety of techniques to combat multipath [LR98].

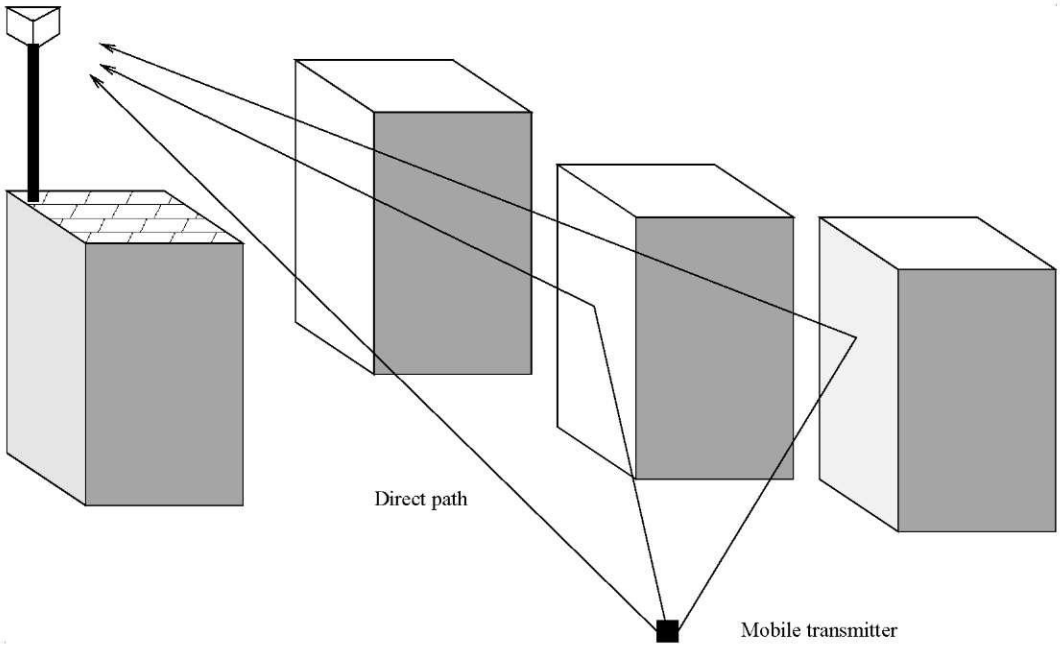

Figure 1.7. Multipath results from scatterers in the mobile radio environment.

Multipath : In mobile and portable radio channels, as shown in Fig. 1.7, there are multiple radio paths between the transmitter and receiver. The longer path result in delayed versions of the desired signal arriving at the receiver. When the difference in delays between the different multipath components, quantified by the time delay spread into one another, leading to intersymbol interference (ISI) at the receiver. This can result in poor signal reception, even when the signal level is high, particulary in TDMA systems. Even when the time delay spread is small, if strong multipath is present, the phases of the multipath signal components can combine destructively over the narrow bandwidth, leading to fading of the received signal level [Rap96].

1.4 Interference cancellation

The goal of this thesis is the investigation of interference cancellation techniques for TD-CDMA with joint data detection (JD). Interference cancellation only will be used as complement of JD in order to try to improve the results of the simulations. Interference cancellation is performed as follows. Firstly, part of the transmitted data symbols and,

thus, of the interference is detected. Next, the contribution of these transmitted data symbols to the compound signal is reconstructed. Then, this reconstructed contribution or interference replica is canceled from the compound signal. Data detection in the first step is performed by a bank of single user detectors, i.e., a number of single user detectors [Koh94]. For each user signal to be detected and cancelled, a single user detector is realized [Koh94].

1.5 Joint Detection

In CDMA mobile radio systems, a number K of independent users are simultaneously active in the same frequency band, only discernible by different user-specific spreading codes. Each data symbol of the data symbol sequence $\underline{\mathbf{d}}$ transmitted by user k is multiplied by the user-specific spreading code. The resulting signal of user k is transmitted over the time-variant multipath mobile radio channel. In the uplink, the mobile radio channels of all K users are in general different. At the receiver of the BS, the superposition of the contributions of all K users appears. At the receiver, transmission over the time-variant mobile radio channels results in both ISI between the data symbols of one and the same user and Multiple Access Interference (MAI) between data symbols of different users. The superposition signal is also disturbed by a sequence $\underline{\mathbf{n}}$ representing intercell interference and thermal noise. The received sequence $\underline{\mathbf{e}}$ containing samples at the chip rate has to be processed at the receiver by a data detection algorithm to determine estimates $\underline{\mathbf{d}}$ of the data symbol sequences $\underline{\mathbf{d}}^{(k)}, k = 1...K$, of all K users. By applying JD schemes like the zero-forcing algorithm, MAI and ISI can be totally eliminated. Therefore, JD schemes goes along with a noise enhancement, which is called signal-to-noise ratio (SNR) degradation [COST99].

1.6 TD-CDMA

Time Division-Code Division Multiple Access (TD-CDMA) is based on a TDMA scheme which is extended by an supplementary CDMA component [KB93], [JS95].

In the case of voice or low rate data transmission, K users are simultaneously active in the same frequency band and time slot, each using a specific CDMA code, which allows signal separation in the receiver. The burst and frame structures of TD-CDMA are shown in Fig. 1.8, where B, T_{fr}, N_{fr} and T_{bu} denote the bandwidth of a frequency band, the duration of a TDMA frame, the number of bursts per TDMA frame, and the burst duration, respectively. A burst consist of a guard interval and two data blocks separated by user specific midamble, which is used for channel estimation. The frame and burst structures are similar to those used in GSM and facilitate beneficially backward compatibility.

In the simulations, directional radio channel models are assumed which set out from a single direction of arrival (DOA) for each user. The corresponding channel impulse responses are based on measurements [FBK93], whereas the angular spread of the radio channels can not be derived from the measurements. The impact of the angular spread of the radio channel on adaptative antennas has been analyzed in [ECSR98], [PMF98], [LP96] and [NB98] among others. A typical feature of TD-CDMA is the application of JD at the receivers, which allows the elimination of ISI and MAI. TD-CDMA easily lends itself to the utilization of adaptative antennas, due to its TDMA component, the number of user signals to be simultaneously treated is much smaller than in systems which work without TDMA.

Most of the receiver concepts utilizing adaptive antenna make use of the knowledge of the DOAs of the desired signals, which opens the posibility of space-time processing at the receiver. The DOAs can be obtained by means of estimation algorithms like MUSIC or ESPRIT [RK89], this algorithms will not be explained in this document. More sophisticated receiver structures are able to consider also information about the not desired interfering signals to maximize the radio of the average power of all desired signals at each antenna to the total interference power. Not only the uplink receivers are able to take advantage of the knowledge about the interfering signals. Also in the downlink it is possible to exploit this knowlegde gained in the uplink by introducing beamforming techniques [SB97]. Therefore, obtainig information about the interfering signals by the estimation algorithms is an important research topic [WP99].

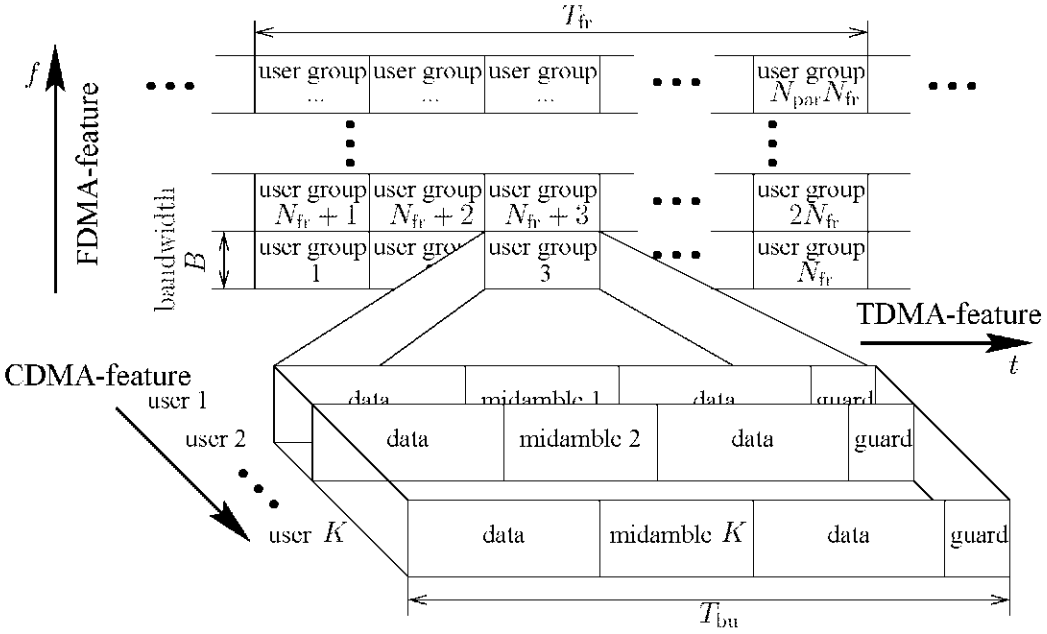

Figure 1.8. Burst and frame structures of TD-CDMA.

1.7 Goals of this thesis

The main objectives of this thesis are the study and development of two novel receiver structures based on interference cancellation together with JD.

The first one will be termed direct interference cancellation. It is based on the interference cancellation principle, see Section 1.4. The achievable performance enhancement will be studied by evaluating the bit error rate (BER).

The second one will be termed interference cancellation after matched filtering. This receiver structure is based on a simplified matched filter, see Apendix A, before an interference cancellation unit. Also by evaluating the BER the performance enhancement achievable with this receiver concept will be studied..

Finally the behaviour of the FEC-coder in the signal reconstruction, for several specific cases:

- Single errors,
- Burst errors and

- error distributions as a function of the distance,

will be studied for specific cases by simulation.

2 System model

2.1 Data estimation

In this section, the discrete time lowpass model of the TD-CDMA uplink receiver with antenna arrays will be presented, see also [BPH] and [WPE98]. The parameters of the TD-CDMA air interface assumed in this document are given in Table 2.1, see also [ETSI97]. In the following complex values are underlined, vectors are represented by

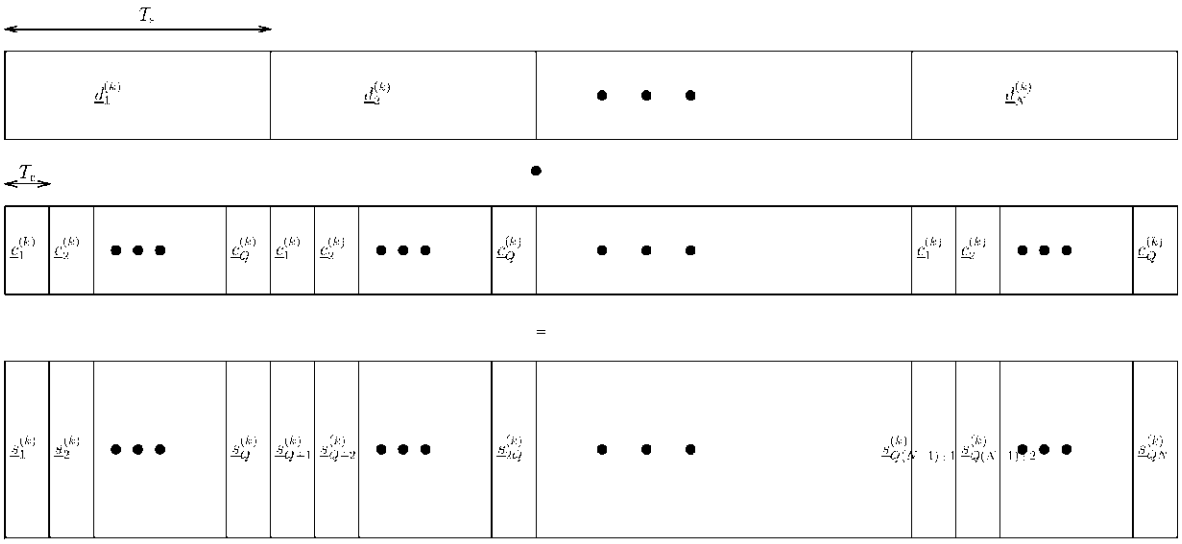

Figure 2.1. Spreading process.

bold face lower case letters, matrices by bold face upper case letters and real values are italic upper case letters. The symbol ˆ means that this variable is an estimation. The symbols * and $^{\mathrm{T}}$ designate complex conjugation and transposition, respectively, of a vector or a matrix [Kl96]. Only the first data block each burst will be considered. The consideration of the second data block is straightforward [WP99].

Each of the K users, see Fig. 2.2. are transmitting simultaneously in the same frequency band and time slot a data sequence see (2.1).

$$\underline{\mathbf{d}}^{(k)} = \left[\underline{d}_1^{(k)}, ..., \underline{d}_N^{(k)}\right]^{\mathrm{T}}, k = 1...K, k \in \mathbb{N}. \tag{2.1}$$

This sequence of N m-ary complex data symbols $\underline{d}_n^{(k)}$ have the symbol duration T_{s}.

These data are elements of the complex set $\{\underline{v}_1, \underline{v}_2, ..., \underline{v}_m\}$. Each of the data symbols $\underline{d}_n^{(k)}$ is spread by a user specific CDMA code of length Q

$$\underline{\mathbf{c}}^{(k)} = \left[\underline{c}_1^{(k)}, ..., \underline{c}_Q^{(k)}\right]^{\mathrm{T}}, k = 1...K, \tag{2.2}$$

at the transmitter. The $\tilde{m}$-ary complex elements $\underline{c}_q^{(k)}$ of (2.2), which are taken from the complex set $\{\underline{v}_{\mathrm{c},1}, \underline{v}_{\mathrm{c},2}, ..., \underline{v}_{,\tilde{m}}\}$, are termed chips. The chip duration T_c equals T_s/Q [WP99]. The spreading process

$$\underline{s}_{ij}^{(k)} = \underline{d}_i^{(k)} \underline{c}_j^{(k)}, i = 1...N, j = 1...Q, \tag{2.3}$$

between data and the code is represented in Fig. 2.1, where $\underline{s}_{ij}$ is the product between $\underline{d}_i$ and $\underline{c}_j$.

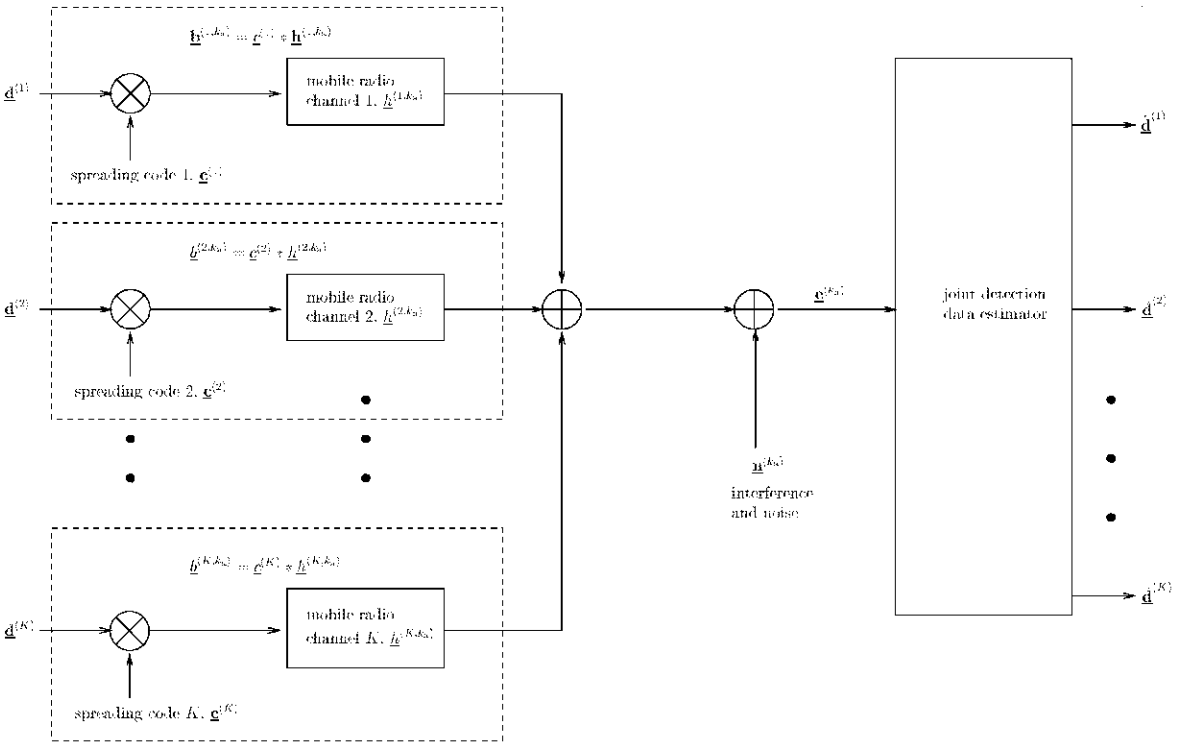

Figure 2.2. System model of the uplink of a CDMA system with a multi-antenna receiver applying joint detection.

At the receiver an antenna array is utilized. The number of elements of the antenna array is K_a, therefore, the transmission of the K user signals takes place over $K \cdot K_\mathrm{a}$

carrier frequency	f_c	1815 MHz
user bandwidth	B	1.6 MHz
number of users	K	8
burst duration	T_{bu}	577 μs
data symbols per data block	N	28
symbol duration	T_s	7.376 μs
chips per symbol	Q	16
chip duration	T_c	0.461 μs
midamble chips	L_{mid}	296
modulation scheme		4PSK
chip impulse filter		GMSK
convolutional encoder(FEC) constrint length rate	 K_c R_c	 5 1/2
interleaving depth	I_d	4 burst

Table 2.1. Parameters used in simulations.

different radio channels. This radio channels are described by the time variant complex impulse responses

$$\underline{\mathbf{h}}^{(k,k_a)}(\tau,t), k = 1...K, k_a = 1...K_a, \tag{2.4}$$

where $\underline{\mathbf{h}}^{(k,k_a)}$ refers to the connection of mobile k with receiver antenna element k_a. τ is the delay parameter and t is the real time [WP99]. In the following, the K channel impulse response between each user k and a reference point (RP) at the BS location, see Fig. 2.3, are called reference channels. The K impulse responses of the reference channels are used to determine the $K \cdot K_a$ above mentioned channel impulse responses. To this purpose the quantities introduced in Fig. 2.3 are required, see also [BPH] and [WPE98]. Relative to the reference line, see Fig. 2.3, the DOA of a signal coming from mobile k is denoted by $\beta^{(k)}$, and the DOA of the k_i-th interfering signal is denoted by $\gamma^{(k_i)}$. The k_a-th array element has distance $l^{(k_a)}$ from RP, and the angle spanned by the reference line and the line connecting the k_a-th array element with RP is termed $\alpha^{(k_a)}$ [WP99]. For each DOA of a desired signal, i.e. for each user k, a discrete time channel impulse response vector

$$\underline{\mathbf{h}}_d^{(k)} = \left[\underline{h}_{d,1}^{(k)}, ..., \underline{h}_{d,W}^{(k)}\right]^T, k = 1...K, \tag{2.5}$$

can be defined corresponding to the link between the k-th user and RP by taking

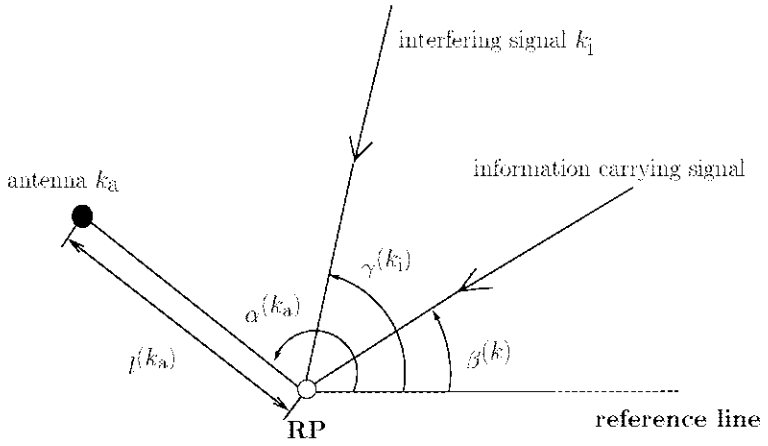

Figure 2.3. Definition of parameters.

W samples $\underline{h}_w^{(k)}$ of the complex channel impulse response at the chip rate $1/T_c$. The channel between the k-th user and the k_a-th antenna element is related to $\underline{\mathbf{h}}^{(k)}$ as follows:

$$\underline{\mathbf{h}}^{(k,k_a)} = \underline{\mathbf{h}}_d \cdot \exp\{j2\pi \frac{l^{(k_a)}}{\lambda} \cos(\beta^{(k)} - \alpha^{(k_a)})\}, \tag{2.6}$$

where λ is the carrier wavelength. The channels from one user are fully correlated at the K_a antennas, so fast fading can not be mitigated by means of space diversity [WP99].

By the convolution of the impulse responses given by (2.6) and the CDMA codes $\underline{\mathbf{c}}^{(k)}$, see (2.2), the effective channel impulse responses

$$\underline{\mathbf{b}}^{(k,k_a)} = [\underline{b}_1^{(k,k_a)}, ..., \underline{b}_{Q+W-1}^{(k,k_a)}]^T = \underline{\mathbf{h}}^{(k,k_a)} * \underline{\mathbf{c}}^{(k)} \tag{2.7}$$

is obtained.

These combined channel impulse responses $\underline{\mathbf{b}}^{(k,k_a)}, k = 1...K, k_a = 1...K_a$, are assumed to be known at the receiver. Using a matrix-vector notation this operation can be

expressed by

$$\begin{pmatrix} \underline{b}_1^{(k,k_\mathrm{a})} \\ \underline{b}_2^{(k,k_\mathrm{a})} \\ \vdots \\ \\ \\ \\ \\ \underline{b}_{Q+W-1}^{(k,k_\mathrm{a})} \end{pmatrix} = \begin{pmatrix} \underline{c}_1^{(k)} & 0 & \dots & & 0 \\ \vdots & \underline{c}_1^{(k)} & 0 & \dots & 0 \\ \underline{c}_Q^{(k)} & \vdots & \underline{c}_1^{(k)} & \dots & 0 \\ 0 & \underline{c}_Q^{(k)} & \vdots & \ddots & 0 \\ \vdots & 0 & \underline{c}_Q^{(k)} & & \underline{c}_1^{(k)} \\ & \vdots & 0 & \ddots & \vdots \\ 0 & 0 & 0 & 0 & \underline{c}_Q^{(k)} \end{pmatrix} \cdot \begin{pmatrix} \underline{h}_1^{(k,k_\mathrm{a})} \\ \underline{h}_2^{(k,k_\mathrm{a})} \\ \vdots \\ \\ \\ \\ \underline{h}_W^{(k,k_\mathrm{a})} \end{pmatrix} \tag{2.8}$$

The spreading code matrix dimension, see (2.8), is $(Q+W-1)\times W$. From (2.7), with the effective channel impulse responses $\underline{\mathbf{b}}^{(k,k_\mathrm{a})}, k=1...K, k_\mathrm{a}=1...K_\mathrm{a}$ the matrix $\underline{\mathbf{A}}^{(k_\mathrm{a})}$ with the dimension $(N\cdot Q+W-1)\times(K\cdot N)$ and the elements

$$\underline{A}_{Q\cdot(n-1)+l,N\cdot(k-1)+n}^{(k_\mathrm{a})} = \begin{cases} \underline{b}_l^{(k,k_\mathrm{a})} \text{ for } k=1...K, \\ \qquad\qquad k_\mathrm{a}=1...K_\mathrm{a}, \\ \qquad\qquad n=1...N, \\ \qquad\qquad l=1...Q+W-1, \\ 0 \qquad \text{else}, \end{cases} \tag{2.9}$$

can be obtained.

Each column of $\underline{\mathbf{A}}^{(k_\mathrm{a})}$ contains the combined channel impulse response $\underline{\mathbf{b}}^{(k,k_\mathrm{a})}$ of user k from the k_a-th antenna element given by (2.7), see (2.11).

$$\underline{\mathbf{A}}^{(k_\mathrm{a})} = \tag{2.10}$$

$$\begin{pmatrix} \underline{b}_1^{(1,k_\mathrm{a})} & 0 & & \dots & & 0 & \underline{b}_1^{(2,k_\mathrm{a})} & 0 & \dots & 0 & \dots & 0 & \underline{b}_1^{(K,k_\mathrm{a})} & \dots \\ 0 & & & & & & & & & & & & & \\ \underline{b}_2^{(1,k_\mathrm{a})} & \vdots & 0 & \dots & 0 & \underline{b}_2^{(2,k_\mathrm{a})} & \vdots & \dots & \vdots & \dots & \vdots & \vdots & \dots & \vdots \\ \vdots & 0 & \vdots & \dots & \vdots & \vdots & 0 & \dots & 0 & \dots & & \underline{b}_{Q+W-1}^{(K,k_\mathrm{a})} & \dots & \\ & \underline{b}_1^{(1,k_\mathrm{a})} & 0 & \dots & 0 & & \underline{b}_1^{(2,k_\mathrm{a})} & 0 & 0 & \dots & & 0 & & \\ \underline{b}_{Q+W-1}^{(1,k_\mathrm{a})} & \vdots & \underline{b}_1^{(1,k_\mathrm{a})} & \dots & 0 & \underline{b}_{Q+W-1}^{(2,k_\mathrm{a})} & \vdots & & 0 & \vdots & \dots & \dots & & \\ 0 & \underline{b}_{Q+W-1}^{(1,k_\mathrm{a})} & \vdots & & 0 & 0 & \underline{b}_{Q+W-1}^{(2,k_\mathrm{a})} & & 0 & \dots & 0 & & & 0 \\ \vdots & 0 & \underline{b}_{Q+W-1}^{(1,k_\mathrm{a})} & & \underline{b}_1^{(1,k_\mathrm{a})} & \vdots & 0 & & \underline{b}_1^{(2,k_\mathrm{a})} & \dots & \underline{b}_1^{(K-1,k_\mathrm{a})} & & & \underline{b}_1^{(K,k_\mathrm{a})} \\ & \vdots & 0 & & \vdots & & \vdots & & \vdots & \dots & \dots & & & \vdots \\ 0 & 0 & 0 & & \underline{b}_{Q+W-1}^{(1,k_\mathrm{a})} & 0 & 0 & 0 & \underline{b}_{Q+W-1}^{(2,k_\mathrm{a})} & \dots & \underline{b}_{Q+W-1}^{(K-1,k_\mathrm{a})} & 0 & & \underline{b}_{Q+W-1}^{(K,k_\mathrm{a})} \end{pmatrix}$$

The vector

$$\underline{\mathbf{d}} = [\underline{\mathbf{d}}^{(1)\mathrm{T}}, \underline{\mathbf{d}}^{(2)\mathrm{T}}, ..., \underline{\mathbf{d}}^{(K)\mathrm{T}}]^\mathrm{T} \tag{2.11}$$

contains the data symbol sequences $\underline{\mathbf{d}}^{(k)}$ of (2.1) for all K users. The dimension of this vector is NK, i.e. NK data symbols $\underline{d}_n^{(k)}, k = 1...K, n = 1...N$, are transmitted by all K users and each of the K users transmit a vector $\underline{\mathbf{d}}^{(k)}, k = 1...K$, respectively [WP99].

The complex additive noise sequences $\underline{\mathbf{n}}^{(k_\mathrm{a})}, k = 1...K, k_\mathrm{a} = 1...K_\mathrm{a}$ of dimension $NQ + W - 1$ at each of the k_a antenna elements, see Fig. 2.2, can be represented by

$$\underline{\mathbf{n}}^{(k_\mathrm{a})} = \left(\underline{n}_1^{(k_\mathrm{a})}, \underline{n}_2^{(k_\mathrm{a})}, ..., \underline{n}_{NQ+W-1}^{(k_\mathrm{a})}\right)^\mathrm{T}. \tag{2.12}$$

With the matrix $\underline{\mathbf{A}}^{(k_\mathrm{a})}$ from (2.9), the vector $\underline{\mathbf{d}}$ from (2.11) and the noise vector $\underline{\mathbf{n}}^{(k_\mathrm{a})}$ from (2.12) the received signal $\underline{\mathbf{e}}^{(k_\mathrm{a})}$ at the k_a-th antenna element is given by

$$\underline{\mathbf{e}}^{(k_\mathrm{a})} = \left[\underline{e}_1^{(k_\mathrm{a})}, \underline{e}_2^{(k_\mathrm{a})}, ..., \underline{e}_{N\cdot Q+W-1}^{(k_\mathrm{a})}\right]^\mathrm{T} = \underline{\mathbf{A}}^{(k_\mathrm{a})}\underline{\mathbf{d}} + \underline{\mathbf{n}}^{(k_\mathrm{a})}. \tag{2.13}$$

This vector $\underline{\mathbf{e}}^{(k_\mathrm{a})}$, with dimension $NQ + W - 1$, see (2.13), can be represented by a matrix-vector multiplication of $\underline{\mathbf{A}}^{(k_\mathrm{a})}$ and $\underline{\mathbf{d}}$ plus the noise $\underline{\mathbf{n}}^{(k_\mathrm{a})}$ for each antenna k_a:

$$\begin{pmatrix} \underline{e}_1^{(k_\mathrm{a})} \\ \underline{e}_2^{(k_\mathrm{a})} \\ \vdots \\ \\ \\ \\ \\ \underline{e}_{NQ+W-1}^{(k_\mathrm{a})} \end{pmatrix} = \tag{2.14}$$

$$\begin{pmatrix}
\underline{b}_1^{(1,k_\mathrm{a})} & 0 & \dots & 0 & \underline{b}_1^{(2,k_\mathrm{a})} & 0 & \dots & 0 & \dots & 0 & \underline{b}_1^{(K,k_\mathrm{a})} & \dots & 0 \\
\underline{b}_2^{(1,k_\mathrm{a})} & \vdots & 0 & \dots & 0 & \underline{b}_2^{(2,k_\mathrm{a})} & \vdots & \dots & \vdots & \dots & \vdots & \vdots & \dots & \vdots \\
\vdots & 0 & \vdots & \dots & \vdots & \vdots & 0 & \dots & 0 & \dots & & \underline{b}_{Q+W-1}^{(K),k_\mathrm{a}} & \cdots & \\
 & \underline{b}_1^{(1,k_\mathrm{a})} & 0 & \dots & 0 & & \underline{b}_1^{(2,k_\mathrm{a})} & 0 & 0 & \dots & & 0 & & \\
\underline{b}_{Q+W-1}^{(1,k_\mathrm{a})} & \vdots & \underline{b}_1^{(1,k_\mathrm{a})} & \dots & 0 & \underline{b}_{Q+W-1}^{(2,k_\mathrm{a})} & \vdots & & 0 & \vdots & \dots & \dots & & \\
0 & \underline{b}_{Q+W-1}^{(1,k_\mathrm{a})} & \vdots & & 0 & 0 & \underline{b}_{Q+W-1}^{(2,k_\mathrm{a})} & & 0 & \dots & 0 & & & 0 \\
\vdots & 0 & \underline{b}_{Q+W-1}^{(1,k_\mathrm{a})} & \underline{b}_1^{(1,k_\mathrm{a})} & \vdots & 0 & & \underline{b}_1^{(2,k_\mathrm{a})} & \dots & \underline{b}_1^{(K-1,k_\mathrm{a})} & & & \underline{b}_1^{(K),k_\mathrm{a}} & \\
 & \vdots & 0 & \vdots & & \vdots & & \vdots & \dots & \dots & & & \vdots & \\
0 & 0 & 0 & \underline{b}_{Q+W-1}^{(1,k_\mathrm{a})} & 0 & 0 & 0 & \underline{b}_{Q+W-1}^{(2,k_\mathrm{a})} & \dots & \underline{b}_{Q+W-1}^{(K-1,k_\mathrm{a})} & 0 & & \underline{b}_{Q+W-1}^{(K,k_\mathrm{a})} &
\end{pmatrix} \cdot \begin{pmatrix} \underline{d}_1^{(1)} \\ \underline{d}_2^{(1)} \\ \vdots \\ \underline{d}_N^{(1)} \\ \underline{d}_1^{(2)} \\ \vdots \\ \underline{d}_N^{(2)} \\ \vdots \\ \underline{d}_N^{(N)} \end{pmatrix} + \begin{pmatrix} \underline{n}_1^{(k_\mathrm{a})} \\ \underline{n}_2^{(k_\mathrm{a})} \\ \vdots \\ \\ \\ \underline{n}_{NQ+W-1}^{(k_\mathrm{a})} \end{pmatrix}$$

In general for all K_a antennas the total system matrix is

$$\underline{\mathbf{A}} = \left[\underline{\mathbf{A}}^{(1)\mathrm{T}}, \underline{\mathbf{A}}^{(2)\mathrm{T}}, ..., \underline{\mathbf{A}}^{(K_\mathrm{a})\mathrm{T}}\right]^\mathrm{T} \tag{2.15}$$

and the combined noise vector is

$$\underline{\mathbf{n}} = \left[\underline{\mathbf{n}}^{(1)\mathrm{T}}, \underline{\mathbf{n}}^{(2)\mathrm{T}}, ... \underline{\mathbf{n}}^{(K_\mathrm{a})\mathrm{T}}\right]^\mathrm{T} \tag{2.16}$$

which represents the intercell MAI. Together with the matrix $\underline{\mathbf{A}}$ from (2.15), the vector $\underline{\mathbf{n}}$ from (2.16) and the vector $\underline{\mathbf{d}}$ from (2.11) the combined received vector becomes

$$\underline{\mathbf{e}} = \left[\underline{\mathbf{e}}^{(1)\mathrm{T}}, \underline{\mathbf{e}}^{(2)\mathrm{T}}, ..., \underline{\mathbf{e}}^{(K_\mathrm{a})\mathrm{T}}\right]^\mathrm{T} = \underline{\mathbf{A}}\,\underline{\mathbf{d}} + \underline{\mathbf{n}}. \tag{2.17}$$

In this equation, $\underline{\mathbf{e}}$ is known at the receiver. This is also approximately true for the system matrix $\underline{\mathbf{A}}$ with the accuracy of $\underline{\mathbf{A}}$ depending on the accuracy of the channel estimates. However the data vector $\underline{\mathbf{d}}$ and the complex additive noise sequence vector $\underline{\mathbf{n}}$ are unknown [WP99]. By (2.17), the transmission model is fully described in matrix-vector notation. (2.17) establishes the relation between the KN data symbols $\underline{d}_n^{(k)}, n = 1...N, k = 1...K$, transmitted by all K users and the received vector $\underline{\mathbf{e}}$. In Fig. 2.2, the discrete-time transmission model described by matrix vector notation is illustrated. The data vector $\underline{\mathbf{d}}^{(k)}$ of user k is transmitted over the channel with the combined channel impulse response $\underline{\mathbf{b}}^{(k,k_\mathrm{a})}$. The superposition of the resulting contribution of user k and the contributions of all other $K-1$ users, disturbed by the noise vector $\underline{\mathbf{n}}^{(k_\mathrm{a})}$, forms the received vector $\underline{\mathbf{e}}^{(k_\mathrm{a})}$. The system matrix $\underline{\mathbf{A}}$ is determined by the combined channel impulse responses $\underline{\mathbf{b}}^{(k,k_\mathrm{a})}, k = 1...K, k_\mathrm{a} = 1...K_\mathrm{a}$, of all users and each antenna [Kl96]. If perfect estimation of the channel impulse responses $\underline{\mathbf{h}}^{(k,k_\mathrm{a})}, k = 1...K, k_\mathrm{a} = 1...K_\mathrm{a}$, is assumed in the receiver and with the knowledge of the CDMA codes $\underline{\mathbf{c}}^{(k)}$ of each user, the system matrix $\underline{\mathbf{A}}$ is perfectly known at the receiver. Furthermore, if we assume to know the covariance matrix

$$\underline{\mathbf{R}}_\mathrm{n} = \mathrm{E}\{\underline{\mathbf{n}}\,\underline{\mathbf{n}}^{*\mathrm{T}}\} \tag{2.18}$$

of $\underline{\mathbf{n}}$ from (2.16) that we will use in our simulations then, applying the zero forcing-block linear equalization algorithm (ZF-BLE), see the Appendix B, to perform JD, a linear estimate

$$\underline{\hat{\mathbf{d}}} = \left(\underline{\mathbf{A}}^{*\mathrm{T}}\underline{\mathbf{R}}_\mathrm{n}{}^{-1}\underline{\mathbf{A}}\right)^{-1}\underline{\mathbf{A}}^{*\mathrm{T}}\underline{\mathbf{R}}_\mathrm{n}{}^{-1}\underline{\mathbf{e}} = \underline{\mathbf{M}}\,\underline{\mathbf{e}} \tag{2.19}$$

for $\underline{\mathbf{d}}$ can be obtained from (2.17), where

$$\underline{\mathbf{M}} = \left(\underline{\mathbf{A}}^{*\mathrm{T}}\underline{\mathbf{R}}_\mathrm{n}{}^{-1}\underline{\mathbf{A}}\right)^{-1}\underline{\mathbf{A}}^{*\mathrm{T}}\underline{\mathbf{R}}_\mathrm{n}{}^{-1}. \tag{2.20}$$

[WP99]. For the following investigations this detection scheme was selected among the many different JD schemes in literature and has already been verified by extensive field tests performed with a TD-CDMA hardware demostrator [MSW97].

2.2 Channel estimation

In the aforementioned section perfect channel estimation is assumed. If the channel impulse responses are not known at the receiver, they must be estimated. The channel estimation technique, which is already state of the art in TD-CDMA, has been proposed by Steiner in [SJ94]. Steiner developed a technique for jointly estimating the channel impulse responses between the links of each active user in the considered cell and a single antenna at the receiver by taking advantage of the midamble section inserted between the two data sections of the burst transmitted by each user $k, k = 1...K$, see the Fig. 1.8. The novelty of the Steiner estimator consists in the design process of the midamble training sequences known at the receiver. If the midamble codes of all users are derived from a single periodic basic code, the portion $\underline{\mathbf{e}}_{\mathrm{m}}$ of the total received signal from all antennas which depends exclusively on the transmitted midamble section and not on the data sections, is given by

$$\underline{\mathbf{e}}_{\mathrm{m}} = \left(\mathbf{I}^{(K_{\mathrm{a}})} \otimes \underline{\mathbf{G}}\right) \underline{\mathbf{h}} + \underline{\mathbf{n}}_{\mathrm{m}}, \tag{2.21}$$

where $\underline{\mathbf{h}}$ is the total channel impulse response vector of lenght $K_{\mathrm{a}}KW$,

$$\underline{\mathbf{h}} = \begin{pmatrix} \underline{h}_1^{(1,1)} \\ \underline{h}_2^{(1,1)} \\ \vdots \\ \underline{h}_W^{(1,1)} \\ \underline{h}_1^{(2,1)} \\ \vdots \\ \underline{h}_W^{(2,1)} \\ \vdots \\ \underline{h}_W^{(N,1)} \\ \underline{h}_1^{(1,2)} \\ \vdots \\ \underline{h}_W^{(2,2)} \\ \vdots \\ \underline{h}_W^{(K,K_{\mathrm{a}})} \end{pmatrix}, \tag{2.22}$$

which can be obtained by serial concatenation of the vectors $\underline{\mathbf{h}}^{(k,k_{\mathrm{a}})}$, $k = 1...K$, $k_{\mathrm{a}} = 1...K_{\mathrm{a}}$, given by (2.6) [WP99]. Each burst has a midamble sequence $\underline{\mathbf{m}}^{(k)}$ of length L_{m},

which is known by the receiver:

$$\underline{\mathbf{m}}^{(k)} = [\underline{m}_1^{(k)}, ..., \underline{m}_{L_\mathrm{m}}^{(k)}]. \tag{2.23}$$

The midamble sequences $\underline{\mathbf{m}}^{(k)}, k = 1...K$, are obtained from a basic periodic code

$$\underline{\mathbf{m}} = [\underline{\mathbf{m}}_1, ..., \underline{\mathbf{m}}_{L_\mathrm{m}+(K-1)W}]^\mathrm{T} \tag{2.24}$$

with the elements

$$\underline{\mathbf{m}}_i = \underline{\mathbf{m}}_{i-P}, i = (P+1)...(L_\mathrm{m} + (K-1)W), P \leq L_\mathrm{m} - W + 1. \tag{2.25}$$

The P elements $\underline{\mathbf{m}}_i, i = 1...P$, form the vector

$$\underline{\mathbf{m}}_\mathrm{P} = (\underline{\mathbf{m}}_1, ..., \underline{\mathbf{m}}_P)^\mathrm{T}, \tag{2.26}$$

which represents one single periode of the basic periodical code $\underline{\mathbf{m}}$ from (2.24).
Since one burst is a concatenation of the first data block, the midamble and the second data block and since the burst is convoluted with a channel impulse response of length W, the last $W-1$ midamble elements are influenced by the first datas of the second data block. The length of the received signal $\underline{\mathbf{e}}_\mathrm{m}$, which depends exclusively on the transmitted midambles without the influence of the adjacent datas is

$$L = L_\mathrm{m} - W + 1. \tag{2.27}$$

If

$$P = L = KW, \tag{2.28}$$

the basic periodic code of (2.24) is

$$\underline{\mathbf{m}} = (\underline{\mathbf{m}}_1, ..., \underline{\mathbf{m}}_{P+KW-1})^\mathrm{T} \tag{2.29}$$

From (2.29) the elements

$$\underline{\mathbf{m}}_i^{(k)} = \underline{\mathbf{m}}_{i+(K-k)W}, i = 1...L_\mathrm{m}, k = 1...K, \tag{2.30}$$

[SJ94] of the midambles $\underline{\mathbf{m}}^{(k)}, k = 1...K$, can be obtained. From the basic periodic code of (2.29) one can determine the square matrix

$$\underline{\mathbf{G}} = \begin{pmatrix} \underline{\mathbf{m}}_P & \underline{\mathbf{m}}_{P-1} & \cdots & \underline{\mathbf{m}}_2 & \underline{\mathbf{m}}_1 \\ \underline{\mathbf{m}}_1 & \underline{\mathbf{m}}_P & \cdots & \underline{\mathbf{m}}_3 & \underline{\mathbf{m}}_2 \\ \vdots & \vdots & & & \vdots \\ \underline{\mathbf{m}}_{P-1} & \underline{\mathbf{m}}_{P-2} & \cdots & \underline{\mathbf{m}}_1 & \underline{\mathbf{m}}_P \end{pmatrix} \tag{2.31}$$

of dimension $(L_{\mathrm{m}} - W + 1)\times(KW)$, which is required for channel estimation in (2.21) [SJ94]. The last vector to describe in (2.21) is $\underline{\mathbf{n}}_{\mathrm{m}}$. which represents the total received intercell MAI from all K_{a} antennas with the covariace matrix

$$\underline{\mathbf{R}}_{\mathrm{m}} = \mathrm{E}\{\underline{\mathbf{n}}_{\mathrm{m}}\, \underline{\mathbf{n}}_{\mathrm{m}}^{*\mathrm{T}}\}. \tag{2.32}$$

From (2.5), a total directional channel impulse response can be defined by

$$\underline{\mathbf{h}}_{\mathrm{d}} = \left[\underline{\mathbf{h}}_{\mathrm{d}}^{(1)\mathrm{T}}, ..., \underline{\mathbf{h}}_{\mathrm{d}}^{(K)\mathrm{T}}\right]^{\mathrm{T}}, \tag{2.33}$$

which has KW complex elements.

The matrix $\underline{\mathbf{A}}_{\mathrm{d}}$ contains the information about the DOAs associated with each com-

ponent of the directional channel impulse response of each user,

$$\underline{\mathbf{A}}_{\mathrm{d}} = \begin{pmatrix}
z^{(1,1)} & \dots & 0 & 0 & \dots & & \dots & 0 & & 0 \\
\vdots & \ddots & 0 & 0 & \dots & & \dots & 0 & & 0 \\
0 & 0 & z^{(1,1)} & 0 & \dots & & \dots & 0 & & 0 \\
0 & \dots & 0 & z^{(2,1)} & \dots & 0 & \dots & 0 & \dots & 0 \\
0 & \dots & 0 & \vdots & \ddots & \vdots & \dots & 0 & \dots & 0 \\
0 & \dots & 0 & 0 & 0 & z^{(2,1)} & \dots & 0 & \dots & 0 \\
0 & \dots & & & & 0 & \dots & z^{(K,1)} & \dots & 0 \\
0 & \dots & & & & 0 & \dots & \vdots & \ddots & \vdots \\
0 & \dots & & & & & \dots & 0 & 0 & z^{(K,1)} \\
z^{(1,2)} & \dots & 0 & 0 & \dots & & \dots & 0 & & 0 \\
\vdots & \ddots & 0 & 0 & \dots & & \dots & 0 & & 0 \\
0 & 0 & z^{(1,2)} & 0 & \dots & & \dots & 0 & & 0 \\
0 & \dots & 0 & z^{(2,2)} & \dots & 0 & \dots & 0 & \dots & 0 \\
0 & \dots & 0 & \vdots & \ddots & \vdots & \dots & 0 & \dots & 0 \\
0 & \dots & 0 & 0 & 0 & z^{(2,2)} & \dots & 0 & \dots & 0 \\
0 & \dots & & & & 0 & \dots & z^{(K,2)} & \dots & 0 \\
0 & \dots & & & & 0 & \dots & \vdots & \ddots & \vdots \\
0 & \dots & & & & & \dots & 0 & 0 & z^{(K,2)} \\
\vdots & \vdots & \vdots & \vdots & \vdots & \vdots & \vdots & \vdots & \vdots & \vdots \\
z^{(1,K_{\mathrm{a}})} & \dots & 0 & 0 & \dots & & \dots & 0 & & 0 \\
\vdots & \ddots & 0 & 0 & \dots & & \dots & 0 & & 0 \\
0 & 0 & z^{(1,K_{\mathrm{a}})} & 0 & \dots & & \dots & 0 & & 0 \\
0 & \dots & 0 & z^{(2,K_{\mathrm{a}})} & \dots & 0 & \dots & 0 & \dots & 0 \\
0 & \dots & 0 & \vdots & \ddots & \vdots & \dots & 0 & \dots & 0 \\
0 & \dots & 0 & 0 & 0 & z^{(2,K_{\mathrm{a}})} & \dots & 0 & \dots & 0 \\
0 & \dots & & & & 0 & \dots & z^{(K,K_{\mathrm{a}})} & \dots & 0 \\
0 & \dots & & & & 0 & \dots & \vdots & \ddots & \vdots \\
0 & \dots & 0 & 0 & 0 & 0 & 0 & 0 & 0 & z^{(K,K_{\mathrm{a}})}
\end{pmatrix} \tag{2.34}$$

with dimension $K_{\mathrm{a}}KW \times KW$ and the components

$$z^{(k,k_{\mathrm{a}})} = \exp\{\mathrm{j}2\pi \frac{l^{(k_{\mathrm{a}})}}{\lambda} \cos(\beta^{(k)} - \alpha^{(k_{\mathrm{a}})})\}, k = 1...K, k_{\mathrm{a}} = 1...K_{\mathrm{a}} \tag{2.35}$$

of $\underline{\mathbf{A}}_{\mathrm{d}}$.

The total channel impulse response vector $\underline{\mathbf{h}}$ can be expressed as

$$\underline{\mathbf{h}} = \underline{\mathbf{A}}_{\mathrm{d}}\, \underline{\mathbf{h}}_{\mathrm{d}}, \tag{2.36}$$

see (2.34) and (2.33).

Then, the total received signal $\underline{\mathbf{e}}_{\mathrm{m}}$ from (2.21) becomes

$$\underline{\mathbf{e}}_{\mathrm{m}} = \left(\mathbf{I}^{(K_{\mathrm{a}})} \otimes \underline{\mathbf{G}}\right) \underline{\mathbf{A}}_{\mathrm{d}} \underline{\mathbf{h}}_{\mathrm{d}} + \underline{\mathbf{n}}_{\mathrm{m}}. \tag{2.37}$$

Since

$$KW < K_{\mathrm{a}} KW \tag{2.38}$$

is valid, the number of unknown channel impulse response components contained in $\underline{\mathbf{h}}_{\mathrm{d}}$ is smaller than the number of unknown channel impulse response components contained in $\underline{\mathbf{h}}$, see (2.21) and (2.38). Since the number of unknown channel impulse response components in both (2.21) and (2.38) is the same, this reduction of the number of the unknown channel impulse response components leads to an improved quality of the channel estimate, see also [PHF97]. According to the maximum-likelihood principle, the channel impulse response estimate of $\underline{\mathbf{h}}_{\mathrm{d}}$is obtained from (2.37) as

$$\hat{\underline{\mathbf{h}}}_{\mathrm{d}} = \left(\underline{\mathbf{A}}_{\mathrm{d}}^{*\mathrm{T}} \left(\mathbf{I}^{(K_{\mathrm{a}})} \otimes \underline{\mathbf{G}}^{*\mathrm{T}}\right) \underline{\mathbf{R}}_{\mathrm{m}}^{-1} \left(\mathbf{I}^{(K_{\mathrm{a}})} \otimes \underline{\mathbf{G}}\right) \underline{\mathbf{A}}_{\mathrm{d}}\right)^{-1} \underline{\mathbf{A}}_{\mathrm{d}}^{*\mathrm{T}} \left(\mathbf{I}^{(K_{\mathrm{a}})} \otimes \underline{\mathbf{G}}^{*\mathrm{T}}\right) \underline{\mathbf{R}}_{\mathrm{m}}^{-1} \underline{\mathbf{e}}_{\mathrm{m}}. \tag{2.39}$$

(2.39) shows that the knowledge of the covariance matrix $\underline{\mathbf{R}}_{\mathrm{m}}$ is required for an maximum-likelihood channel estimation, which is the optimum estimation [WP99].

2.3 Novel receiver structures for interference cancellation

In this section, the two receiver structures, which have been developed, will be presented. In the Fig. 2.5 and 2.8 the receiver block diagrams are shown. The structures are similar, only some blocks are different. The differences between the two receiver diagrams will be explained in the Subsections 2.3.1 and 2.3.2. The two diagrams are a simplified version of the real receptor, which is more complex. Basically, the two receivers have two steps, data and channel are estimated two times. First, the receiver performs JD, by applying a ZF-BLE, see Apendix B, where the first estimations of coded data $\hat{\underline{\mathbf{d}}}_{c_1}^{(k)}, k = 1...K$, of all users are obtained. After this, the data must be deinterleaved and decoded by a Forward Error Correction-decoder (FEC-decoding). The FEC-Encoder,which is shown in Fig. 2.4, has a constraint length L_{c} equal to 5, a code rate R_{c} equal to 1/2 and a 23, 35 non systematic convolutional code. This encoder will

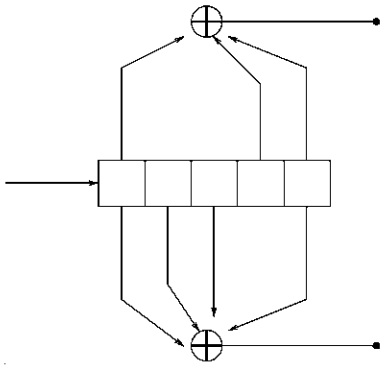

Figure 2.4. FEC-Encoder.

be explained more in detail in following sections.

Thus, we have the first estimation of uncoded data $\hat{\underline{\mathbf{d}}}_{u_1}^{(k)}, k = 1...K$. From this estimated uncoded data, $\hat{\underline{\mathbf{d}}}_{u_1}^{(k)}, k = 1...K$, we can obtain an estimated received signal $\hat{\underline{\mathbf{e}}}_{\mathrm{r}}^{(k_{\mathrm{a}})}, k_{\mathrm{a}} = 1...K_{\mathrm{a}}$, termed noise-free received signal. The two receivers differ here. The two receivers perform different ways to obtain the modified signal $\underline{\mathbf{e}}_{\mathrm{mo}}$. This different modifications will be explained in the following subsections. After this modification in the receiver a second estimation under consideration of JD, taking into account the estimated interference covariance matrix $\underline{\mathbf{R}}_{\mathrm{n}}$, which is obtained before, see (2.18), (2.19) and (2.20), and FEC-decoding is performed. The construction of the modified signal $\underline{\mathbf{e}}_{\mathrm{mo}}$ will depend on, e.g., the channel $\underline{\mathbf{h}}$, the number of antennas K_{a}, number of users K and of the deinterleaving and the FEC-decoding. Finally the second estimation of uncoded data $\hat{\underline{\mathbf{d}}}_{u_2}^{(k)}, k = 1...K$, will be obtained as the output of the deinterleaver and the FEC-decoding block. This second estimation will be the output of both receivers.

2.3.1 Direct interference cancellation

In this subsection the first receiver structure will be presented. The receiver structure, see Fig. 2.5, has a block termed interference cancellation. This block will be described more in detail in this subsection, since the other blocks have been described before. There are three inputs to the interence cancellation block:

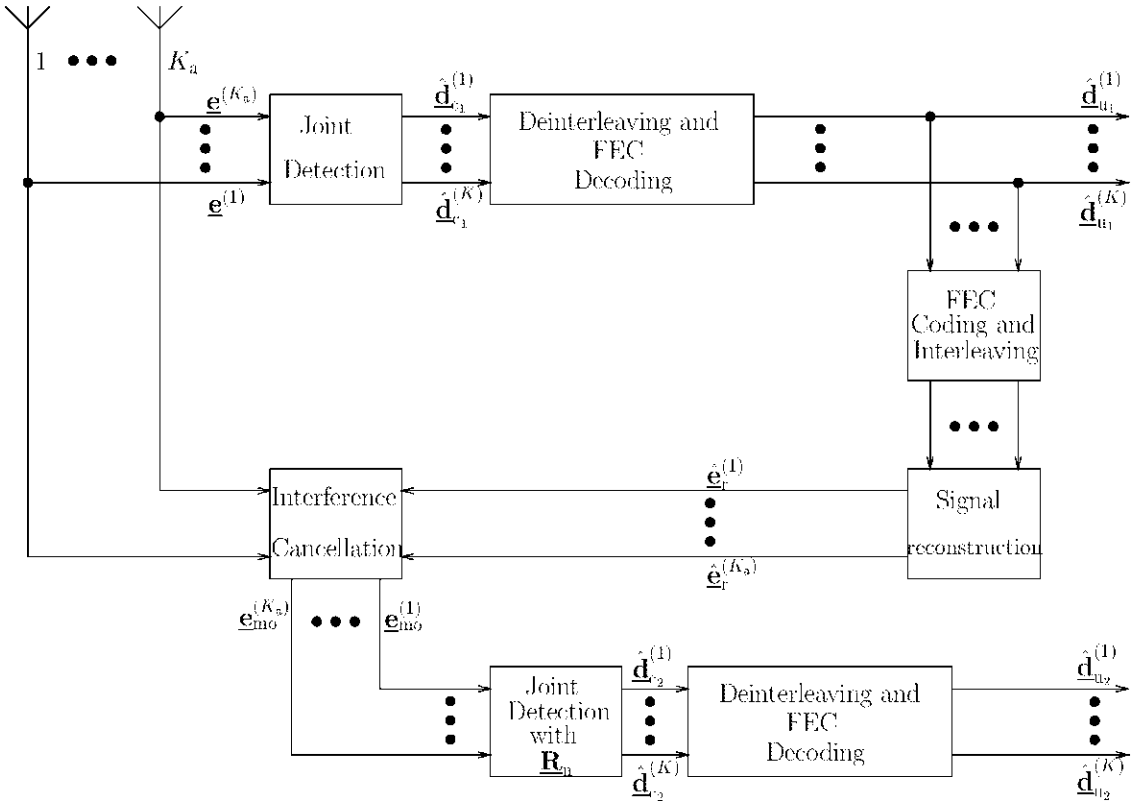

Figure 2.5. Receiver block diagram Interference cancellation.

- received signal $\underline{\mathbf{e}}$,
- noise-free signal $\underline{\hat{\mathbf{e}}}_r$
- interference power P_{INT}.

The first one, the received signal $\underline{\mathbf{e}}$, is obtained directly from the antenna array. From the estimated data $\underline{\hat{\mathbf{d}}}_{u1}^{(k)}, k = 1...K$ the noise-free signal $\underline{\hat{\mathbf{e}}}_r^{(k_a)}, k_a = 1...K_a$, is determined by signal reconstruction, i.e. by applying coding, interleaving and modulation, see Table 2.1, and represents one of the input signals of the interference cancellation block. Together with the received signal $\underline{\mathbf{e}}$ an estimation

$$\underline{\hat{\mathbf{n}}} = \underline{\mathbf{e}} - \underline{\hat{\mathbf{e}}}_r \tag{2.40}$$

of the noise vector $\underline{\mathbf{n}}$ is obtained by substracting $\underline{\hat{\mathbf{e}}}_r$ from $\underline{\mathbf{e}}$. Now with this noise estimation $\underline{\hat{\mathbf{n}}}$ from (2.40), the properties of noise are known, with the accuracy of $\underline{\hat{\mathbf{n}}}$

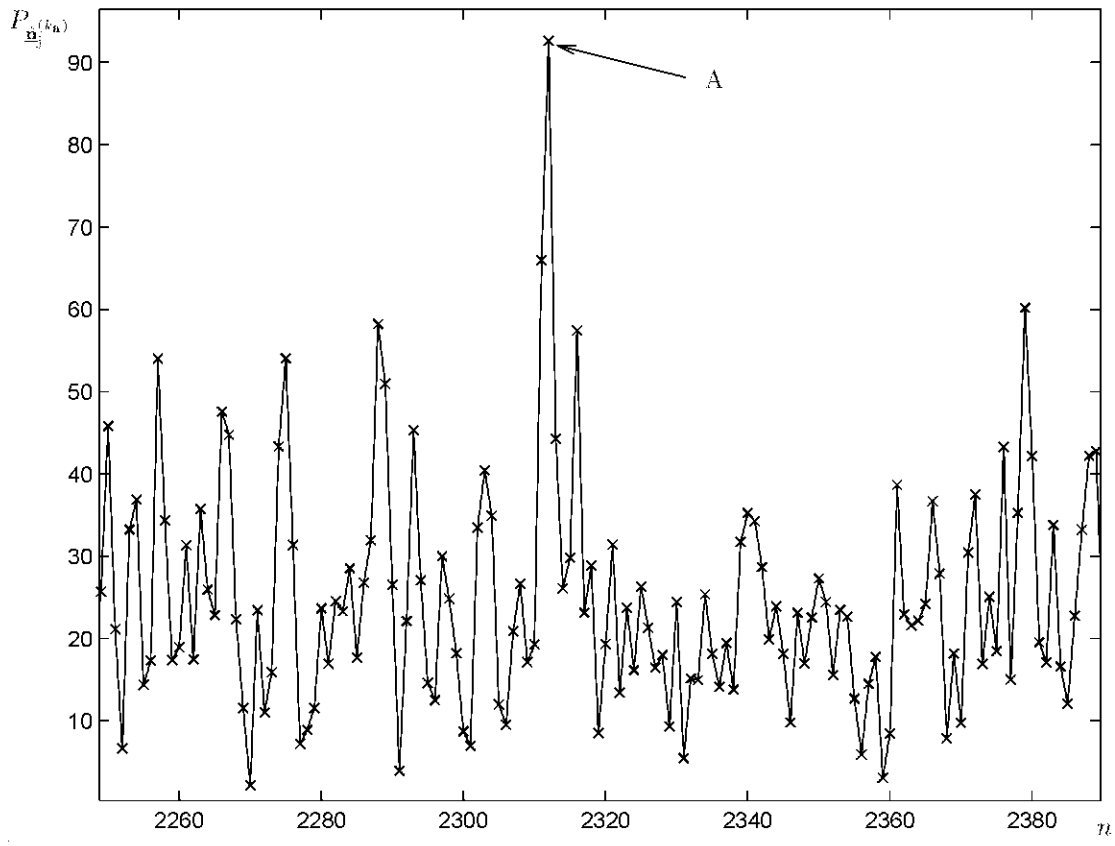

Figure 2.6. Power $P_{\underline{\hat{n}}_n}^{(k_a)}$ of (2.41) of noise samples $n_j^{(k_a)}$.

depending on the accuracy of the data estimation. Observing $\underline{\hat{n}}$ in Fig. 2.6, the big amplitudes of the noise, see point A in Fig. 2.6, in theory, leads to detection errors. If it would be possible to choose a bound to decide which noise amplitudes causes detection errors, then it would be possible to locate errors and subsequently to correct them in order to improve the system bit error performance. The last input of the interference cancellation block is the interference power P_{INT}. It can be obtained by two ways. The power control of the antenna allows that a mobile adapts the required power to transmit data. Therefore, the interference power can be calculated. This principle is used in GSM systems. The second possibility to get information about P_{INT} is to calculate an estimation of the mean interference power P_{INT} from the estimated interference vector $\underline{\hat{n}}$ of (2.40).

The modified received signals $\underline{\mathbf{e}}_{\mathrm{mo}}^{(k_a)}, k_a = 1...K_a$, are the block outputs. It is assumed

that this modified signals, $\underline{\mathbf{e}}_{\mathrm{mo}}^{(k_\mathrm{a})}, k_\mathrm{a} = 1...K_\mathrm{a}$, are affected by less interference. Fig. 2.7 shows the stream diagram of the interference cancellation block. From (2.40) one can calculate the instantaneous interference power,

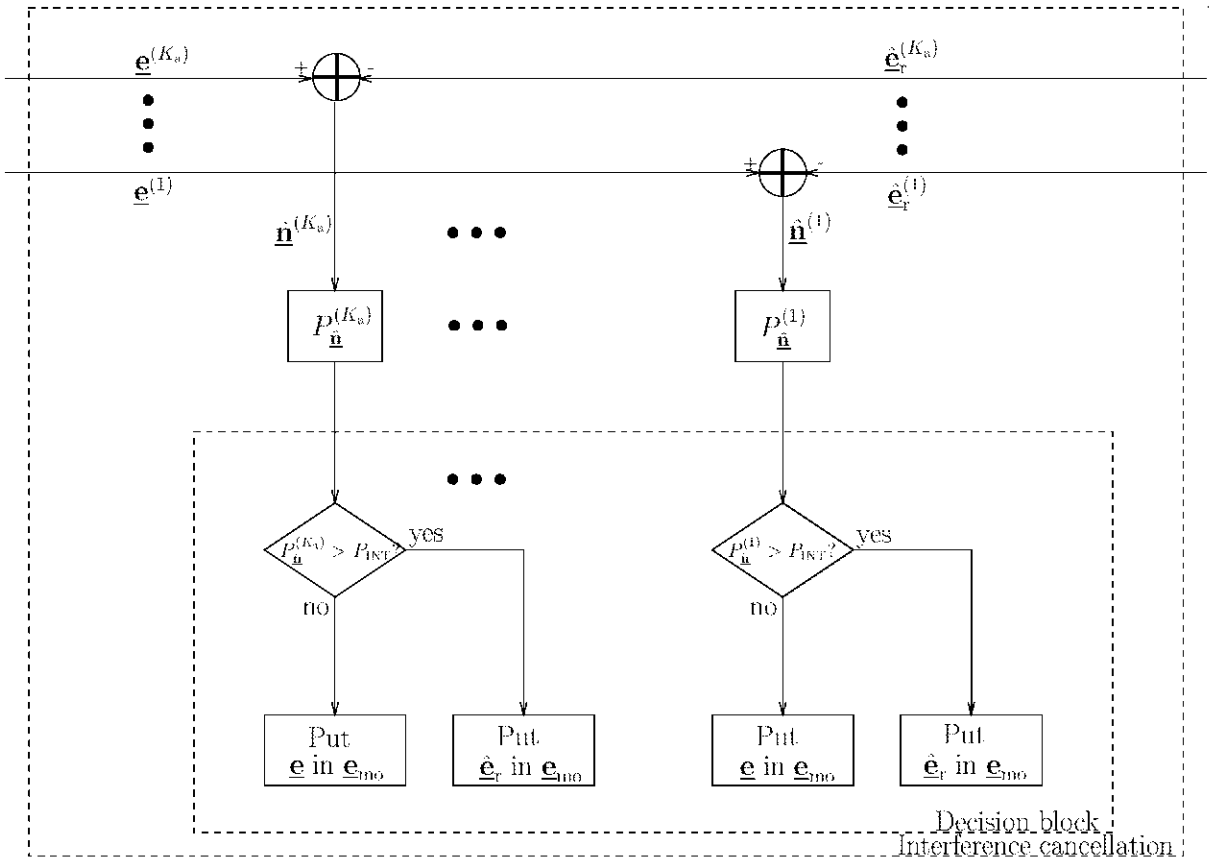

Figure 2.7. Block interference cancellation.

$$P_{\underline{\hat{\mathbf{n}}}_j^{(k_\mathrm{a})}} = \sqrt{(\underline{\hat{n}}_{r,j}^{(k_\mathrm{a})})^2 + (\underline{\hat{n}}_{i,j}^{(k_\mathrm{a})})^2}, j = 1...NQ + W - 1, k_\mathrm{a} = 1...K_\mathrm{a} \tag{2.41}$$

with the real parts $\underline{\hat{n}}_{r,n}^{(k_\mathrm{a})}$ of the noise samples and the imaginary parts $\underline{\hat{n}}_{i,n}^{(k_\mathrm{a})}$. The instantaneous power $P_{\underline{\hat{\mathbf{n}}}j}^{(k_\mathrm{a})}, j = 1...NQ + W - 1, k_\mathrm{a} = 1...K_\mathrm{a}$, is compared with a threshold, which is equal to P_{INT}. Then, the interference cancellation block will decide which samples of the signals $\underline{\mathbf{e}}$ and $\hat{\underline{\mathbf{e}}}_\mathrm{r}^{(k_\mathrm{a})}$ will be taken as samples of the modified signal $\underline{\mathbf{e}}_{\mathrm{mo}}$, see Fig. 2.7. With this block termed interference cancellation, the received signal $\underline{\mathbf{e}}$ leads to a modified signal $\underline{\mathbf{e}}_{\mathrm{mo}}$. The direct interference cancellation block can detect in the noise vector $\hat{\underline{\mathbf{n}}}$ the samples which are assumed to have a high amplitude of noise, by calculating the instantaneous interference power. After this, if one insert in the

modified signal $\underline{\mathbf{e}}_{\mathrm{mo}}$ the samples of the signal $\hat{\underline{\mathbf{e}}}_{\mathrm{r}}$, it will be assumed, that the errors will be corrected, by eliminating the high components of noise and inserting samples of the signal $\hat{\underline{\mathbf{e}}}_{\mathrm{r}}$, since $\hat{\underline{\mathbf{e}}}_{\mathrm{r}}$ has a bit error reduction through FEC-decoding.

2.3.2 Interference cancellation after matched filtering

In this subsection the second receiver structure will be presented. Besides one additional input, the inputs of the interference cancellation block are the same than in the previous section. This new input is the vector $\hat{\underline{\mathbf{d}}}_{FEC}^{(k)}, k = 1...K$, see Fig. 2.8, which represents the estimated data after interleaving and FEC-coding. The output $\underline{\mathbf{e}}_{\mathrm{mo}}$ of this block is the same than in the direct interference cancellation of Section 2.3.1.

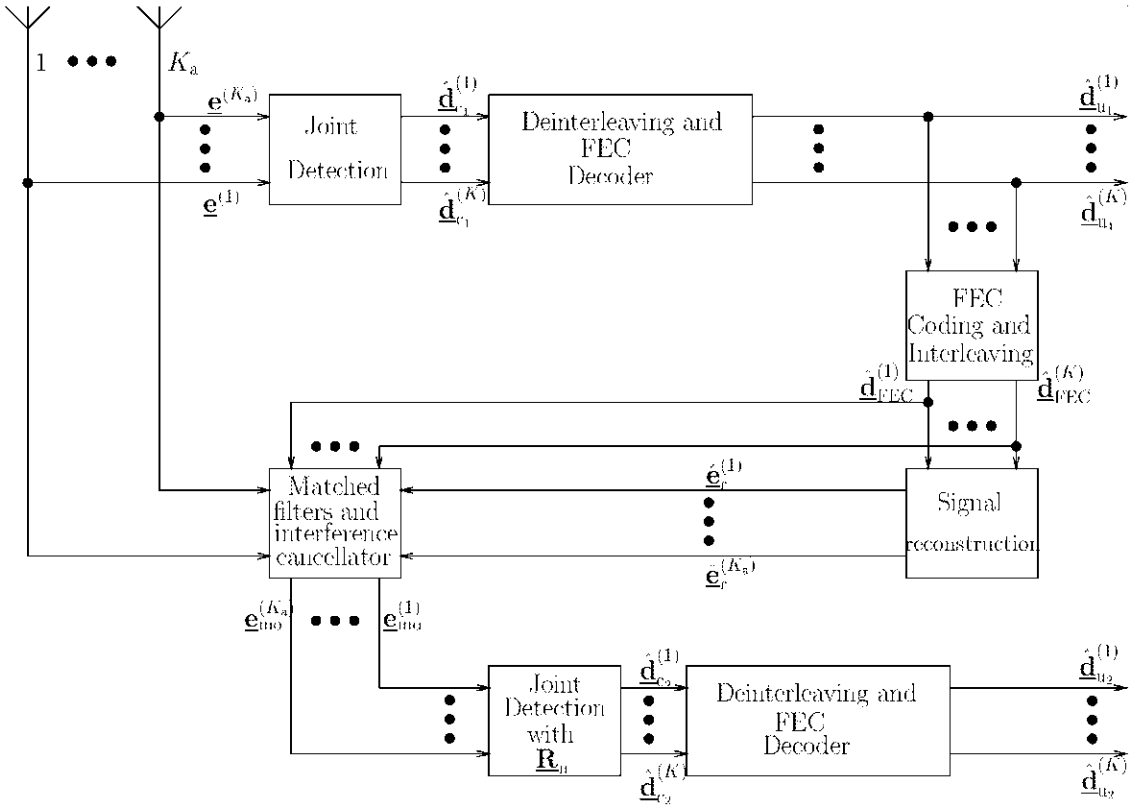

Figure 2.8. Receiver block diagram for interference cancellation after matched filtering.

In the following, the inputs and outputs of the interference cancellation block will be

presented. First the received signal $\underline{\mathbf{e}}$ is filtered by a matched filter, see Apendix A,

$$\underline{\mathbf{d}}_{\underline{\mathbf{A}}^{*\mathrm{T}}}^{(k)} = \underline{\mathbf{A}}^{*\mathrm{T}} \cdot \underline{\mathbf{e}}, k = 1...K. \tag{2.42}$$

The estimation $\hat{\underline{\mathbf{d}}}_{\underline{\mathbf{A}}^{*\mathrm{T}}}$ is the product between the conjugate transponse of the system Matrix $\underline{\mathbf{A}}$ and the received signal $\underline{\mathbf{e}}$. A more detailed notation is given by

$$\begin{pmatrix} \underline{d}_1^{(1)} \\ \underline{d}_2^{(1)} \\ \vdots \\ \underline{d}_N^{(1)} \\ \underline{d}_1^{(2)} \\ \vdots \\ \underline{d}_N^{(2)} \\ \vdots \\ \underline{d}_N^{(N)} \end{pmatrix} = \begin{pmatrix} \underline{r}_1^{(1,k_\mathrm{a})} & \cdots & \underline{r}_{Q+1}^{(1,k_\mathrm{a})} & \cdots & \underline{r}_{Q+W-1}^{(1,k_\mathrm{a})} & 0 & \cdots & 0 \\ 0 & \cdots & \underline{r}_1^{(1,k_\mathrm{a})} & \cdots & & \underline{r}_{Q+W-1}^{(1,k_\mathrm{a})} & \cdots & 0 \\ \vdots & & \vdots & & & & & \\ 0 & \cdots & 0 & & & \underline{r}_1^{(1,k_\mathrm{a})} & \cdots & \underline{r}_{Q+W-1}^{(1,k_\mathrm{a})} \\ \underline{r}_1^{(2,k_\mathrm{a})} & \cdots & \underline{r}_{Q+1}^{(2,k_\mathrm{a})} & \cdots & \underline{r}_{Q+W-1}^{(2,k_\mathrm{a})} & 0 & \cdots & 0 \\ 0 & \cdots & \underline{r}_1^{(2,k_\mathrm{a})} & \cdots & & \underline{r}_{Q+W-1}^{(1,k_\mathrm{a})} & \cdots & 0 \\ \vdots & & \vdots & & & \vdots & & \vdots \\ \underline{r}_1^{(N,k_\mathrm{a})} & \cdots & \underline{r}_{Q+W-1}^{(N,k_\mathrm{a})} & 0 & \cdots & & & 0 \\ \vdots & & \vdots & & & & & \vdots \\ 0 & & & & \underline{r}_1^{(N,k_\mathrm{a})} & \cdots & & \underline{r}_{Q+W-1}^{(N,k_\mathrm{a})} \end{pmatrix} \cdot \begin{pmatrix} \underline{e}_1^{(k_\mathrm{a})} \\ \underline{e}_2^{(k_\mathrm{a})} \\ \vdots \\ \\ \\ \\ \\ \\ \underline{e}_{NQ+W-1}^{(k_\mathrm{a})} \end{pmatrix}, \tag{2.43}$$

where $\hat{\underline{\mathbf{d}}}_{\underline{\mathbf{A}}^{*\mathrm{T}}}$ has dimension NK, $\underline{\mathbf{e}}$ has dimension $NQ+W-1$ and $\underline{\mathbf{A}}^{*\mathrm{T}}$ has the dimension $(NQ+W-1)\times(NQ)$. $\underline{r}_h^{(k,k_\mathrm{a})}, h = 1...Q+W-1, k = 1...K$, is the conjugated complex of effective channel impulse responses $\underline{b}_h^{(k,k_\mathrm{a})}, h = 1...Q+W-1, k = 1...K$.

The basic insight is the following:

Single high samples of the interference migth not be the reason for bit errors at the output of the detector, as it is assumed in the direct interference cancellation structure. The matched filter operation maximizes the SNR. If after matched filtering the received signal $\underline{\mathbf{e}}$, the interference is still so high that a bit error occurs, then also the reconstructed signals $\hat{\underline{\mathbf{e}}}_\mathrm{r}^{(k_\mathrm{a})}, k_\mathrm{a} = 1...K_\mathrm{a}$, are corrupted, unless the bit error is eliminated by FEC-decoding. If the received signal $\underline{\mathbf{e}}$ now is matched filtered and becomes $\hat{\underline{\mathbf{d}}}_{\underline{\mathbf{A}}^{*\mathrm{T}}}$ it might include more bit errors than the corresponding signal $\hat{\underline{\mathbf{d}}}_\mathrm{FEC}$, where some of the bit errors are eliminated by decoding.

If $\hat{\underline{\mathbf{d}}}_\mathrm{FEC}$ is not equal to $\hat{\underline{\mathbf{d}}}_{\underline{\mathbf{A}}^{*\mathrm{T}}}$ this undoubtly is expected to be a result of the bit error reduction through FEC-decoding. Therefore, in this cases the corresponding components of the received signal vector $\underline{\mathbf{e}}^{(K_\mathrm{a})}, k_\mathrm{a} = 1...K_\mathrm{a}$ are replaced by the corresponding components of $\hat{\underline{\mathbf{e}}}_\mathrm{r}^{(k_\mathrm{a})}, k_\mathrm{a} = 1...K_\mathrm{a}$. to form $\underline{\mathbf{e}}_\mathrm{IMO}$.

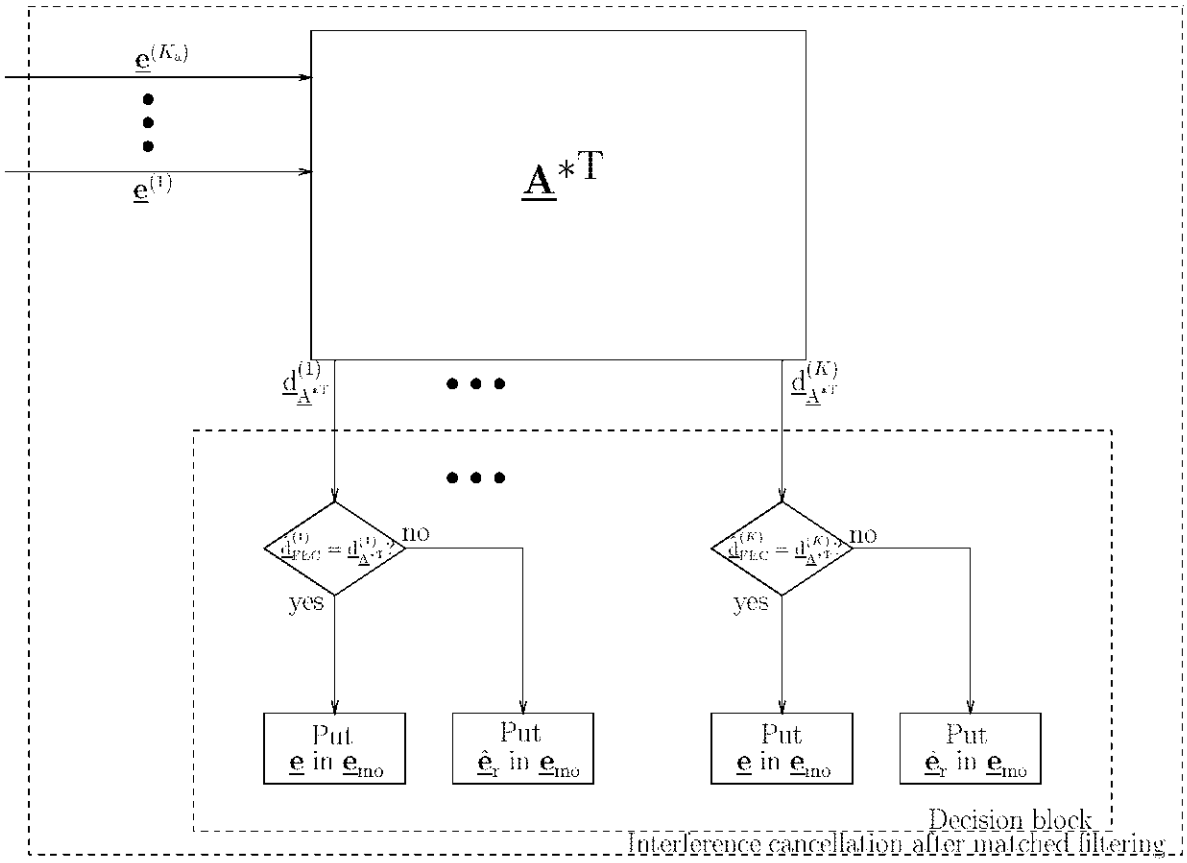

Figure 2.9. Block interference cancellation after matched filtering.

2.4 Limits in the reconstruction quality

As it has been seen in previous sections, the reconstruction of the signal play a important role in the two receivers. Clearly, the FEC-coder is necessary to generate the signal $\hat{\underline{e}}_r$. In this section the reconstruction limits due to the use of the FEC-decoder will be studied.

In the following, the quality of the signal reconstruction is investigated, whereas the channel impulse responses are assumed to be known in the receiver. If we define the received signal of the k-th user $\underline{e}^{(k)}$ without noise and the noise-free signal of the k-th user $\hat{\underline{e}}_r^{(k)}$

$$R_e^{(k)} = \frac{\mathrm{E}\{|\underline{e}^{(k)} - \hat{\underline{e}}_r^{(k)}|^2\}}{\mathrm{E}\{|\underline{e}^{(k)}|^2\}}, k = 1...K, \tag{2.44}$$

then R_e is the reconstruction error [Wec99]. In the numerator we will have the mean error energy of the k-th user and in the denominator the mean energy of the received signal.

The general structure of the reconstruction is showed in Fig. 2.10, where P_b is the BER in the first uncoded data estimation $\hat{\underline{\mathbf{d}}}_{u_1}$ and P_FEC is the BER after the FEC-coder.

The features of the FEC-coder have been refered before, see Section 2.3 and Fig. 2.4, the constraint lenght L_c is 5 and the code rate R_c is 1/2 [Wec99].

In the sequel the influence of only one wrong bit in the input of the coder will be studied, so it will be assumed that there is only one wrong bit in a bit stream. With the coder features, the links with the X-ors and the number of tappings, there will be seven wrong bits in the output of the coder. The shifting of the wrong bit in the register, see Fig. 2.4, will produce an error by each link with the X-or. While a wrong bit is shifted through the coder, ten bits will be generated. The first, second, fourth, sixth, seventh, ninth and tenth will be also wrong.

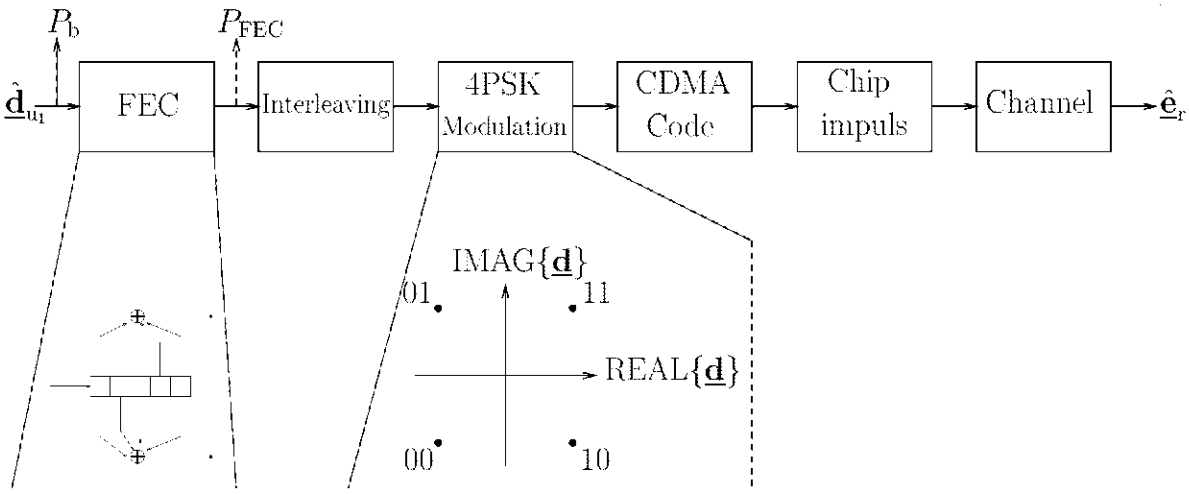

Figure 2.10. General structure of the signal reconstructor.

Therefore the BER P_FEC in the output of the coder with the first uncoded data estimation for single error is

$$P_\mathrm{FEC} = 7R_\mathrm{c}P_\mathrm{b}. \tag{2.45}$$

Thus the BER in the output of the coder P_FEC is a factor 3,5 bigger than in the input [Wec99]. This BER will be the same in the output of the signal reconstructor, since

neither interleaving, nor 4 PSK modulation , nor the spreading with the k-th CDMA code nor the convolution with the channel will not leads to any changes [Wec99]. Letting the previous conditions the error recontruction will be derived next.

With regard to the 5 registers of the coder, see Fig. 2.4 and Fig. 2.10, in two cases it will be produced two mistakes in the output and in the other only one mistake, due to the links between the X-ors.

With regard to the 4 PSK modulation which is used, if there are two mistakes, for example B in Fig. 2.11, there is an energy

$$En = (a+a)^2 + (b+b)^2 \tag{2.46}$$

which in this case is four. With only one bit error per symbol, for example the case A in Fig. 2.11, En is two.

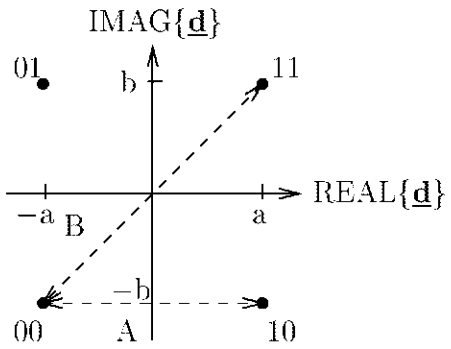

Figure 2.11. 4 PSK modulation.

If N is the number of the input bits of the coder, $2N$ is the number in the output bits and $P_{\mathrm{b}}^{(k)}$ is the BER in the first uncoded data estimation, then the recontruction error of the user k-th is

$$R_e^{(k)} = \frac{\frac{2}{5}\cdot 4\cdot L_{\mathrm{c}}\cdot P_{\mathrm{b}}\cdot N + \frac{3}{5}\cdot 2\cdot L_{\mathrm{c}}\cdot P_{\mathrm{b}}\cdot N}{2N\cdot R_{\mathrm{c}}} = 14P_{\mathrm{b}}^{(k)} \tag{2.47}$$

[Wec99].

In the sequel, the influence of errors which appears in burst in a bit stream in the signal reconstruction process will be studied. All the users will be active simultaneously but only the uncoded BER $P_{\mathrm{b}}^{(1)}$ of the first user, the error reconstruction $R_e^{(1)}$ and the BER after the coder $P_{\mathrm{FEC}}^{(1)}$ of the first user will be considered. A burst error of length

X is inserted in a error free detected bit stream to obtain Fig. 2.12. This Fig. 2.12 shows the BER $P_{\mathrm{b}}^{(1)}$, the BER after the coder $P_{\mathrm{FEC}}^{(1)}$, the reconstructed error $R_e^{(1)}$ and the relations $R_e^{(1)}/P_{\mathrm{b}}{}^{(1)}$ and $P_{\mathrm{FEC}}{}^{(1)}/P_{\mathrm{b}}{}^{(1)}$ for the first user signal. When X is one the

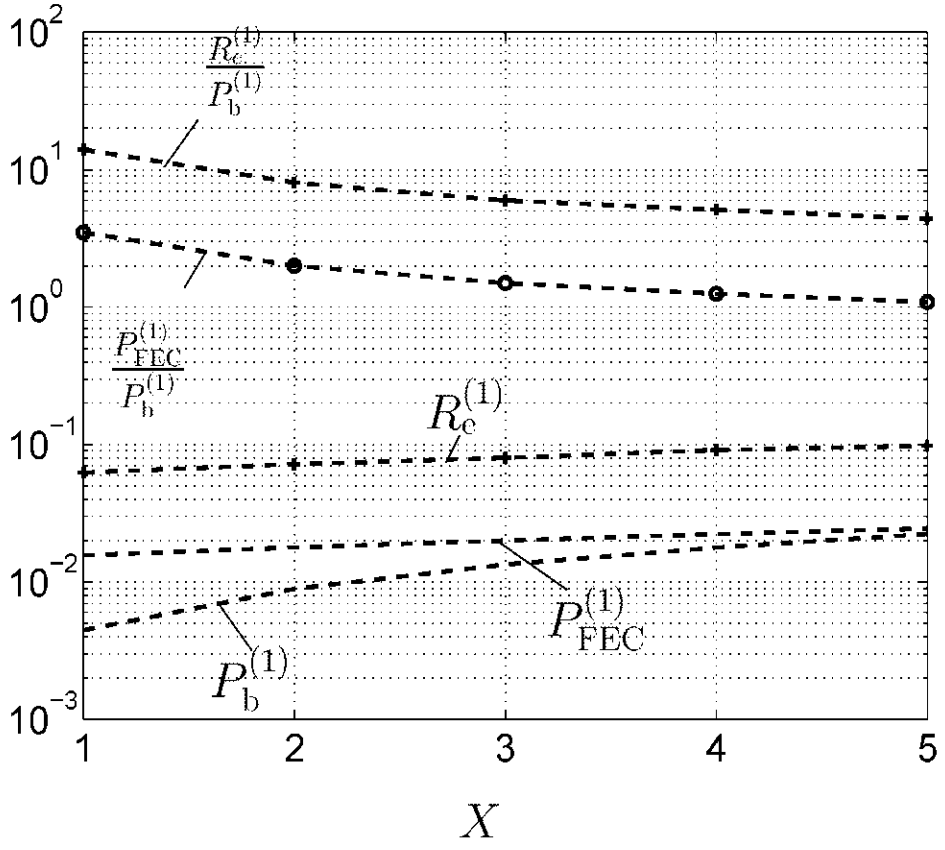

Figure 2.12. Uncoded BER $P_{\mathrm{b}}^{(1)}$, BER after the coder $P_{\mathrm{FEC}}^{(1)}$ and reconstruction error $R_e^{(1)}$ as a function of burst error of length X [Wec99].

relations $R_e^{(1)}/P_{\mathrm{b}}{}^{(1)}$ and $P_{\mathrm{FEC}}^{(1)}/P_{\mathrm{b}}{}^{(1)}$ in (2.45) and (2.47) are fulfilled, see Fig. 2.12. Furthermore, the BER after the coder $P_{\mathrm{FEC}}^{(1)}$ is 3,5 times bigger than the uncoded BER $P_{\mathrm{b}}^{(1)}$, see (2.45) and Fig. 2.12. With X equal to five errors, the BER after the coder $P_{\mathrm{FEC}}^{(1)}$ is equal to the uncoded BER $P_b^{(1)}$ and the reconstruction error $R_e^{(1)}$ is 4,2 times bigger than the uncoded $P_{\mathrm{b}}^{(1)}$. The relations $R_e^{(1)}/P_{\mathrm{b}}^{(1)}$ and $P_{\mathrm{FEC}}^{(1)}/P_{\mathrm{b}}^{(1)}$ are smaller with $X = 5$, due to the fact that the possibity that two errors being simultaneously in the register of the coder compensate each other by the X-or operation, is higher when having errors in bursts than having single errors.

In the following in a bit stream, every Y-th bit is wrong. For Y equal to one, the

complete bit stream is wrong, the uncoded BER $P_{\mathrm{b}}^{(1)}$ is one, the BER after the coder $P_{\mathrm{FEC}}^{(1)}$ will be equal to $P_{\mathrm{FEC}}^{(1)}/P_{\mathrm{b}}^{(1)}$ and the same is true for the other relations and the error reconstruction $R_e^{(1)}$, see Fig. 2.13. The curves $P_{\mathrm{FEC}}^{(1)}$ and $R_e^{(1)}$ show oscillations, due to the structure of the coder. In these cases two mistakes can be canceled in two links of one X-or. Y will not be greater than five because this is the case $X = 1$. For $Y = 5$ $R_e^{(1)}/P_{\mathrm{b}}^{(1)}$ is 14 and $P_{\mathrm{FEC}}^{(1)}/P_{\mathrm{b}}^{(1)}$ is 3,5 like the Fig. 2.12 for $X = 1$.

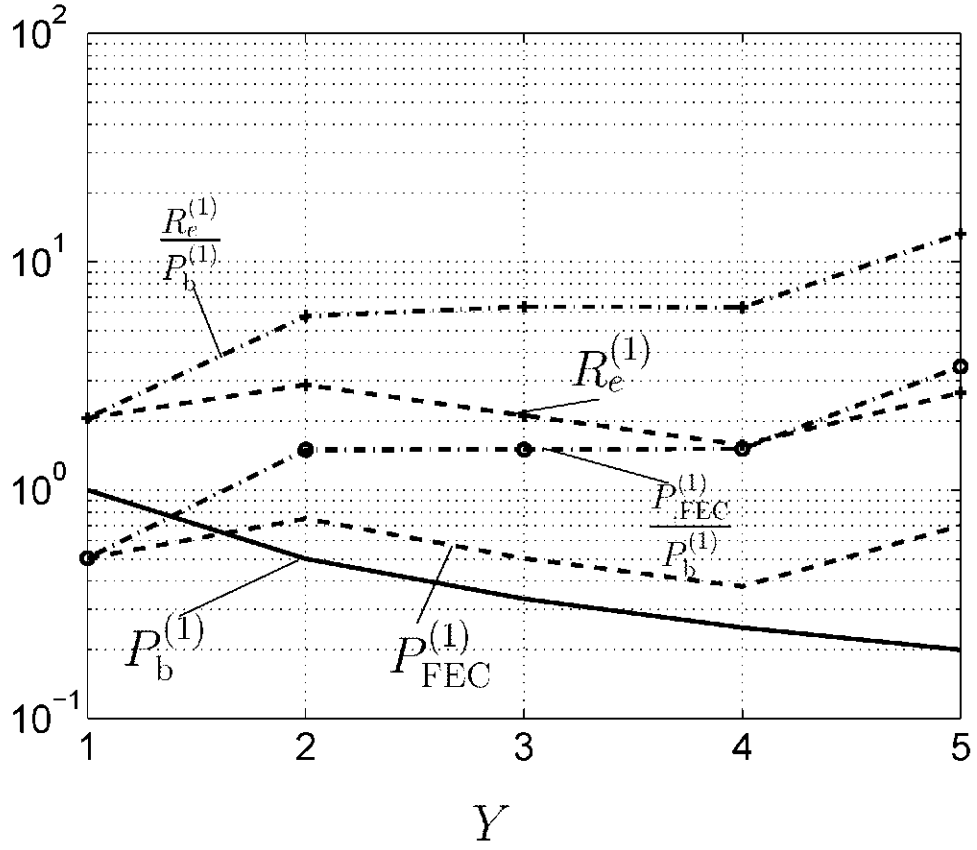

Figure 2.13. Uncoded BER $P_{\mathrm{b}}^{(1)}$, BER after the coder and reconstruction error $R_e^{(1)}$ as a function of Y [Wec99].

In the sequel, the study of the distance between errors, in several specific receiver points, see Fig. 2.14, will be realized.

With three simulations, see Table 2.4, to find out the FEC-encoder and the FEC decoder behaviour with errors will be analized. In the simulations only one the first user is taken into account, i.e., all the users will be active but only the first one will be considered. The points that will be checked:

Users	Antennas	C/I
8	4	-12
4	4	-12
8	1	-5

Table 2.2. Values in the simulations.

- Before the decoder in the first data estimation, point A, see Fig. 2.14.
- Before the encoder in the signal reconstruction process, point B, see Fig. 2.14.
- After the encoder in the signal reconstruction process, point C, see Fig. 2.14.

The distance between errors will be termed Δn, i.e., there are Δn correct bits between two errors. The error distribution as a function of the error distance $N_{\text{err}}(\Delta\text{n})$ will be the ratio that one find an error distance Δn. N_{total} is the total number of errors found in the bit stream of the first user.

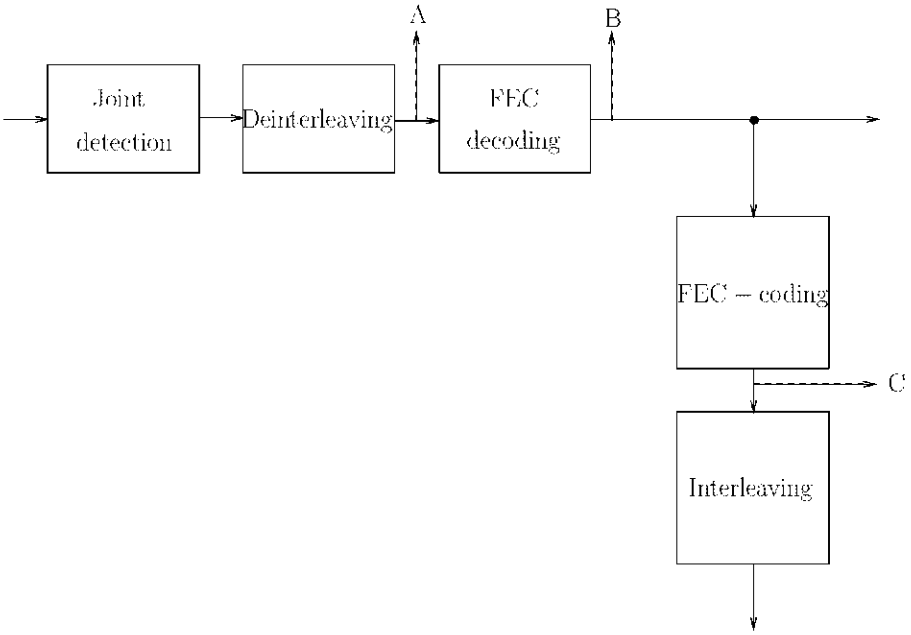

Figure 2.14. First data estimation and the FEC-coding and interleaving process.

The quotient between the error distribution $N_{\text{err}}(\Delta\text{n})$ and the total of errors N_{total}

$$\frac{N_{\text{err}}(\Delta\text{n})}{N_{\text{total}}} \tag{2.48}$$

will be termed the normalized error distribution. In the Figures, you can see the normalized error distribution $N_{\mathrm{err}}(\Delta \mathrm{n})/\mathrm{N}_{\mathrm{total}}$ before the decoder, point A, in the first data estimation, see Fig. 2.15, 2.21 and 2.27, for the three given situations. Most errors are close to each other, i.e., the high amplitudes are close to zero. The decoder, which we will observe in the following, can not correct all the errors. For the following point, before the encoder in the signal reconstruction, see Fig. 2.17, 2.23 and 2.29, it can be observed a decrease in the errors distribution $N_{\mathrm{err}}(\Delta \mathrm{n})$ but also a narrowing of errors, i.e., there are only burst errors. At the point C, see Fig. 2.14, after the encoder in the signal reconstruction, an increased number of errors according to Fig. 2.12 and Fig. 2.13 can be observed, since there are errors at the encoder input.

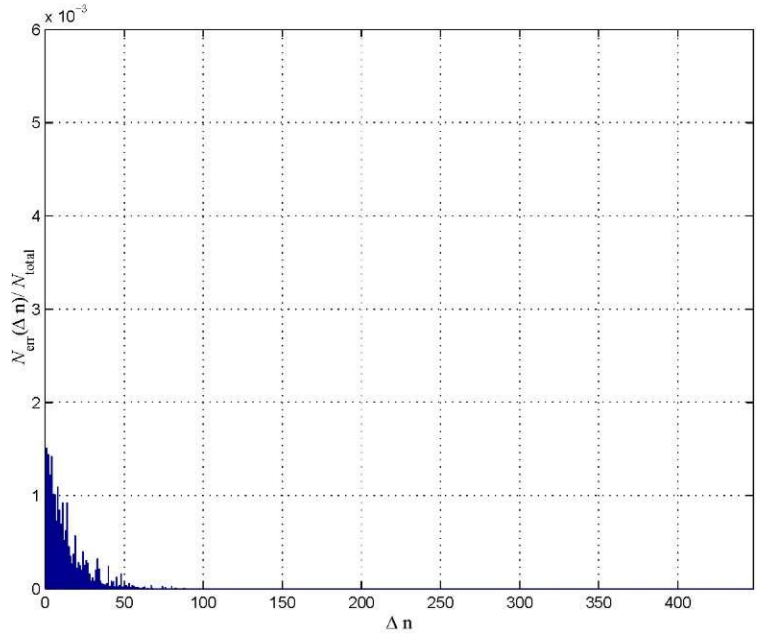

Figure 2.15. Normalized error distribution $N_{\mathrm{err}}(\Delta \mathrm{n})/\mathrm{N}_{\mathrm{total}}$ as a function of the distance Δn between errors for 8 users, 4 antenna, C/I=-12, before FEC-decoding.

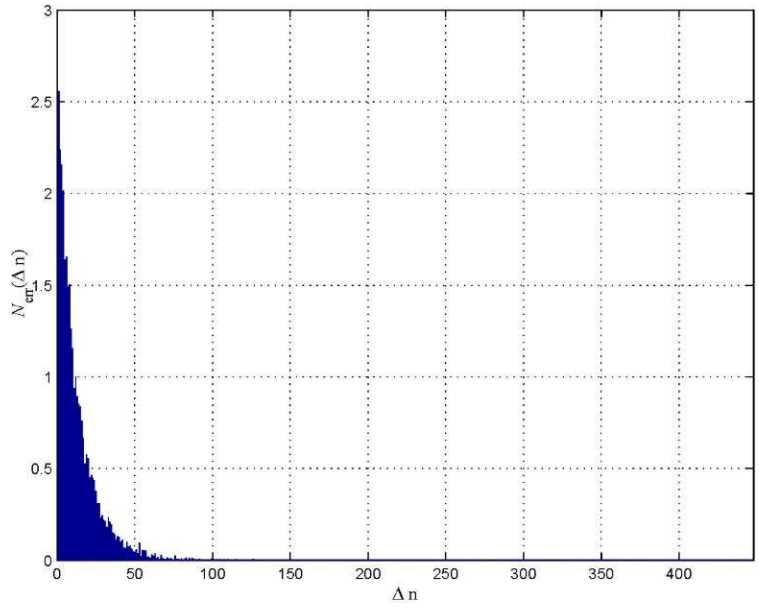

Figure 2.16. Error distribution $N_{\mathrm{err}}(\Delta \mathrm{n})$ as a function of the distance Δn between errors for 8 users, 4 antenna, C/I=-12, before FEC-decoding.

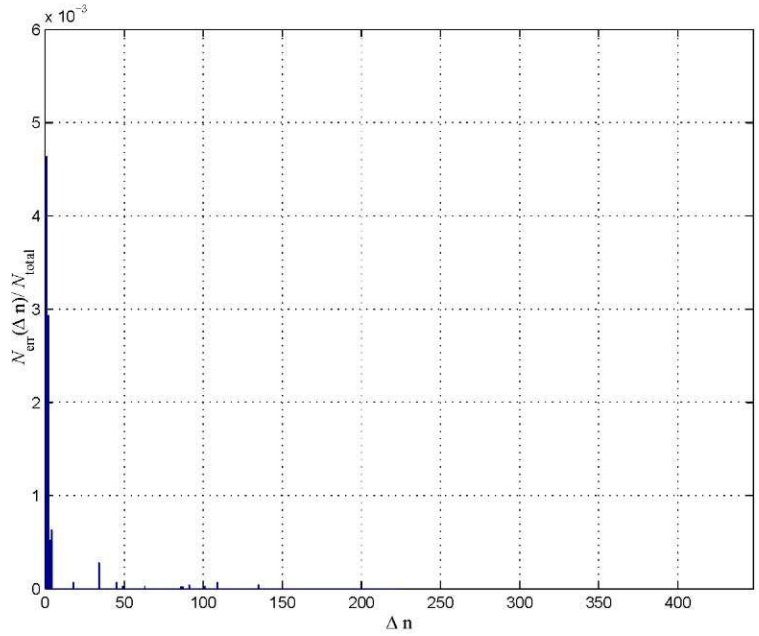

Figure 2.17. Normalized error distribution $N_{\mathrm{err}}(\Delta \mathrm{n})/\mathrm{N}_{\mathrm{total}}$ as a function of the distance Δn between errors for 8 users, 4 antenna C/I=-12, before FEC-coding.

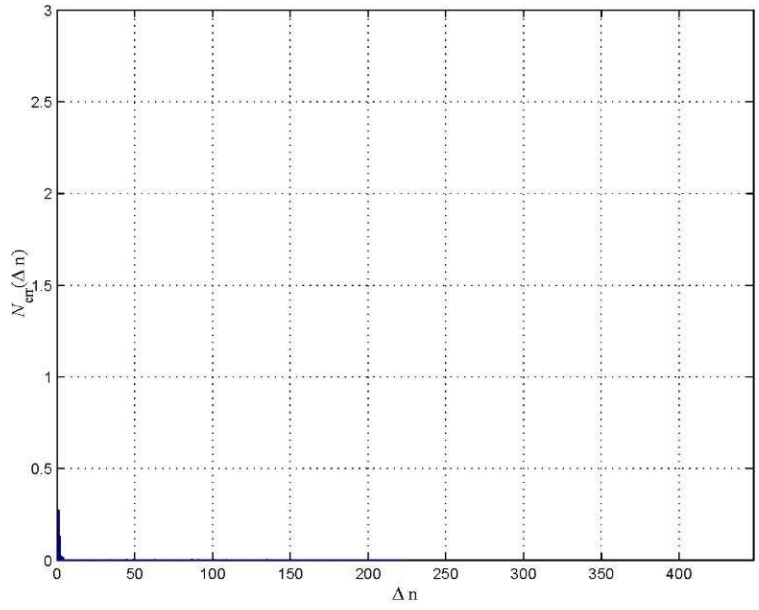

Figure 2.18. Error distribution $N_{\mathrm{err}}(\Delta \mathrm{n})$ as a function of the distance Δn between errors for 8 users, 4 antenna, C/I=-12, before FEC-coding.

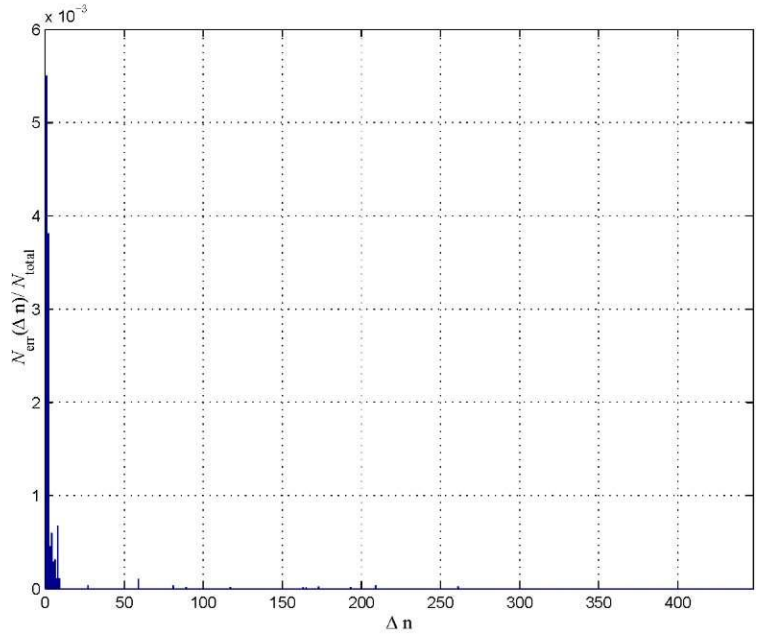

Figure 2.19. Normalized error distribution $N_{\mathrm{err}}(\Delta \mathrm{n})/\mathrm{N}_{\mathrm{total}}$ as a function of the distance Δn between errors for 8 users, 4 antenna C/I=-12, after FEC-coding.

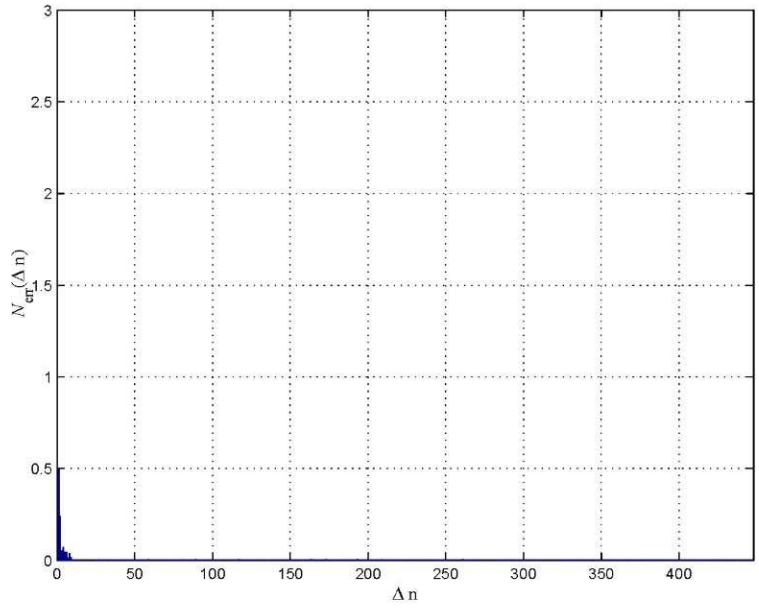

Figure 2.20. Error distribution $N_{\mathrm{err}}(\Delta \mathrm{n})$ as a function of the distance Δn between errors for 8 users, 4 antenna C/I=-12, after FEC-coding.

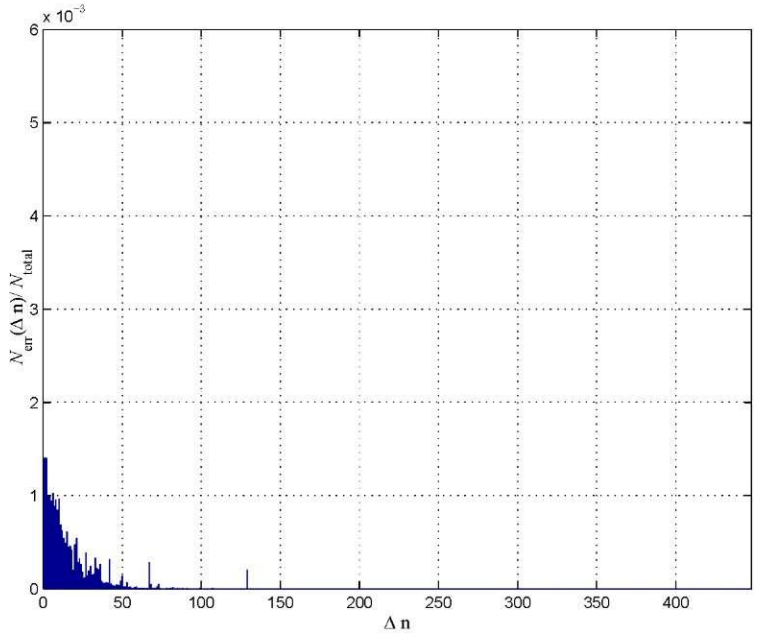

Figure 2.21. Normalized error distribution $N_{\mathrm{err}}(\Delta \mathrm{n})/\mathrm{N}_{\mathrm{total}}$ as a function of the distance Δn between errors for 4 users, 4 antenna C/I=-12, before FEC-decoding.

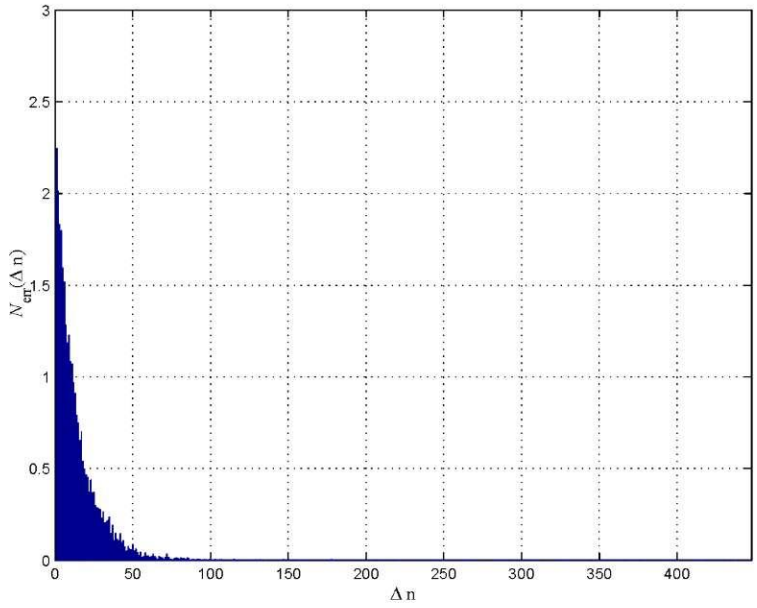

Figure 2.22. Error distribution $N_{\mathrm{err}}(\Delta \mathrm{n})$ as a function of the distance Δn between errors for 4 users, 4 antenna C/I=-12, before FEC-decoding.

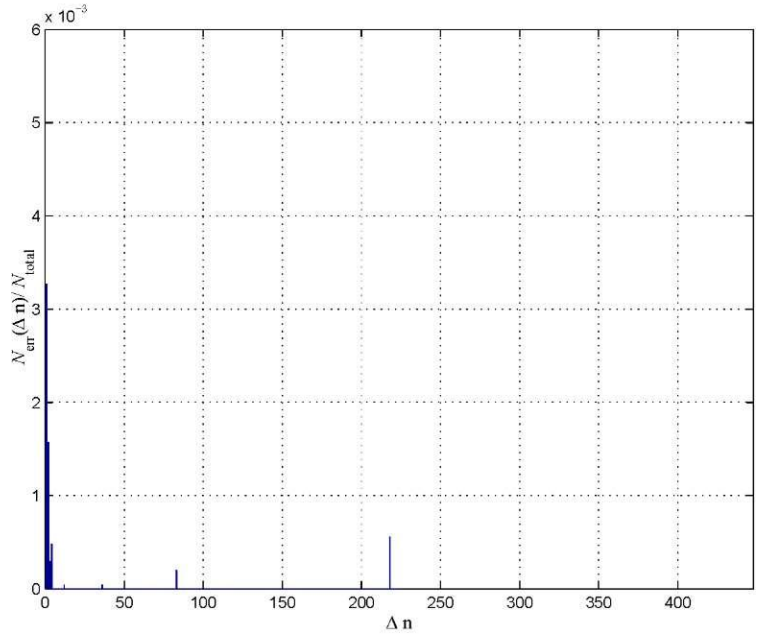

Figure 2.23. Normalized error distribution $N_{\mathrm{err}}(\Delta \mathrm{n})/\mathrm{N}_{\mathrm{total}}$ as a function of the distance Δn between errors for 4 users, 4 antenna C/I=-12, before FEC-coding.

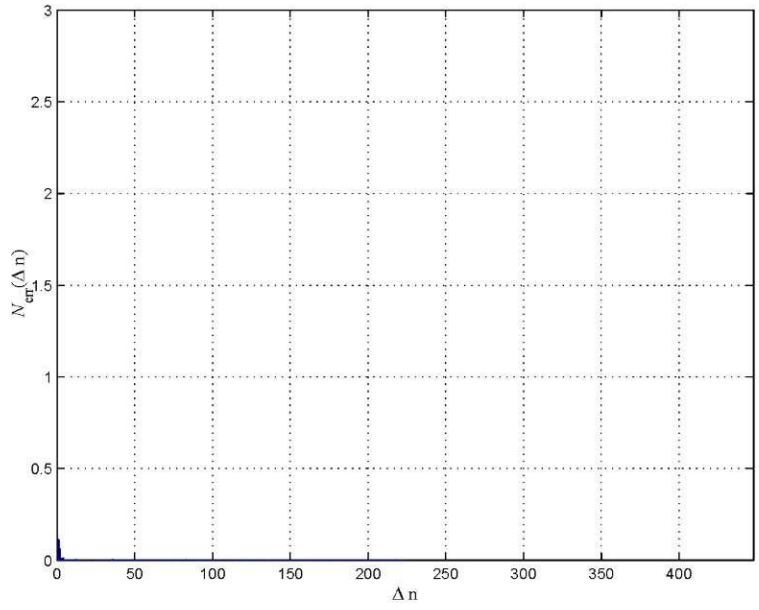

Figure 2.24. Error distribution $N_{\mathrm{err}}(\Delta \mathrm{n})$ as a function of the distance Δn between errors for 4 users, 4 antenna C/I=-12, before FEC-coding.

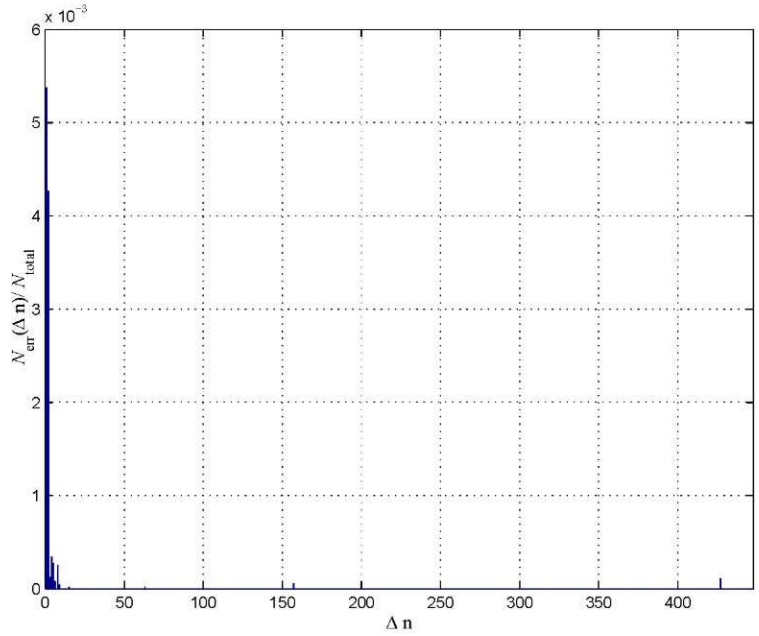

Figure 2.25. Normalized error distribution $N_{\mathrm{err}}(\Delta \mathrm{n})/\mathrm{N}_{\mathrm{total}}$ as a function of the distance Δn between errors for 4 users, 4 antenna C/I=-12, after FEC-coding.

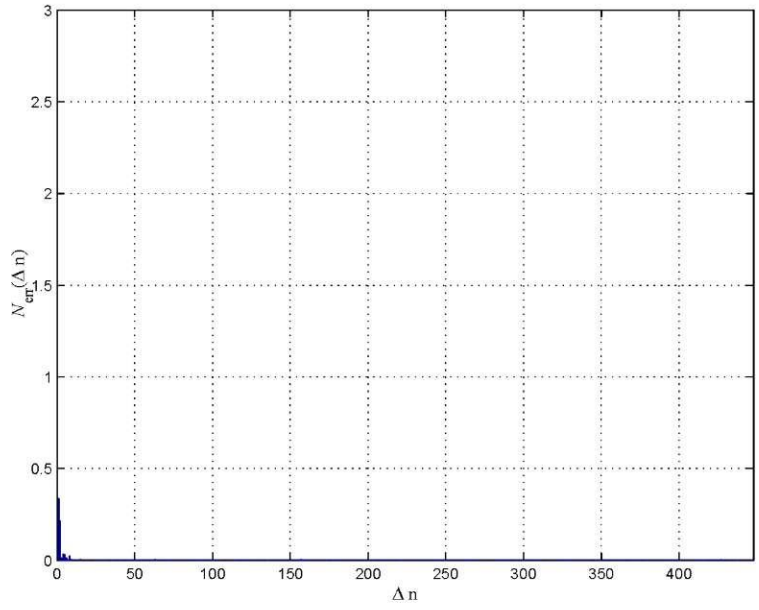

Figure 2.26. Error distribution $N_{\mathrm{err}}(\Delta \mathrm{n})$ as a function of the distance Δn between errors for 4 users, 4 antenna C/I=-12, after FEC-coding.

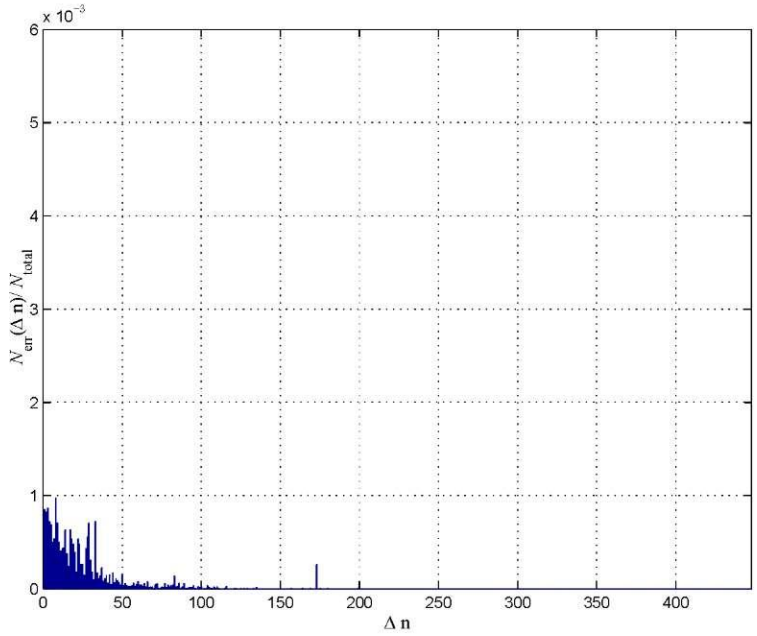

Figure 2.27. Normalized error distribution $N_{\mathrm{err}}(\Delta \mathrm{n})/\mathrm{N}_{\mathrm{total}}$ as a function of the distance Δn between errors for 8 users, 1 antenna C/I=-5, before FEC-decoding.

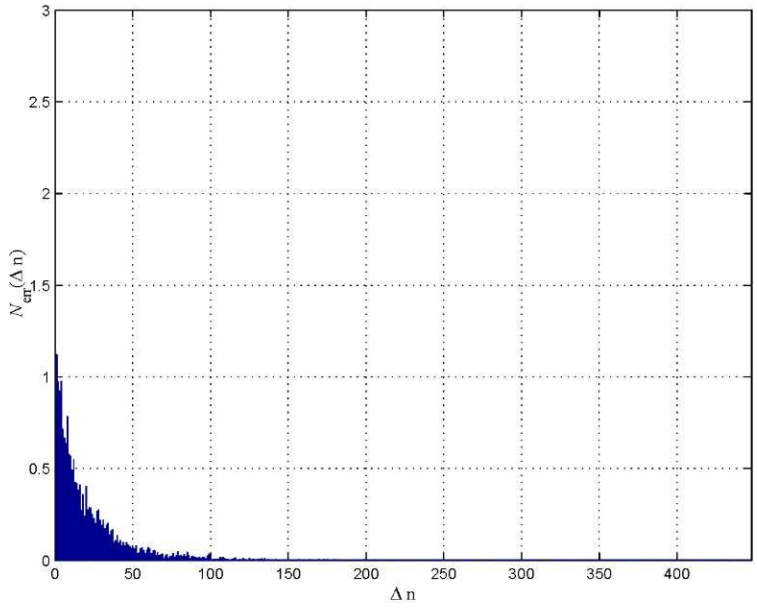

Figure 2.28. Error distribution $N_{\mathrm{err}}(\Delta \mathrm{n})$ as a function of the distance Δn between errors for 8 users, 1 antenna C/I=-5, before FEC-decoding.

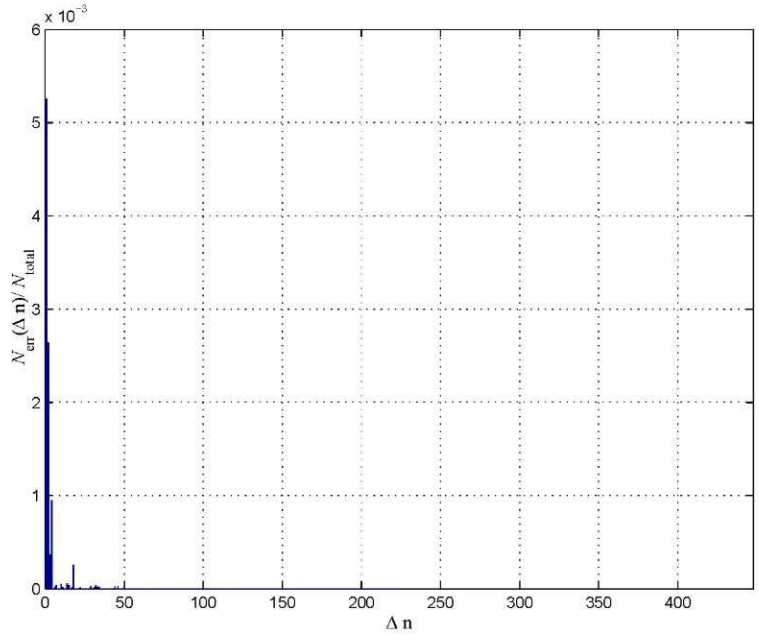

Figure 2.29. Normalized error distribution $N_{\mathrm{err}}(\Delta \mathrm{n})/\mathrm{N}_{\mathrm{total}}$ as a function of the distance Δn between errors for 8 users, 1 antenna C/I=-5, before FEC-coding.

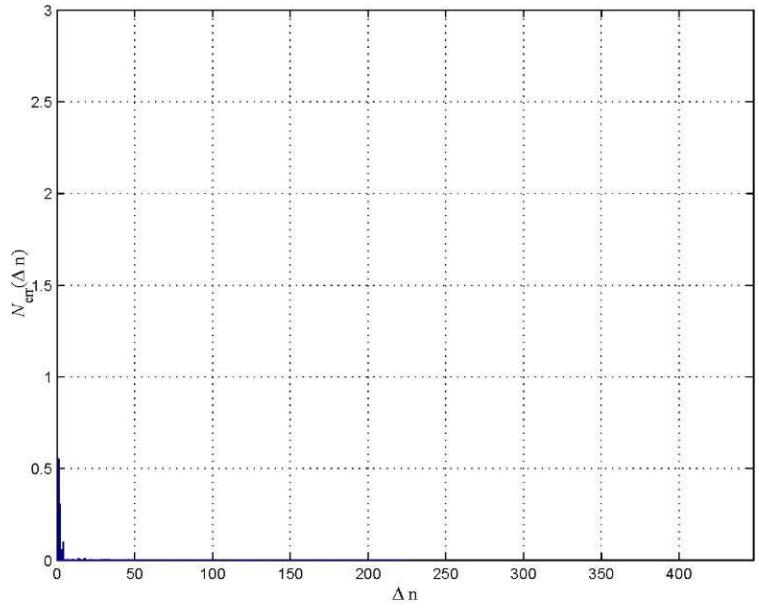

Figure 2.30. Error distribution $N_{\mathrm{err}}(\Delta \mathrm{n})$ as a function of the distance Δn between errors for 8 users, 1 antenna C/I=-5, before FEC-coding.

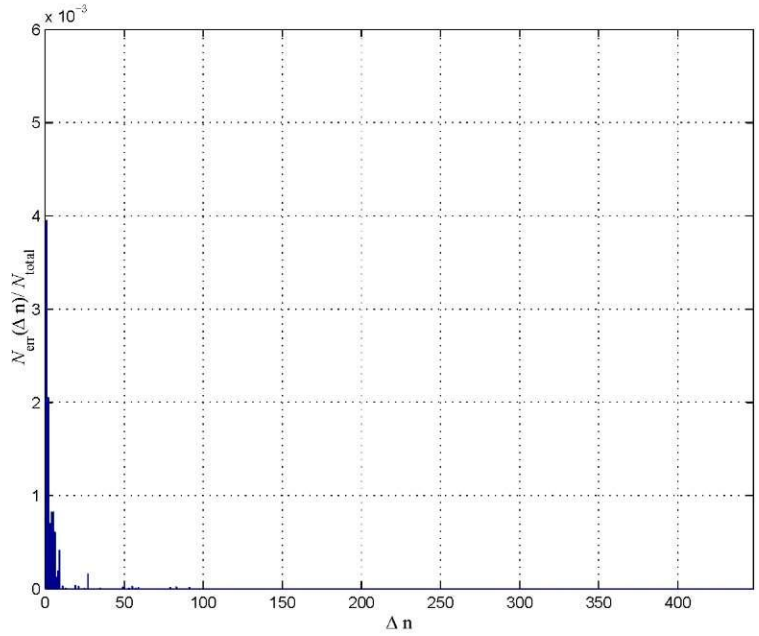

Figure 2.31. Normalized error distribution $N_{\mathrm{err}}(\Delta \mathrm{n})/\mathrm{N}_{\mathrm{total}}$ as a function of the distance Δn between errors for 8 users, 1 antenna C/I=-5, after FEC-coding.

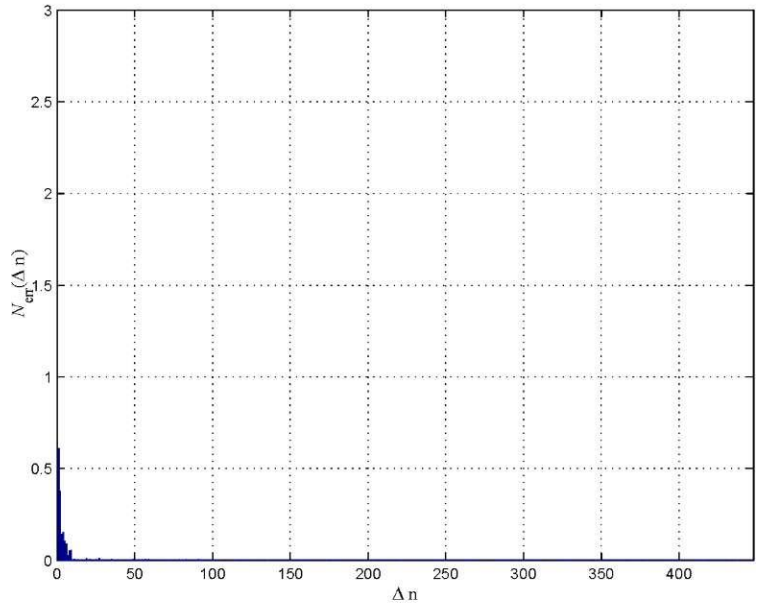

Figure 2.32. Error distribution $N_{\mathrm{err}}(\Delta \mathrm{n})$ as a function of the distance Δn between errors for 8 users, 1 antenna C/I=-12, after FEC-coding.

3 Channel model

The channel impulse response $\underline{h}(\tau, t)$ is calculated by adding E exponential oscillations of phases $\vartheta_i, i = 1...E$, Doppler frequencies $f_{\mathrm{d},i}, i = 1...E$ and delays $\tau_i, i = 1...E$. The phases $\vartheta_i, i = 1...E$ are randomly taken from the set $[0, 2\pi[$. The E Doppler frequencies $f_{\mathrm{d},i}, i = 1...E$ depend on the user speed v and the user direction of movement φ_{v}. Fig 3.3 shows the situation when there is no Line of Sight (LOS) between the mobile and the RP. We will suppose that the mobile is only moving along a circle around the RP.

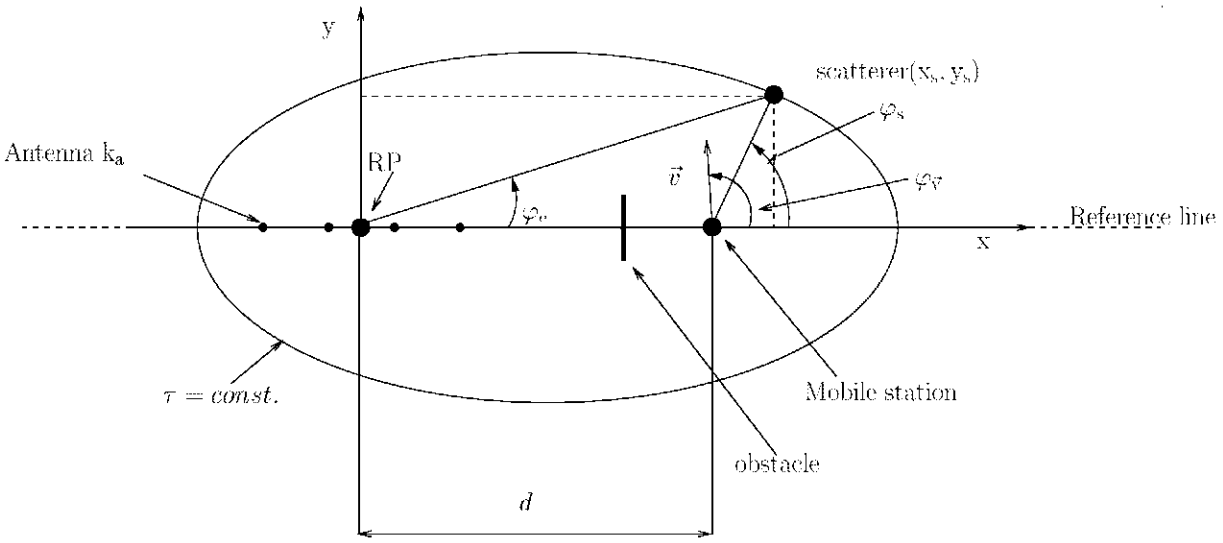

Figure 3.1. Definition of the position of a scatterer.

Due to the fact that there is no LOS between transmitter and receiver, a scatterer (x_{s},y_{s}) exists. We will take into account only the reflexions, scattering and diffractions. For each tuple $(\tau, \varphi_{\mathrm{e}})$ the coordinates (x_{s},y_{s}) of the scatterer can be unequivocally determined:

$$x_{\mathrm{s}}(\tau, \varphi_{\mathrm{e}}) = \frac{(c_0^2\tau^2 - d^2)\cos(\varphi_{\mathrm{e}})}{2(c_0\tau - d\cos(\varphi_{\mathrm{e}}))}\,, \tag{3.1}$$

$$y_{\mathrm{s}}(\tau, \varphi_{\mathrm{e}}) = \frac{(c_0^2\tau^2 - d^2)\sin(\varphi_{\mathrm{e}})}{2(c_0\tau - d\cos(\varphi_{\mathrm{e}}))}\,, \tag{3.2}$$

$$r_1 = \frac{(c_0^2\tau^2 - 2dc_0\tau\cos(\varphi_{\mathrm{e}}) + d^2)}{2(c_0\tau - d\cos(\varphi_{\mathrm{e}}))}\,, \tag{3.3}$$

$$\varphi_{\mathrm{s}} = \arccos(\frac{x_{\mathrm{s}} - d}{r_1}) \cdot \mathrm{sign}(y_{\mathrm{s}}), \text{with } d = 10 \text{ m}. \tag{3.4}$$

The Doppler frequency shift is given by:

$$f_{\mathrm{d},i} = \frac{v \cdot f_0}{c_0} = \frac{v}{\lambda} \cdot \cos(\varphi_{\mathrm{s}} - \varphi_{\mathrm{v}}). \tag{3.5}$$

The used channel model is characterized by:

- The number of taps (6 in our case),
- the relative delays of those taps with regard to the first one,
- the average power of the taps with regards to the maximum power taps,
- the Doppler spectrum $S_c(0, f_{\mathrm{d}})$.

The Doppler spectrum indicates the average power of the received signal with the Doppler frequency f_{d}.
The channel impulse response $\underline{h}(\tau, t)$ of our model will be expressed as:

$$\underline{h}_{\mathrm{tap}}(\tau, t) = \lim_{E \to \infty} \frac{1}{\sqrt{E}} \sum_{w=1}^{W} \sum_{i=1}^{\mathrm{Prob}(\tau_w)E} \exp(\mathrm{j}\vartheta_{i,w}) \exp(\mathrm{j}2\pi f_{\mathrm{d},i,w} t) \delta(\tau - \tau_w). \tag{3.6}$$

Where

- $\underline{h}_{\mathrm{tap}}(\tau, t)$ is the channel impulse response with discrete delays $\tau_w, w = 1...W$,
- W is the number of taps (in our channel, between 4 and 6),
- E is the number of exponential oscillations ($E \to \infty$ for the perfect model),
- $f_{\mathrm{d,i,w}}$ is the i-th Doppler frequency for the w-th tap,
- $\vartheta_{i,w}$ is the i-th phase for the w-th tap,
- τ_w is the delay for the w-th tap, it depens on the select model,
- $\mathrm{Prob}(\tau_w)$ is the probability of taps with delay τ_w. It is proportional to the number of Doppler frequencies and to the number of phases for the w-th tap,

- Prob(τ_w)E is the number of Doppler frequencies and the number of phases for the w-th tap.

To consider the directional anisotropy in the wave propagation in a radio mobile channel, we must assign a direction of propagation to the channel impulse response. Next, this direction of propagation will be modeled for a user k. For the others it is calculated in a similar way.

1. The user movement is expressed with the variable v_{T}, which can take values from 1-3 km/h for indoor environment. The Doppler frequency shifts are calculated from 3.5 depending on the user velocity v_{T}, the direction of movement φ_{v} and the DOA φ_{s} of the desired signal.

2. For other parameters we will use the ITU specifications. In our case, the models Indoor Office A (ITU IO A) and Indoor Office B (ITU IO B).

	Channel A Delay Spread = 35 ns P(A)= 50%		Channel B Delay Spread = 100 ns P(A)= 45%	
Tap	Rel. Delay / ns	Avg. Power / dB	Rel. Delay / ns	Avg. Power / dB
1	0	0	0	0
2	50	-3	100	-3.6
3	110	-10	200	-7.2
4	170	-18	300	-10.8
5	290	-26	500	-18
6	310	-32	700	-25.2

Table 3.1. ITU-Indoor-Office Parameter.

3. We will use E=300 in our simulations. Table 3.2 shows the distribution of the number of waves per tap for a 6 taps model.

4. If we would have a LOS between the BS and the mobile, it will be indicated in a simulation mode.

5. K_{d} is the number of directions of propagation of the desired signals $\beta^{(k,k_{\mathrm{d}})}, k = 1...K, k_{\mathrm{d}} = 1...K_{\mathrm{d}}$, see Fig. 2.3.

Tap	Number of received signals
1	174
2	76
3	34
4	14
5	2
6	0

Table 3.2. ITU-IO-B

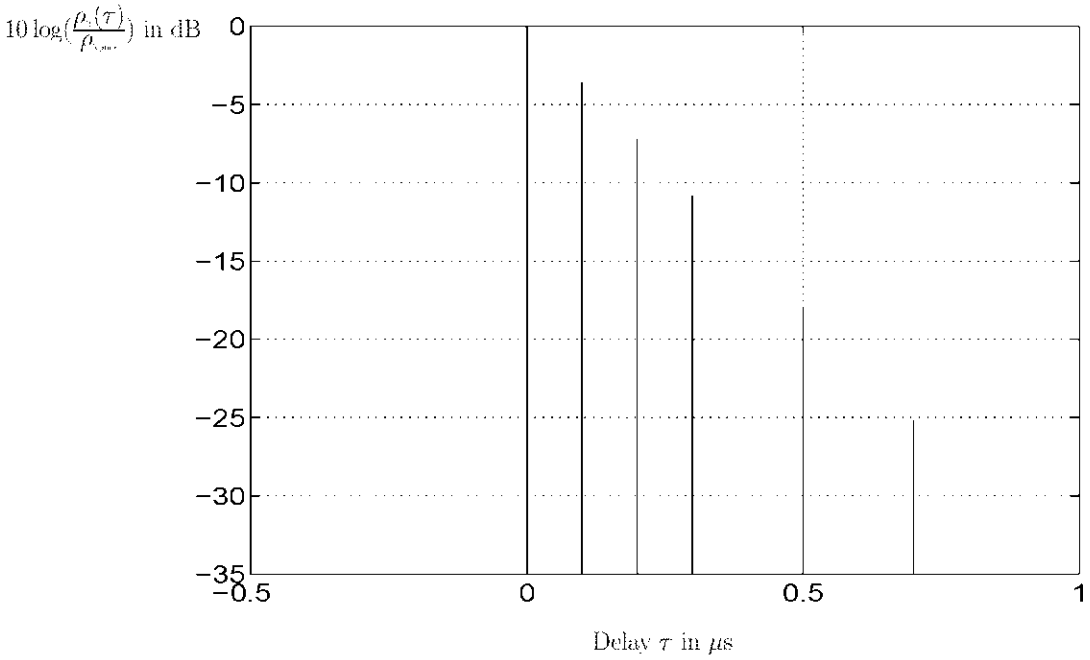

Figure 3.2. Delay-power spectrum for ITU model Indoor-office-B.

6. With a parameter called Richtung IL it is specfied for which data blocks we must apply the K_d DOAs.

Finally, the channel impulse response defined in 3.7, taking into account the DOAs, will be represented as

$$\begin{aligned} \underline{h}_{\mathrm{tap}}(\tau,t,\varphi) &= \lim_{E\to\infty}\frac{1}{\sqrt{E}}\sum_{w=1}^{W}\sum_{i=1}^{\mathrm{Prob}(\tau_w)E}\exp(\mathrm{j}\vartheta_{i,w})\exp(\mathrm{j}2\pi f_{\mathrm{d},i,w}t)\delta(\tau-\tau_w)\delta(\varphi-\varphi_{\mathrm{e},i,w}) \\ w &= 1...W, \\ i &= 1...Prob(\tau_w)E. \end{aligned} \tag{3.7}$$

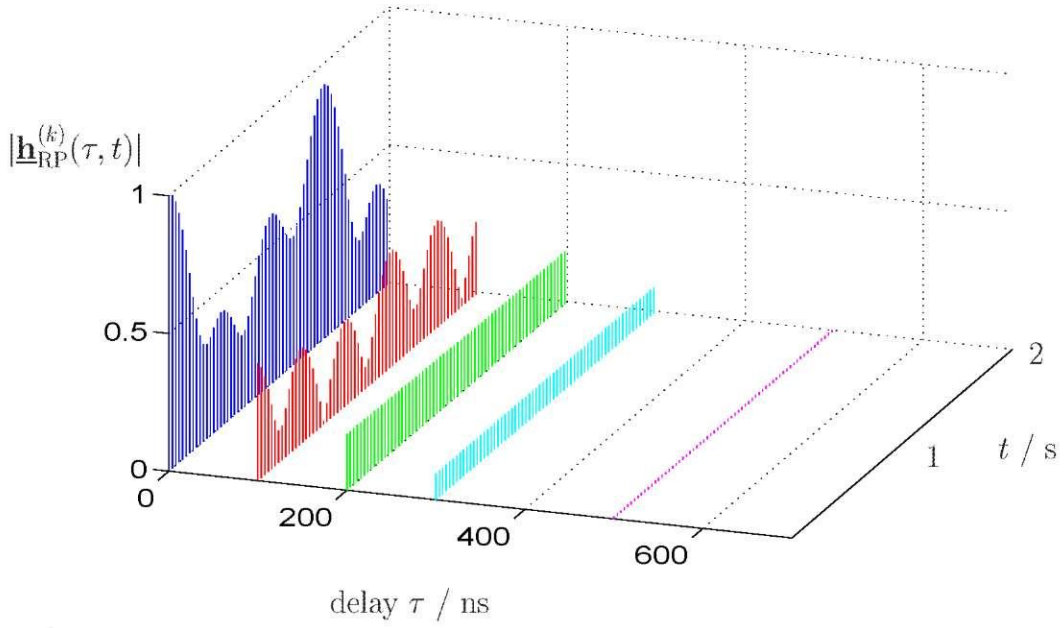

Figure 3.3. Channel impulse response.

where i is the $i-$th exponential for the $w-$th tap

e $= 1...K_{\mathrm{d}}$ [Poh99].

4 Results

4.1 General

In this section, the results obtained in the simulation of the two receivers are presented. These simulations are made in the uplink of a TD-CDMA mobile radio system. It will be assumed that the ITU indoor/office B channels are known at the receiver, see Section 3. The main parameters of the TD-CDMA mobile radio system used for the simulations are given in Table 2.1. With regard to intercell MAI, see Fig. 4.1, it is assumed to be created by very large number of pairwise uncorrelated interfering signals with a uniform distribution of their DOAs over the total range $[0,2\pi]$ in azimuth and are also.

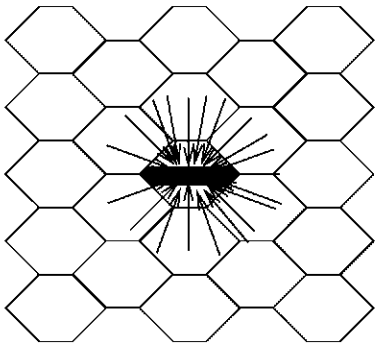

Figure 4.1. Uniformly distributed interfering signals over all directions.

In the receiver with direct interference cancellation two kinds of antenna configurations are used. The antenna configurations are URA 2 2 and ULA 1. The first one has K_a

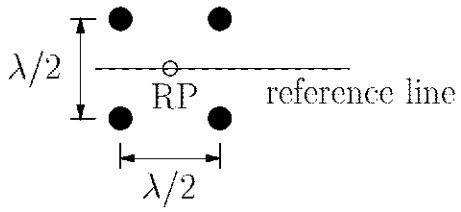

Figure 4.2. Square array structure with K_a=4, URA 2 2.

equal to 4 antennas, see Fig. 4.2, with a sepatarion of half of the carrier wavelength

λ. The second one is a single antenna. In the second receiver with interference cancellation after matched filtering three kinds of antenna are used. Besides one additional antenna structure, the antenna structures are the same than in the receiver with direct interference cancellation. This new antenna structure is RING 8, with K_a equal to 8 antenna elements in a circle, see Fig. 4.3, with a separation of half of the carrier wavelength λ. The users are assumed to have a velocity of 3 km/h and they are assumed to be randomly distributed on a circle around the BS.

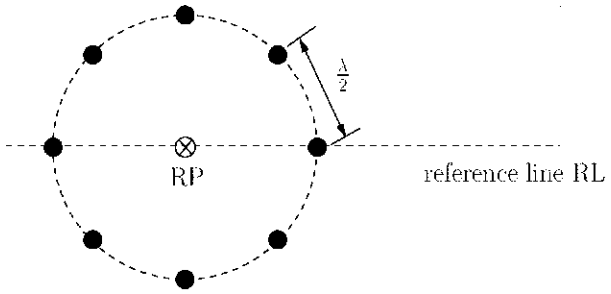

Figure 4.3. Circle array structure with K_a=8, RING 8.

The relation of the average power of a desired information carrying signal to the average total interference power σ^2 with respect to a single receiver antenna is called average carrier-to-interference ratio C/I. The average coded and uncoded BER P_b as a function of the average C/I is determined by Monte Carlo simulations of data transmission in a single cell.

The simulation program measures the BER in the first and the second data estimation. In each one of them, two kinds of BER will be measured.

The first, which is the uncoded BER, is the BER between the antennas, the transmitter and the receiver, where as the coded BER is the BER measured before FEC-coding in the transmitter and after FEC-decoding in the receiver, see Fig. 4.4. In this document $P_{b,c1}$ and $P_{b,c2}$ will be the coded BER of the first and second data estimation and $P_{b,u1}$ and $P_{b,u2}$ will be the uncoded BER of the first and the second data estimation.

Three situations with respect to the number of antennas and the number of users have been simulated with the receiver with direct interference cancellation. The simulation results for 8 users 1 antenna, 8 users 4 antenna and 4 users 4 antenna will be presented in the following section. For the receiver with interference cancellation after matched

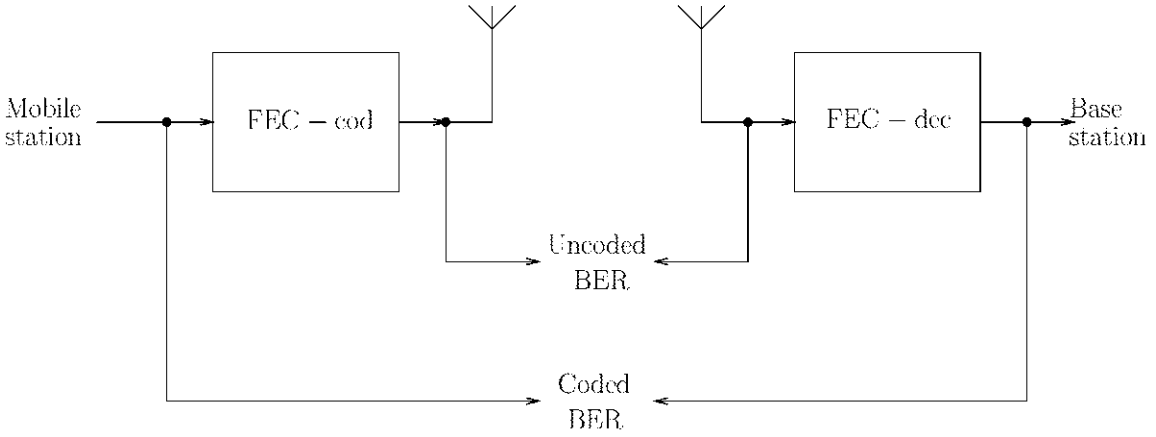

Figure 4.4. Coded and uncoded BER

filtering, the situations 4 users 8 antennas, 8 users 4 antennas, 4 users 4 antennas and 8 users one antenna have been simulated.

4.2 Simulation results by considering the interference cancellation receiver

In this section, the results obtained with the receiver with interference cancellation, see Subsection 2.3.1, are presented. First, some variables will be described which are used in the figures, related with the receiver. Second all the features used in the simulations will be explained and finally the results of the simulations will be presented.
Furthermore, a variable to measure the insertion rate of the signal $\underline{\hat{\mathbf{e}}}_{\mathrm{r}}$ is introduced. This variable is termed percentage of replacement p_r. If N_r is the number of samples of the signal $\underline{\hat{\mathbf{e}}}_{\mathrm{r}}$ in the modified signal $\underline{\mathbf{e}}_{\mathrm{mo}}$ and N_{c} is the total number of received samples of signal $\underline{\mathbf{e}}$, the percentage of replacement is

$$p_r = \frac{N_r}{N_c}. \tag{4.1}$$

As said before, this simulation program measures four kinds of BER but with this receiver only two. The uncoded BER $P_{\mathrm{b,u1}}$ of the first data detection and the uncoded BER $P_{\mathrm{b,u2}}$ of the second data detection. The reason why there is no improvement in the coded BER, is that there is the same value for $P_{\mathrm{b,c1}}$ and for $P_{\mathrm{b,c2}}$, i.e., there is no gain. This is due to the influence of the direct interference cancellation block. This

block only eliminates the interference of the received signal $\underline{\mathbf{e}}$, see Subsection 2.3.1, but the errors spreaded in the recontruction signal process still will be in the signal $\underline{\hat{\mathbf{e}}}_{\mathrm{r}}$ and in the modified signal $\underline{\mathbf{e}}_{\mathrm{mo}}$. In the second data detection we will not take advantage of the estimation of the interference covariance matrix $\underline{\underline{\mathbf{R}}}_{\mathrm{u}}$. Therefore, we will reduce the errors only with JD and finally we will have the same coded BER $P_{\mathrm{b,c2}}$ than in the first data detection.

The interference power P_{INT} used in the first receiver, see Subsection 2.3.1, has been multiplied by a constant REL to observe its influence on the simulations. The values of REL

35	30	25	20	15	10	5	1	0.5

are between 35 and 0.5. Further on it is shown that its influence is important. Clearly REL is inversely proportional to the percentage of replacement p_r, see (4.1). In the next subsections, this percentage will be plotted versus the C/I ratio. In this receiver in each situation and for each REL there will be one figure showing the uncoded BER $P_{\mathrm{b,u1}}$ and uncoded BER $P_{\mathrm{b,u2}}$ as a function of the C/I ratio and another with the percentage of replacement p_r as a function of the C/I ratio. Another figure with all the percentages of replacement for all situations and one figure with all the uncoded BER $P_{\mathrm{b,u2}}$ including only one uncoded BER $P_{\mathrm{b,u1}}$ as a reference will be presented. For the three situations, eight users four antennas, four users four antennas and eight users one antenna, a comparison of the results of these three situations is shown.

4.2.1 Simulation results with eight users and four antennas

Regarding the obtained results in the following Figures, it can be seen that when the constant REL is big, e.g. $REL = 35$, see Fig. 4.5, the value of the percentage of replacement p_r is low. Furthermore uncoded BER $P_{\mathrm{b,u2}}$ is worse than the uncoded BER $P_{\mathrm{b,u1}}$. Whenever REL takes a value higher than five, we have more than 95% of percentage of replacement p_r. Due to the low value of $REL \cdot P_{\mathrm{INT}}$, almost all the signal $\underline{\hat{\mathbf{e}}}_{\mathrm{r}}$ is inserted in the modified signal $\underline{\mathbf{e}}_{\mathrm{mo}}$, it can be observed a better BER in the second data detection with compared to the first data detection. With a percentage

of replacement p_r of about 100% the system improves more. E.g. for REL equal to 1 and a BER equal to 10^{-3} we have a gain of about seven dB. This is a very good result, but the only problem is the coded BER, where we can not get an improvement, always the second data detection leads to the same BER value than the first. In Fig. 4.23, all the uncoded BER curves with dotted lines of the second data detection are presented. It can be observed that when making the constant REL lower the curves improve. The solid line correspond to the first uncoded data detection for having a general reference curve. The last Figure ,see 4.24, shows the tendency of all the percentage of replacement p_r curves.

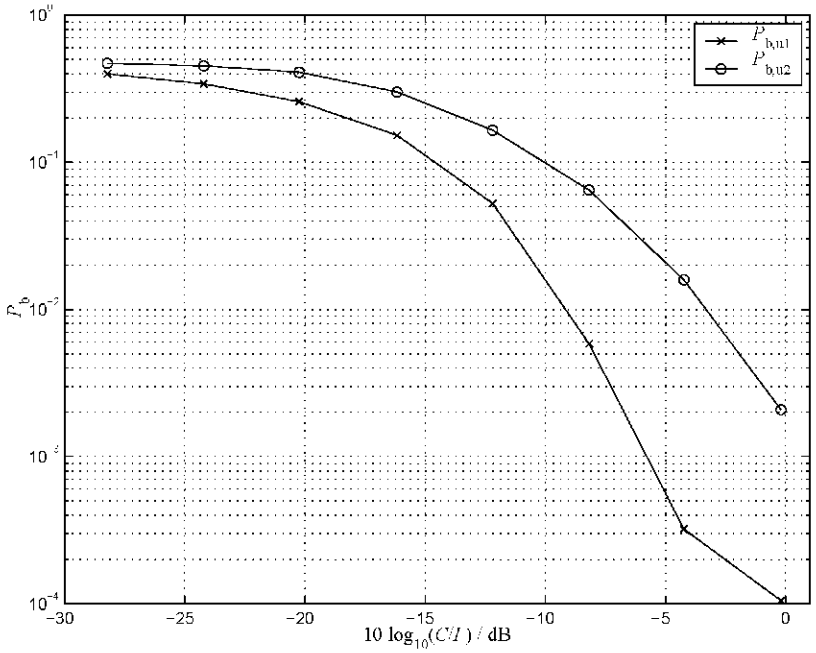

Figure 4.5. Eight users, four antenna, URA 2 2, uncoded BER $P_{\mathrm{b,u1}}$ and $P_{\mathrm{b,u2}}$ as a function of C/I with $REL = 35$.

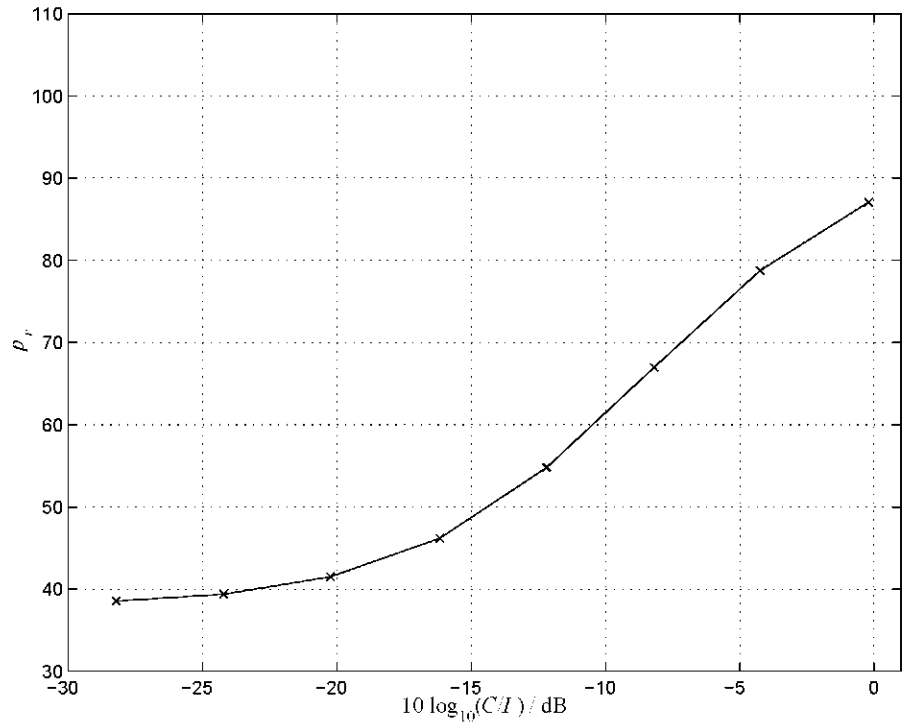

Figure 4.6. Eight users, four antenna, URA 2 2, percentage of replacement, p_r, as a function of C/I with $REL = 35$.

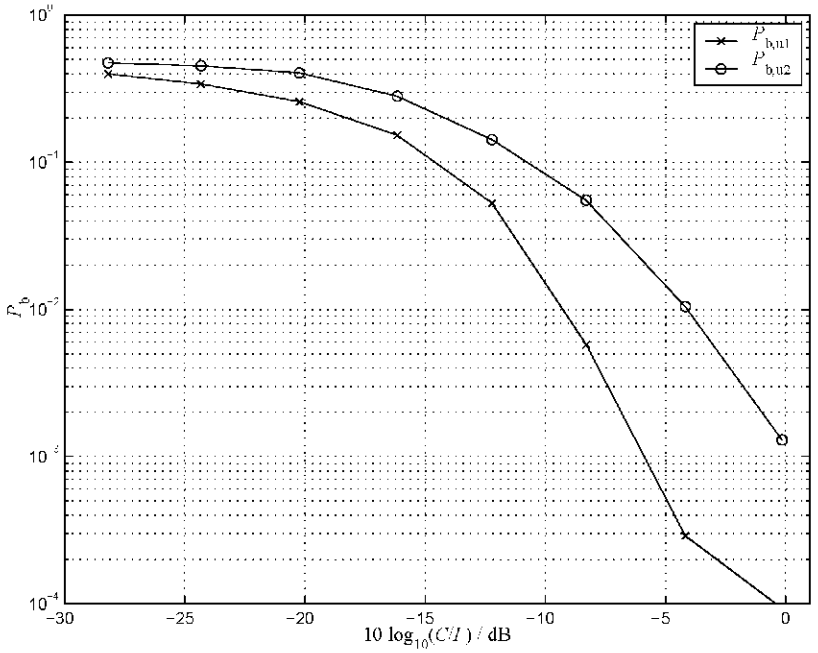

Figure 4.7. Eight users, four antenna, URA 2 2, uncoded BER $P_{\mathrm{b,u1}}$ and $P_{\mathrm{b,u2}}$ as a function of C/I with $REL = 30$.

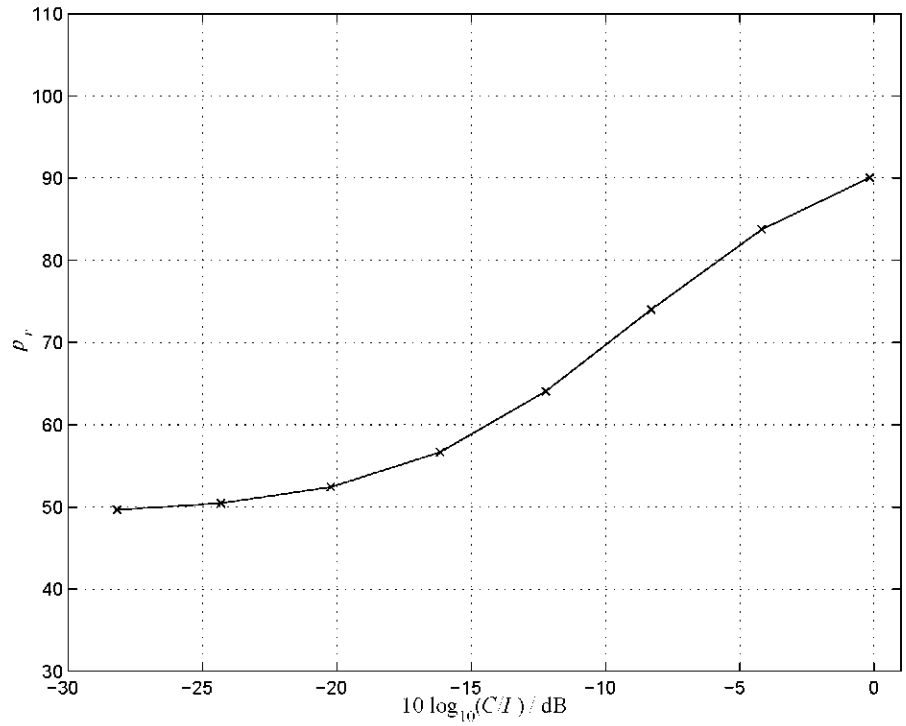

Figure 4.8. Eight users, four antenna, URA 2 2, percentage of replacement, p_r, as a function of C/I with $REL = 30$.

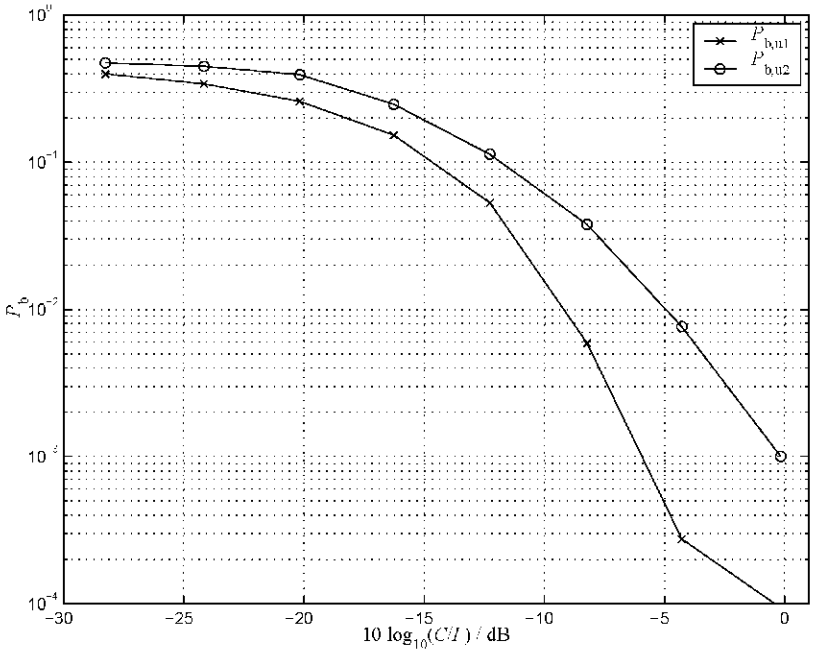

Figure 4.9. Eight users, four antenna, URA 2 2, uncoded BER $P_{\mathrm{b,u1}}$ and $P_{\mathrm{b,u2}}$ as a function of C/I with $REL = 25$.

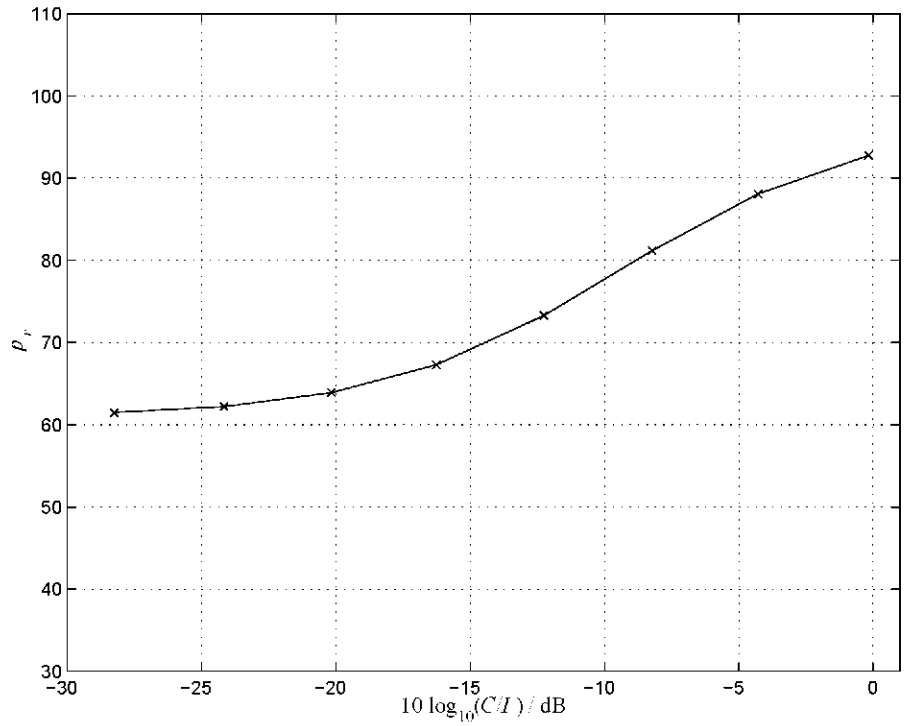

Figure 4.10. Eight users, four antenna, URA 2 2, percentage of replacement, p_r, as a function of C/I with $REL = 25$.

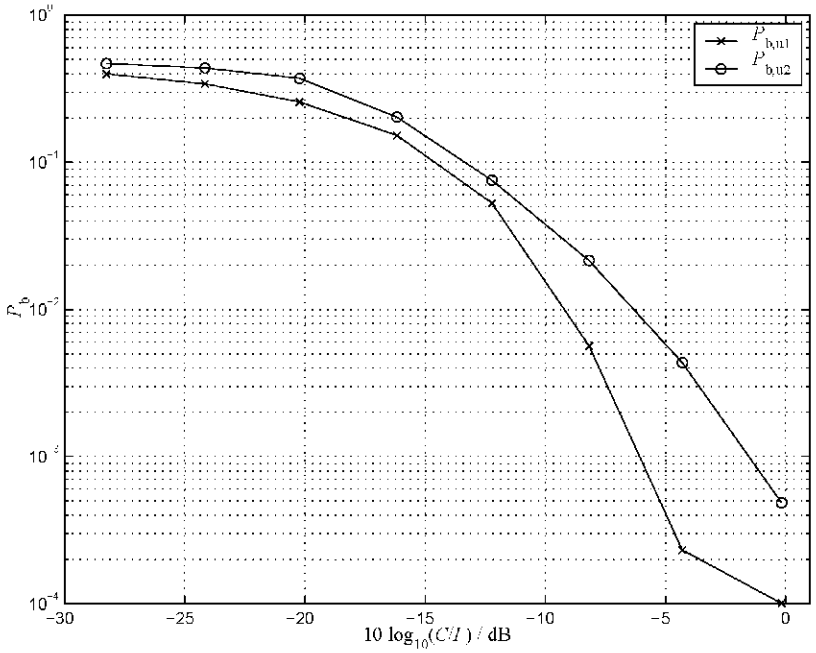

Figure 4.11. Eight users, four antenna, URA 2 2, uncoded BER $P_{\mathrm{b,u1}}$ and $P_{\mathrm{b,u2}}$ as a function of C/I with $REL = 20$.

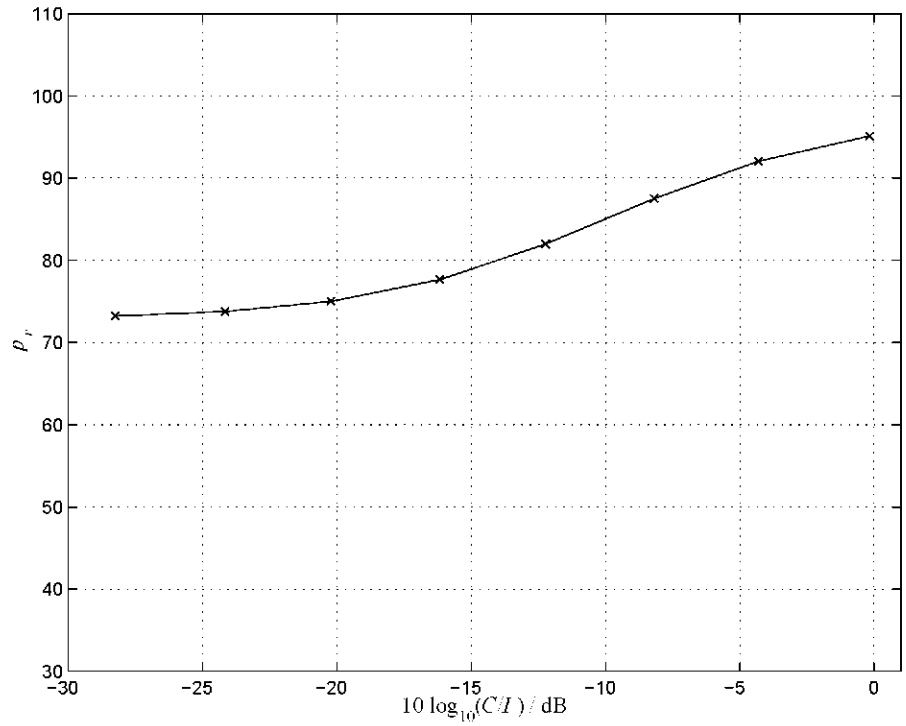

Figure 4.12. Eight users, four antenna, URA 2 2, percentage of replacement, p_r, as a function of C/I with $REL = 20$.

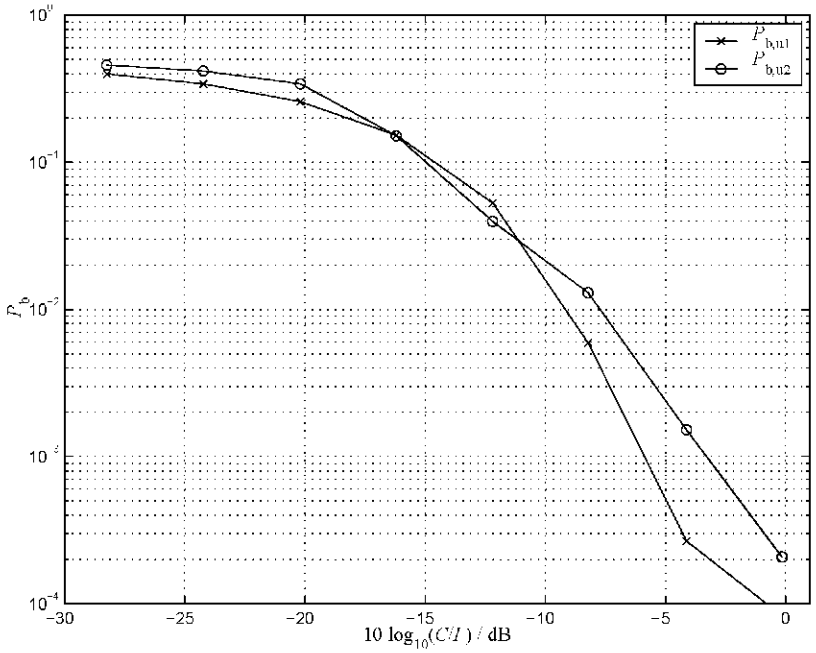

Figure 4.13. Eight users, four antenna, URA 2 2, uncoded BER $P_{\mathrm{b,u1}}$ and $P_{\mathrm{b,u2}}$ as a function of C/I with $REL = 15$.

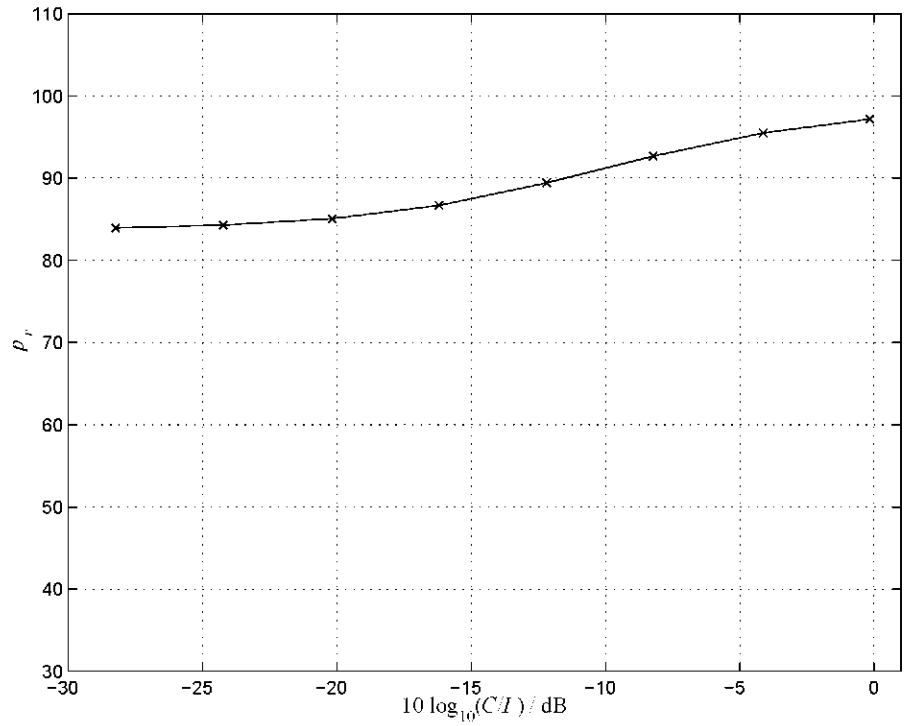

Figure 4.14. Eight users, four antenna, URA 2 2, percentage of replacement, p_r, as a function of C/I with $REL = 15$.

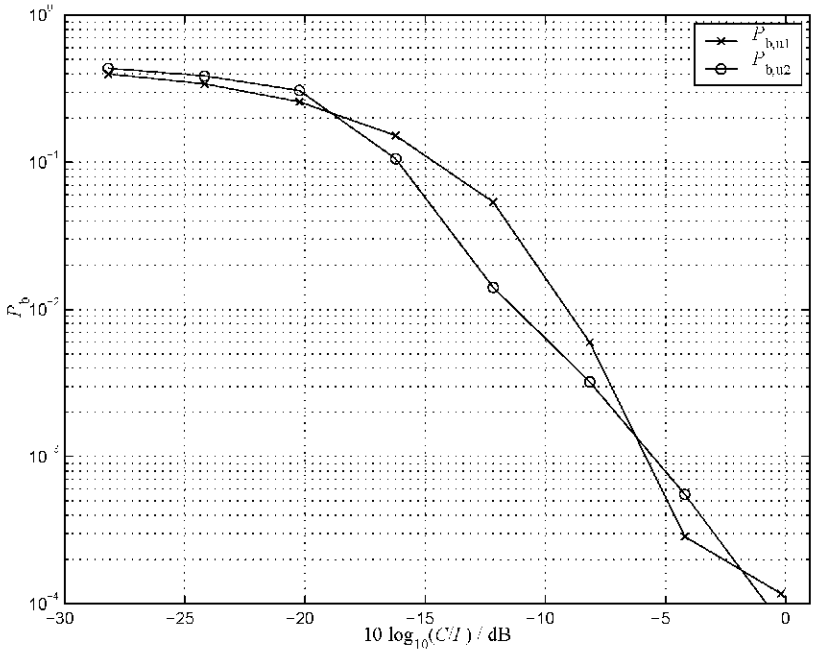

Figure 4.15. Eight users, four antenna, URA 2 2, uncoded BER $P_{\mathrm{b,u1}}$ and $P_{\mathrm{b,u2}}$ as a function of C/I with $REL = 10$.

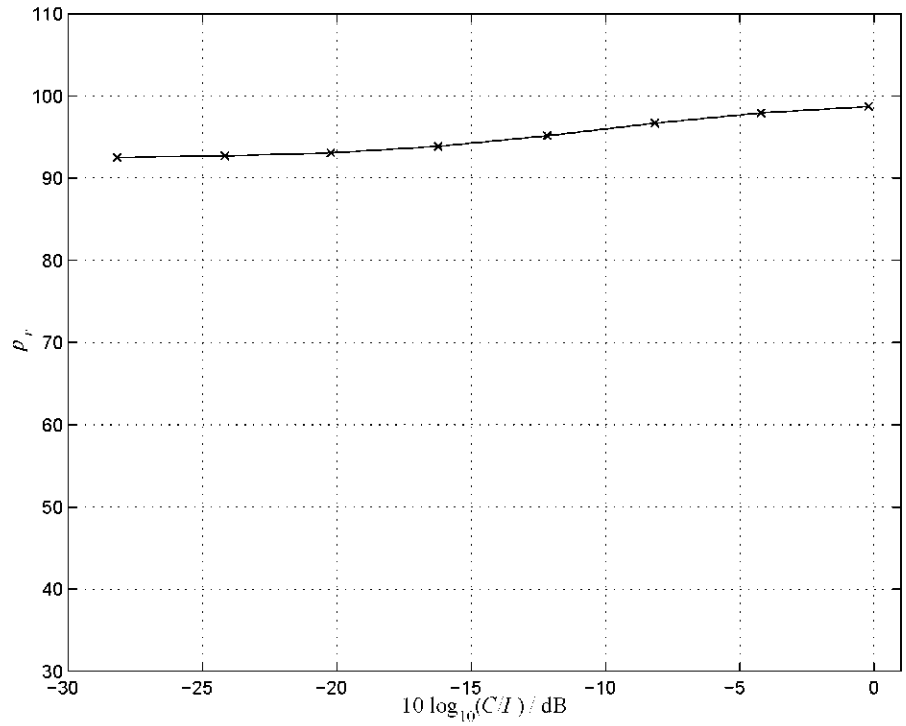

Figure 4.16. Eight users, four antenna, URA 2 2, percentage of replacement, p_r, as a function of C/I with $REL = 10$.

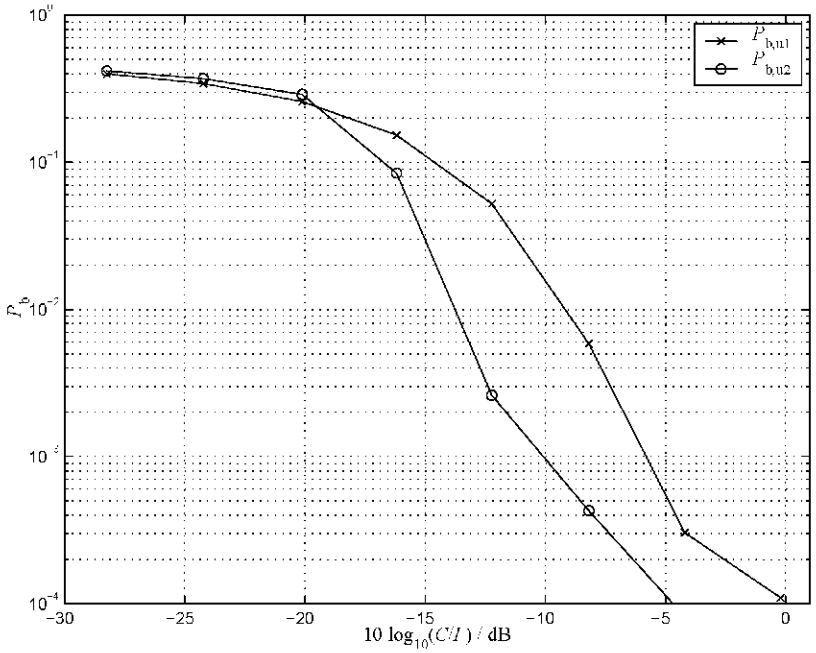

Figure 4.17. Eight users, four antenna, URA 2 2, uncoded BER $P_{\mathrm{b,u1}}$ and $P_{\mathrm{b,u2}}$ as a function of C/I with $REL = 5$.

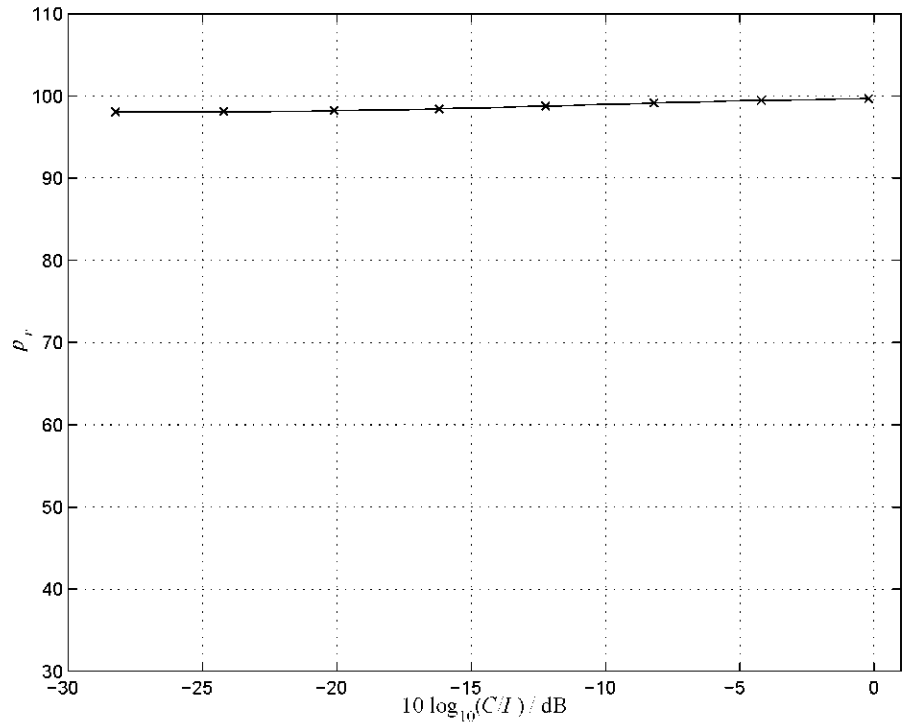

Figure 4.18. Eight users, four antenna, URA 2 2, percentage of replacement, p_r, as a function of C/I with $REL = 5$.

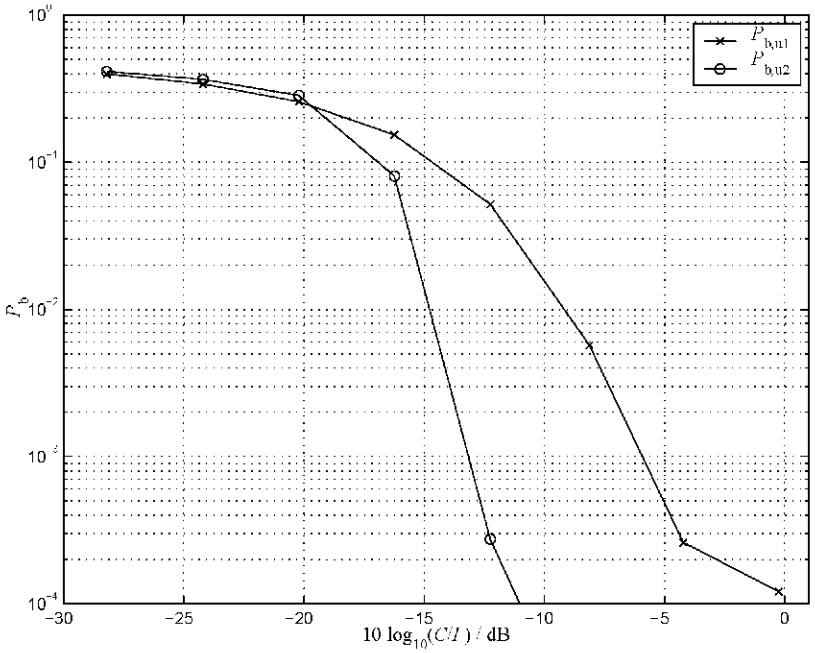

Figure 4.19. Eight users, four antenna, URA 2 2, uncoded BER $P_{\mathrm{b,u1}}$ and $P_{\mathrm{b,u2}}$ as a function of C/I with $REL = 1$.

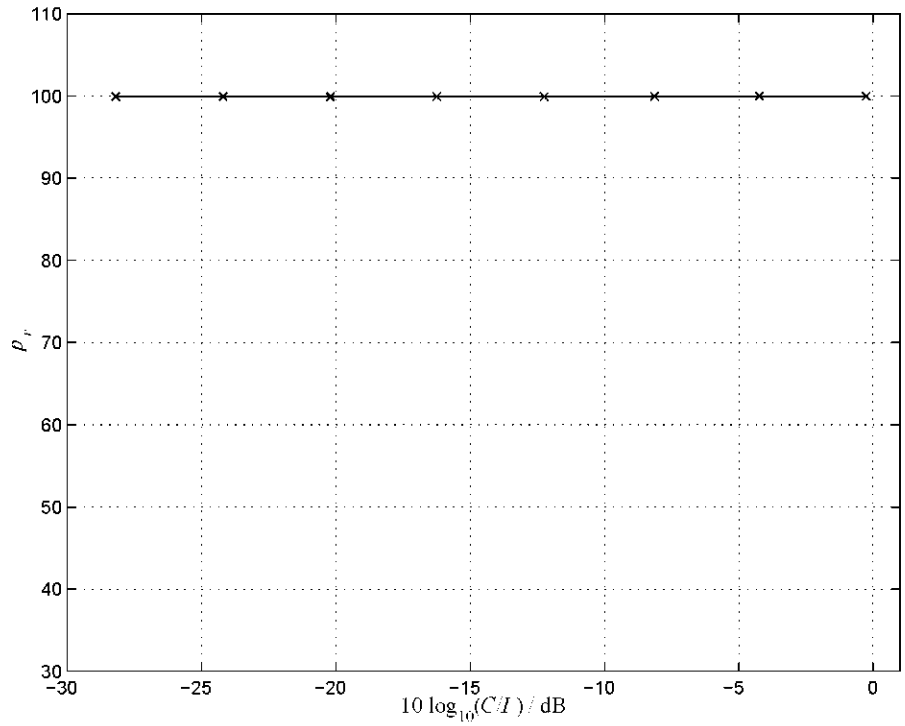

Figure 4.20. Eight users, four antenna, URA 2 2, percentage of replacement, p_r, as a function of C/I with $REL = 1$.

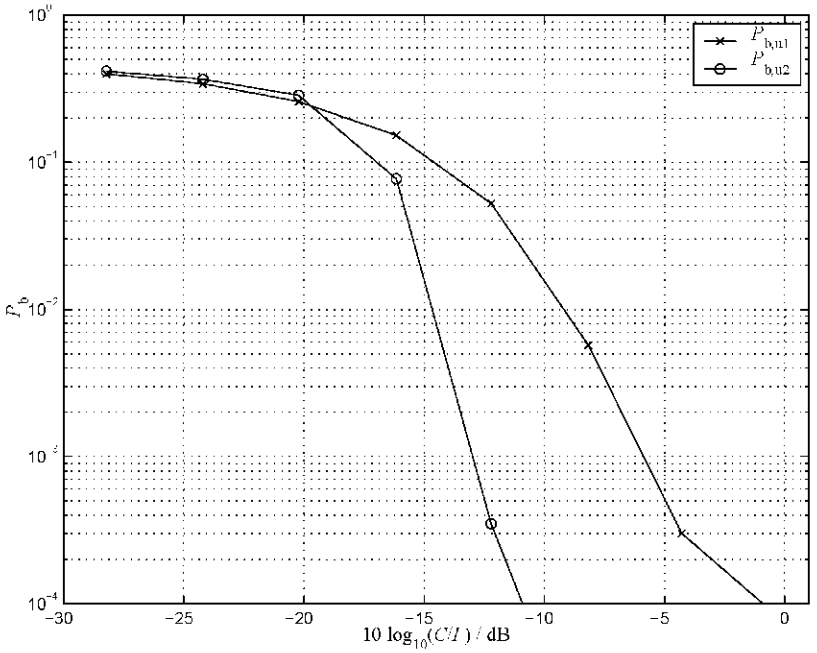

Figure 4.21. Eight users, four antenna, URA 2 2, uncoded BER $P_{\mathrm{b,u1}}$ and $P_{\mathrm{b,u2}}$ as a function of C/I with $REL = 0,5$.

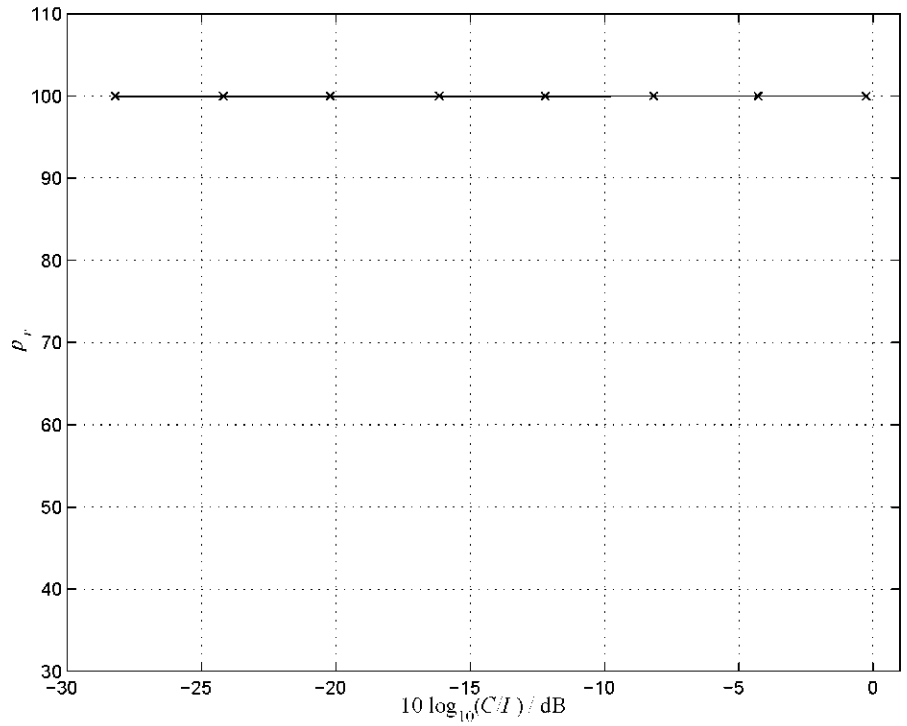

Figure 4.22. Eight users, four antenna, URA 2 2, percentage of replacement, p_r, as a function of C/I with $REL = 0,5$.

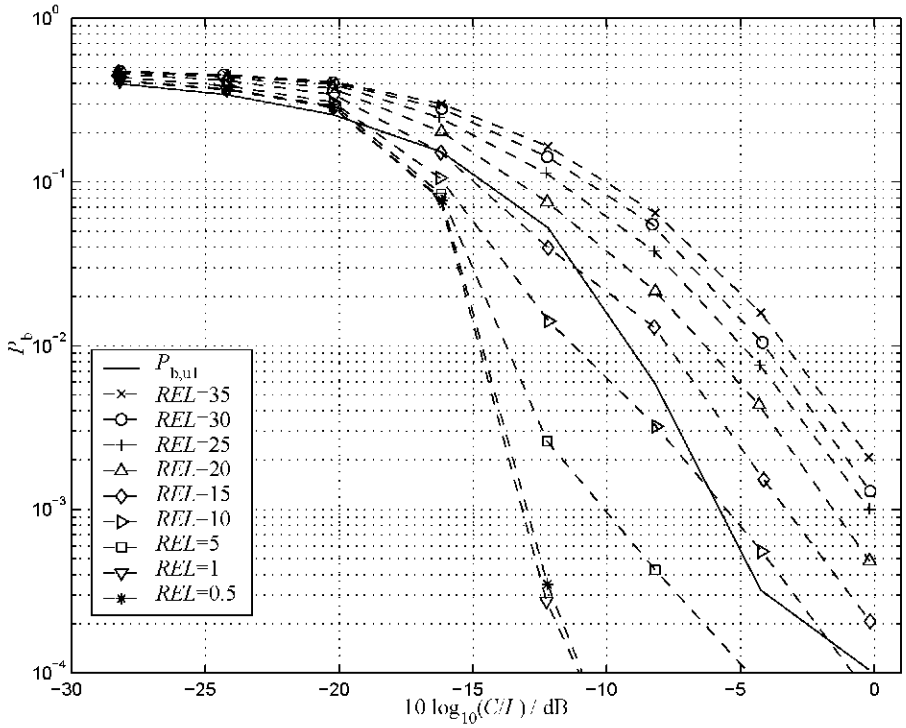

Figure 4.23. Eight users, four antenna, URA 2 2, comparison with all the uncoded $P_{\mathrm{b,u2}}$ and a uncoded $P_{\mathrm{b,u1}}$ as a function of C/I.

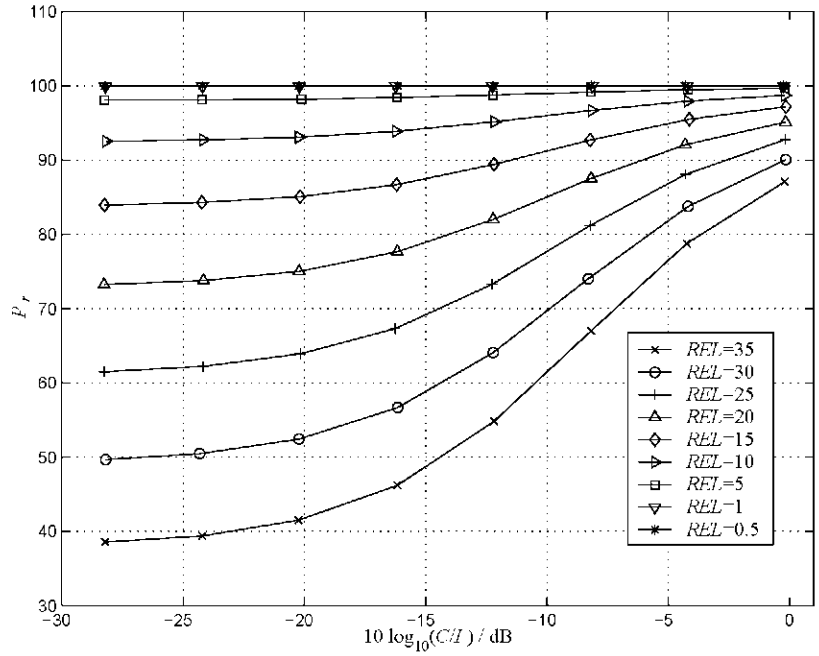

Figure 4.24. Eight users, four antenna, URA 2 2, all the percentage of replacements as a function of C/I.

4.2.2 Simulation results considering four users and four antennas

Considering four users and four antennas in the simulations it can be observed, in the following figures that a similar tendency to the previous situation. If REL decreases, the percentage replacement p_r also the C/I ratio can be reduced to achieve the same BER. If REL is between 15 and 10, then the uncoded BER $P_{\mathrm{b,u2}}$ is smaller than the uncoded BER $P_{\mathrm{b,u1}}$ for certain C/I ratio, i.e., there is a gain of C/I in dB. For REL between 5 and 0.5, with a percentage of replacement p_r of almost 100%, we obtain the best results. For a BER of 10^{-3} we obtain 6 dB of C/I improvement. This good results can only be achieved for the uncoded BER. The Fig. 4.43 is similar to the Fig. 4.23, it shows all the uncoded BER $P_{\mathrm{b,u2}}$ for all $RELs$ in dotted lines and only one uncoded BER $P_{\mathrm{b,u1}}$ as a reference curve. The Fig. 4.44 shows a summary of all the percentages of replacement p_r.

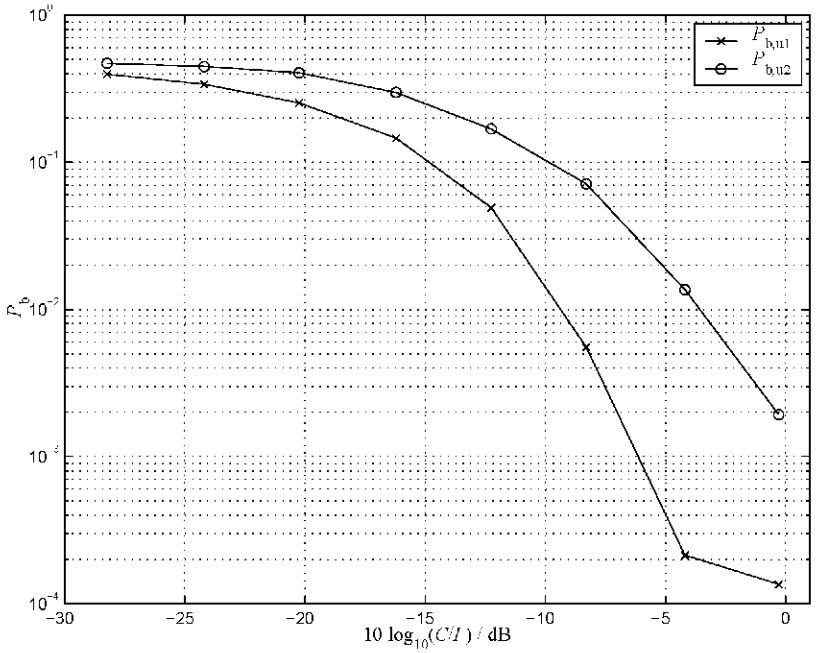

Figure 4.25. Four users, four antenna, URA 2 2, uncoded BER $P_{\mathrm{b,u1}}$ and $P_{\mathrm{b,u2}}$ as a function of C/I with $REL = 35$.

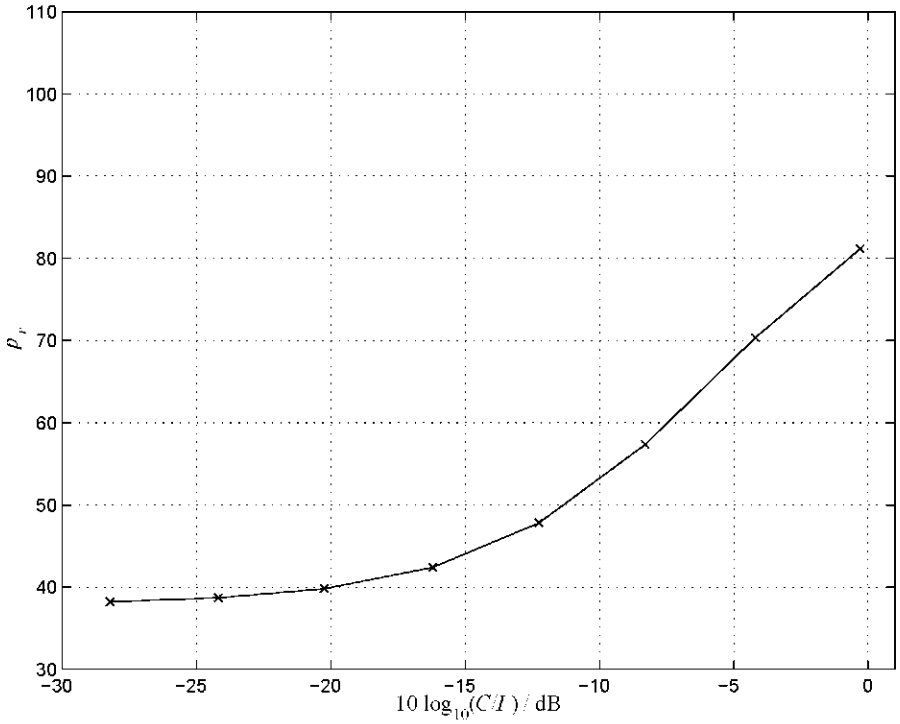

Figure 4.26. Four users, four antenna, URA 2 2, percentage of replacement, p_r, as a function of C/I with $REL = 35$.

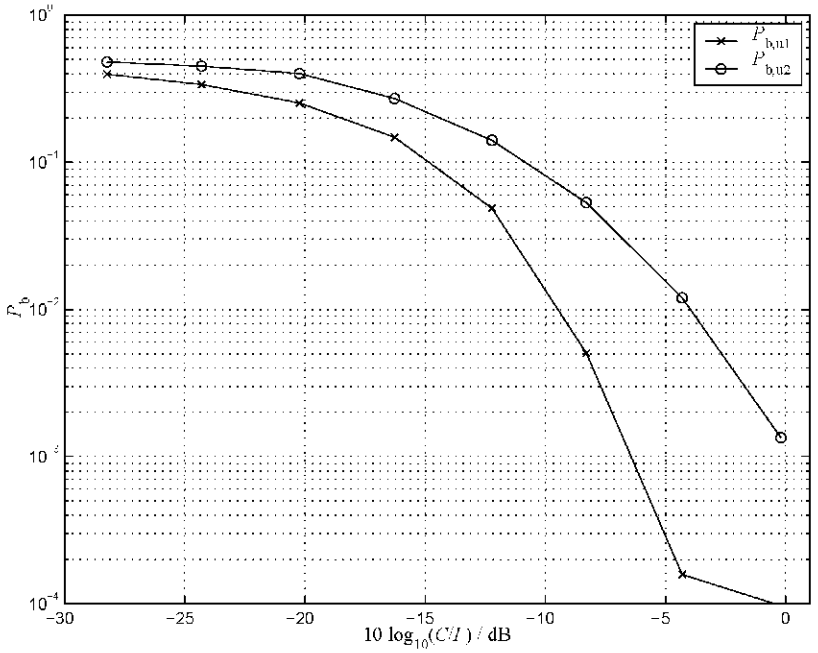

Figure 4.27. Four users, four antenna, URA 2 2, uncoded BER $P_{\mathrm{b,u1}}$ and $P_{\mathrm{b,u2}}$ as a function of C/I with $REL = 30$.

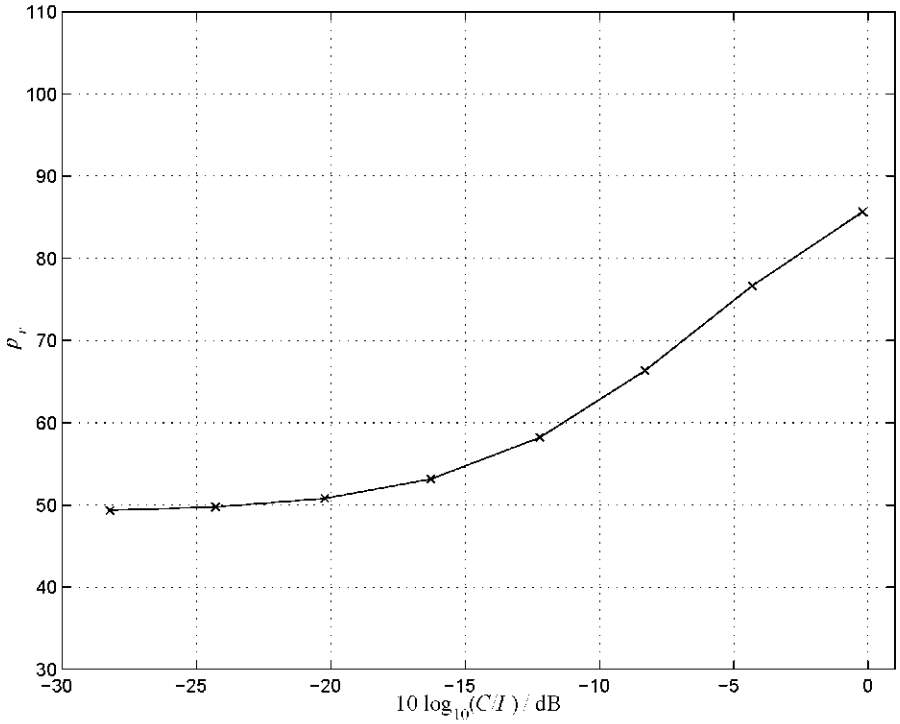

Figure 4.28. Four users, four antenna, URA 2 2, percentage of replacement, p_r, as a function of C/I with $REL = 30$.

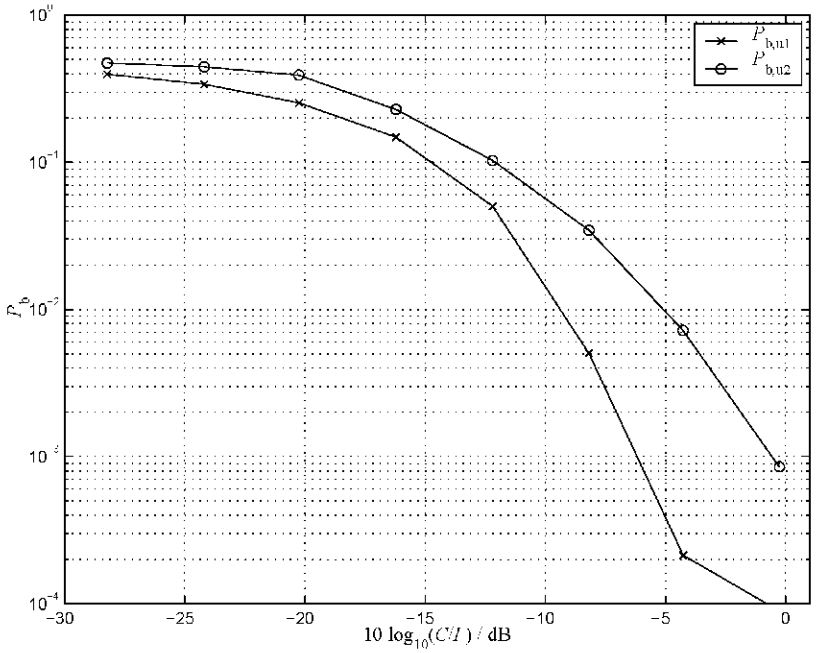

Figure 4.29. Four users, four antenna, URA 2 2, uncoded BER $P_{\mathrm{b,u1}}$ and $P_{\mathrm{b,u2}}$ as a function of C/I with $REL = 25$.

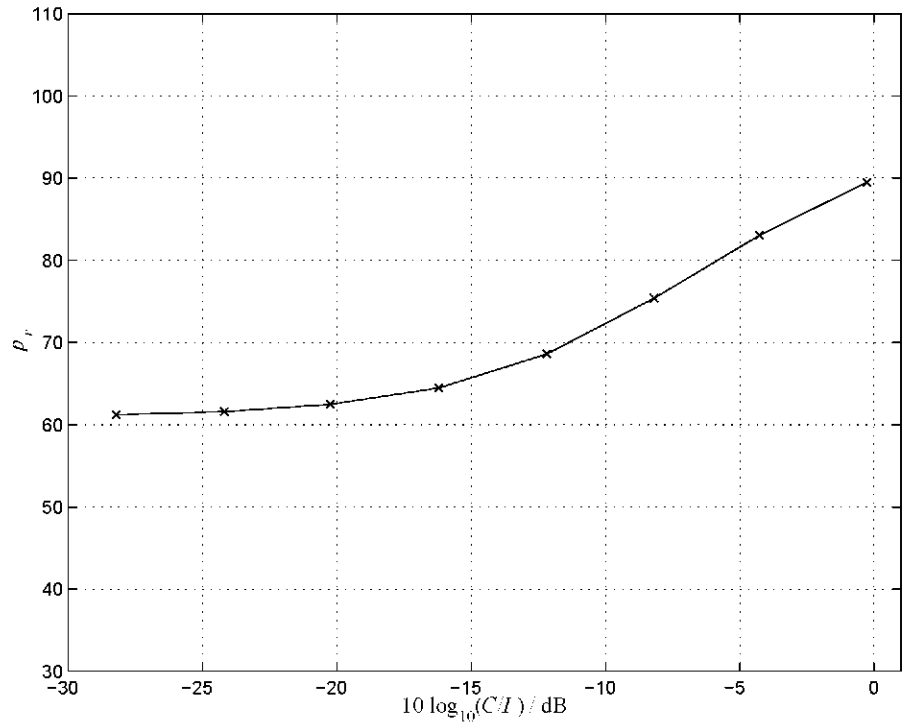

Figure 4.30. Four users, four antenna, URA 2 2, percentage of replacement, p_r, as a function of C/I with $REL = 25$.

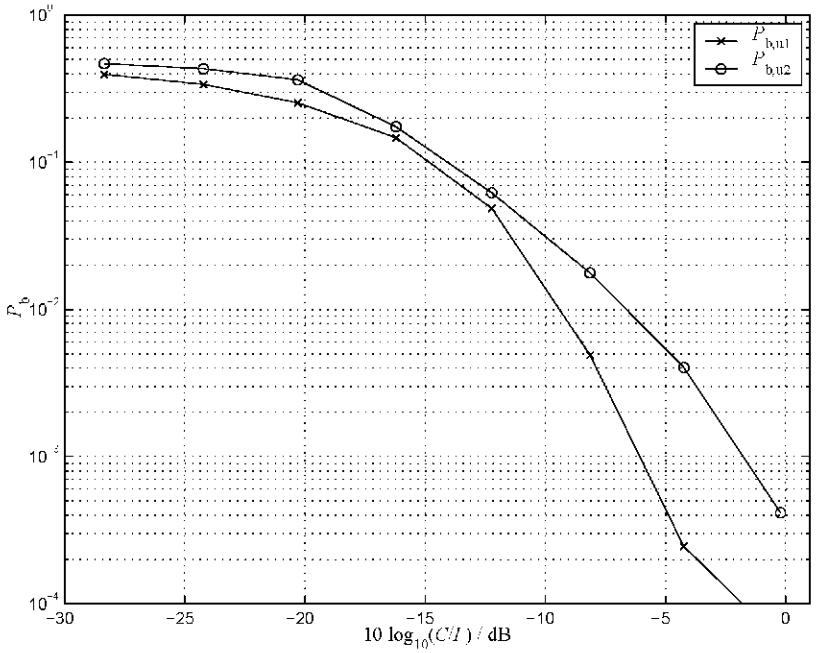

Figure 4.31. Four users, four antenna, URA 2 2, uncoded BER $P_{\mathrm{b,u1}}$ and $P_{\mathrm{b,u2}}$ as a function of C/I with $REL = 20$.

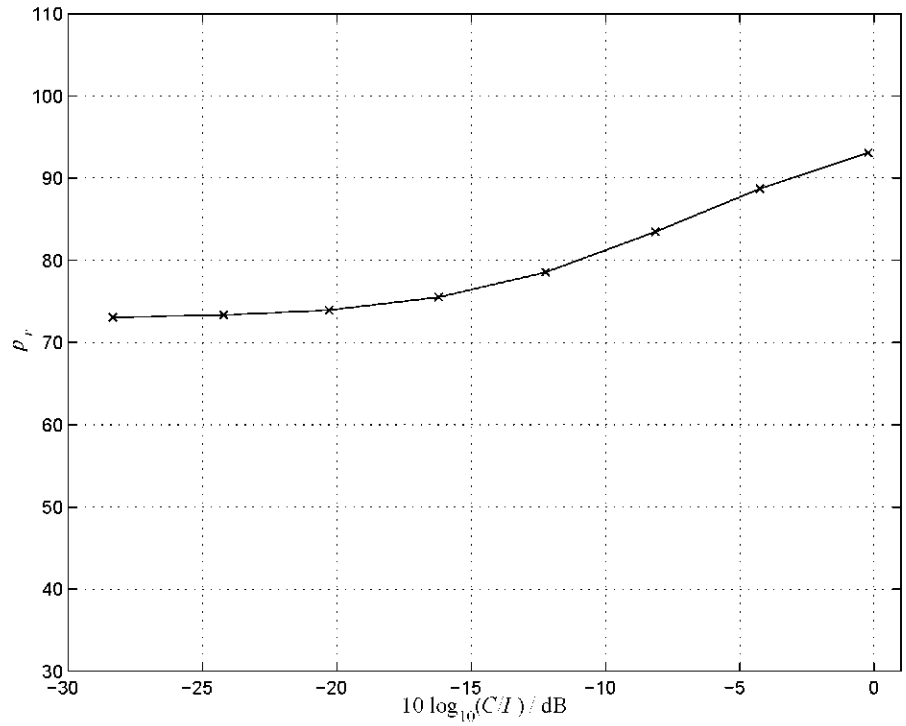

Figure 4.32. Four users, four antenna, URA 2 2, percentage of replacement, p_r, as a function of C/I with $REL = 20$.

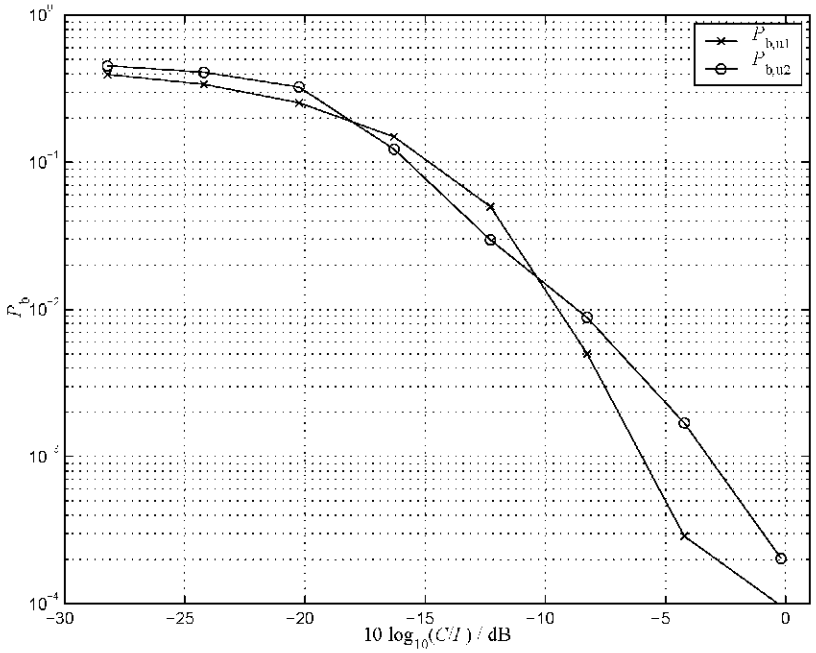

Figure 4.33. Four users, four antenna, URA 2 2, uncoded BER $P_{\mathrm{b,u1}}$ and $P_{\mathrm{b,u2}}$ as a function of C/I with $REL = 15$.

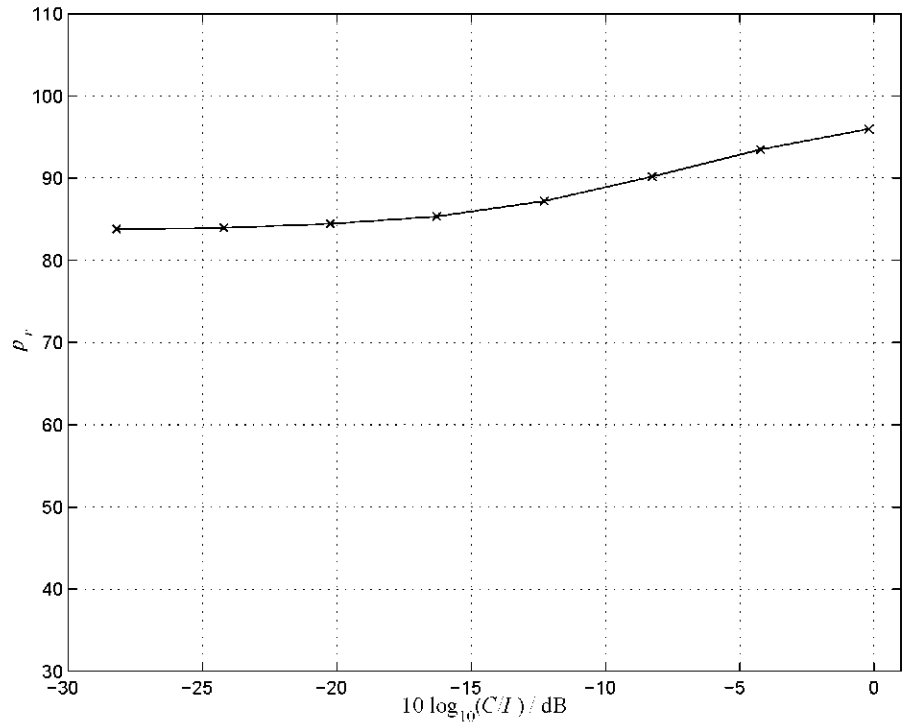

Figure 4.34. Four users, four antenna, URA 2 2, percentage of replacement, p_r, as a function of C/I with $REL = 15$.

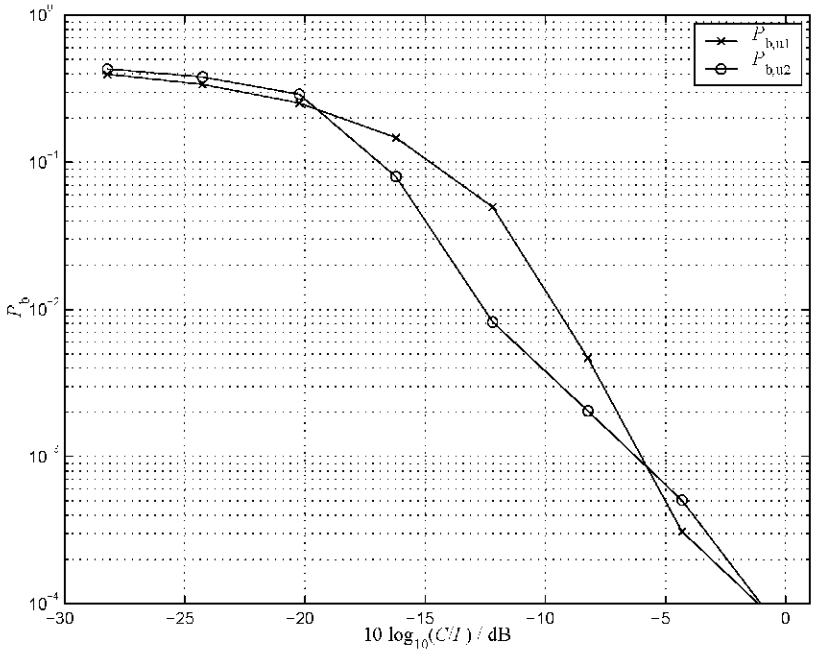

Figure 4.35. Four users, four antenna, URA 2 2, uncoded BER $P_{\mathrm{b,u1}}$ and $P_{\mathrm{b,u2}}$ as a function of C/I with $REL = 10$.

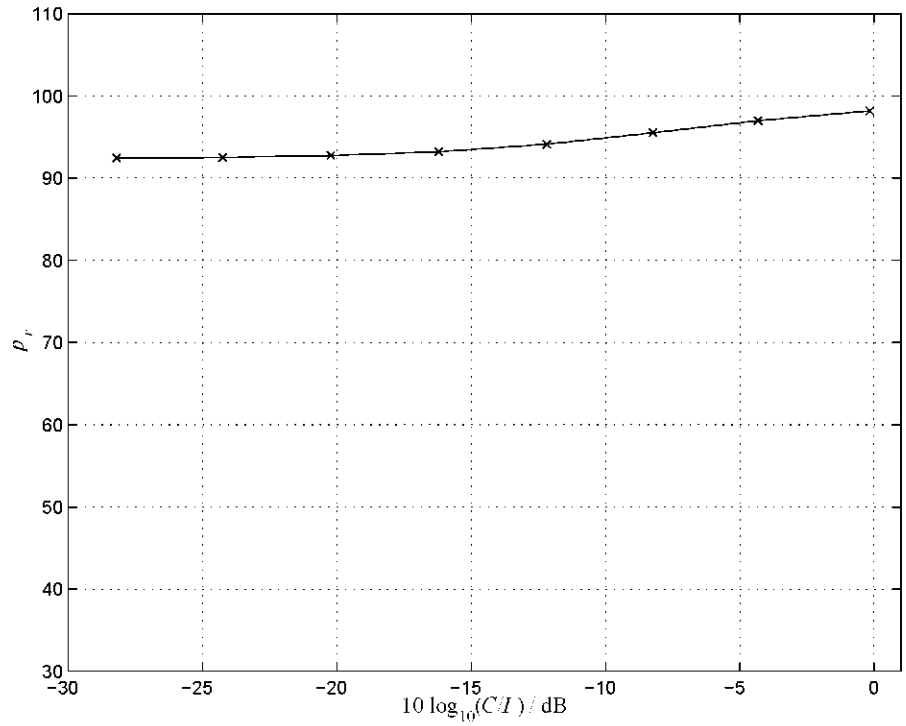

Figure 4.36. Four users, four antenna, URA 2 2, percentage of replacement, p_r, as a function of C/I with $REL = 10$.

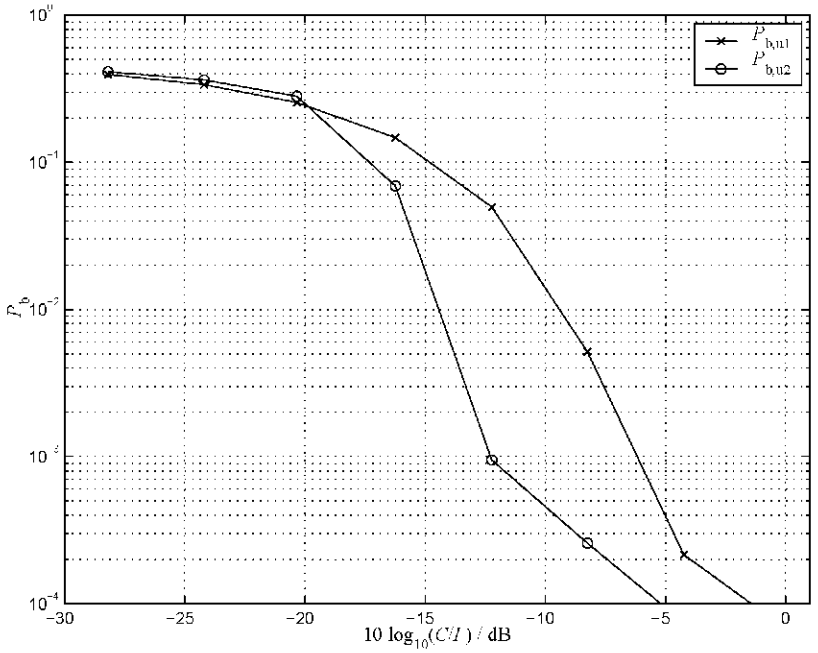

Figure 4.37. Four users, four antenna, URA 2 2, uncoded BER $P_{\mathrm{b,u1}}$ and $P_{\mathrm{b,u2}}$ as a function of C/I with $REL = 5$.

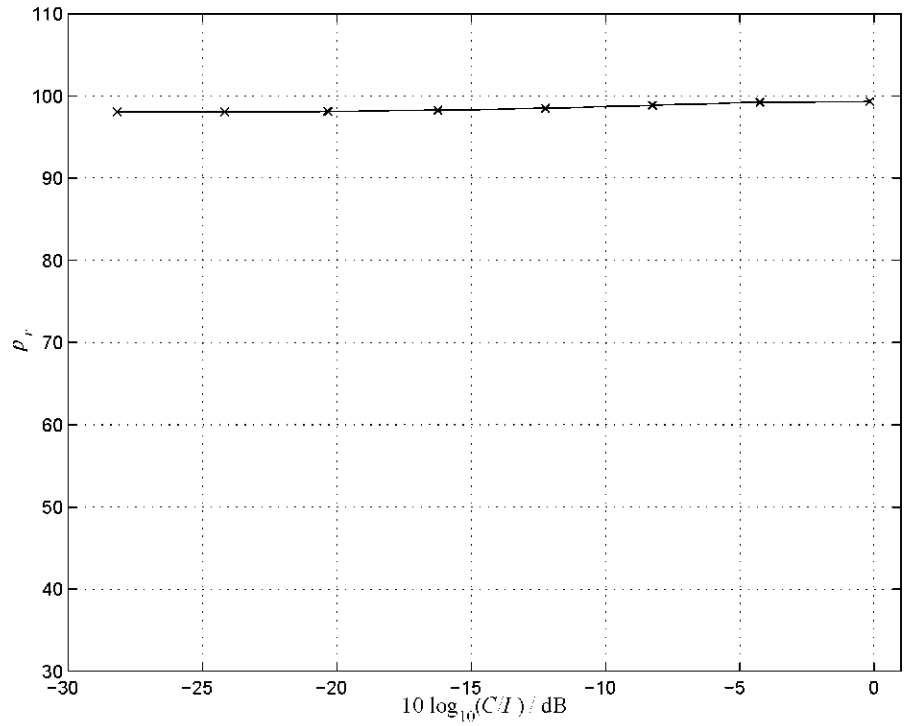

Figure 4.38. Four users, four antenna, URA 2 2, percentage of replacement, p_r, as a function of C/I with $REL = 5$.

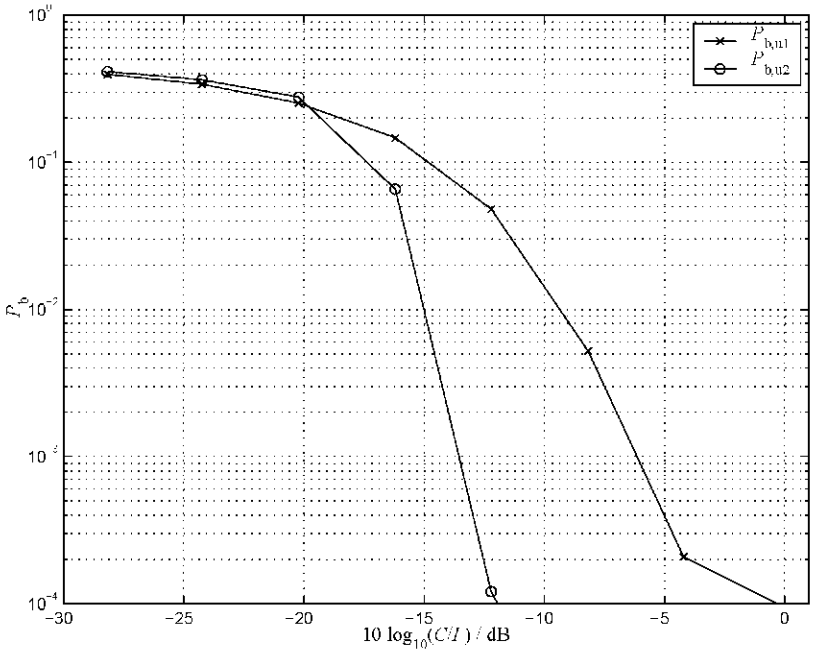

Figure 4.39. Four users, four antenna, URA 2 2, uncoded BER $P_{\mathrm{b,u1}}$ and $P_{\mathrm{b,u2}}$ as a function of C/I with $REL = 1$.

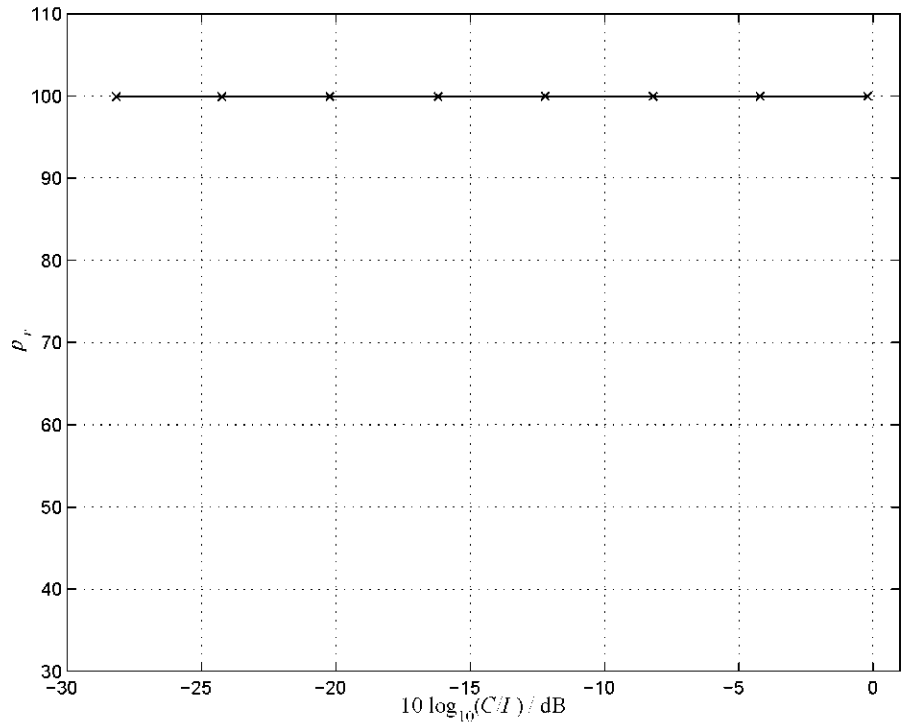

Figure 4.40. Four users, four antenna, URA 2 2, percentage of replacement, p_r, as a function of C/I with $REL = 1$.

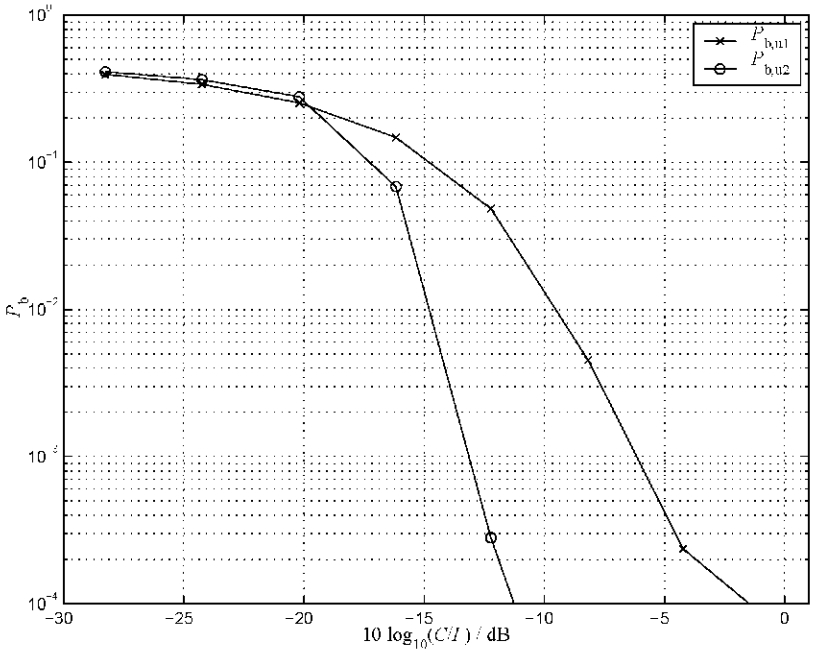

Figure 4.41. Four users, four antenna, URA 2 2, uncoded BER $P_{\mathrm{b,u1}}$ and $P_{\mathrm{b,u2}}$ as a function of C/I with $REL = 0, 5$.

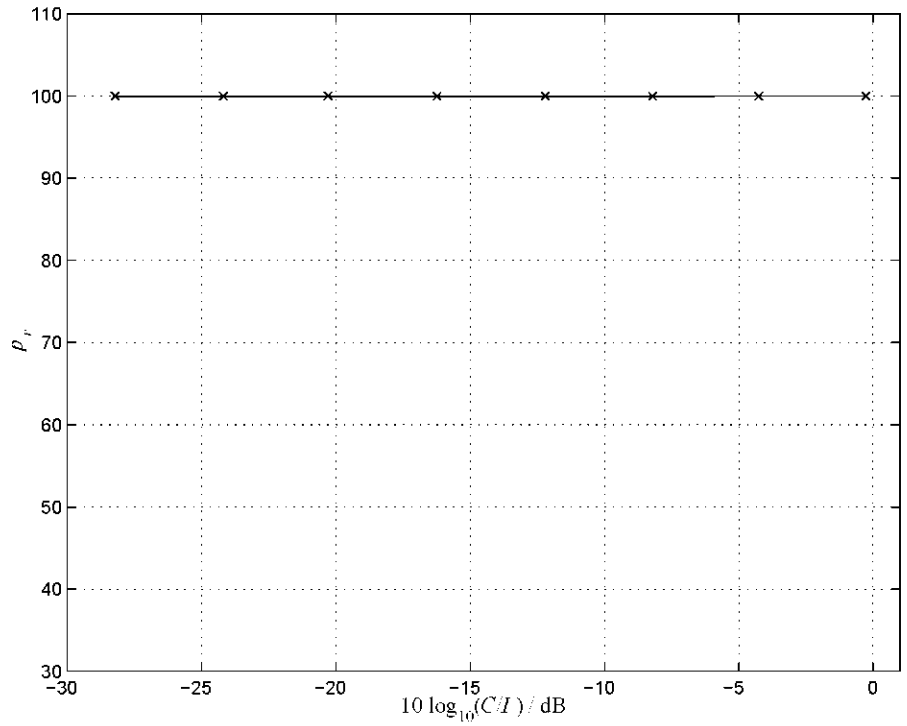

Figure 4.42. Four users, four antenna, URA 2 2, percentage of replacement, p_r, as a function of C/I with $REL = 0, 5$.

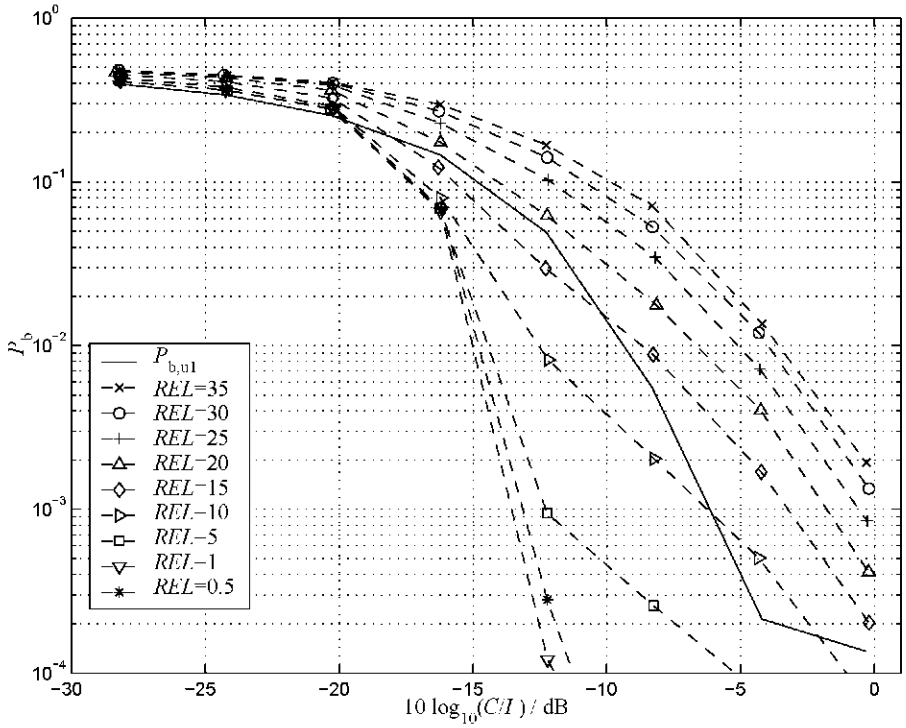

Figure 4.43. Four users, four antenna, URA 2 2, comparison with all the uncoded $P_{\mathrm{b,u2}}$ and an uncoded $P_{\mathrm{b,u1}}$ as a function of C/I.

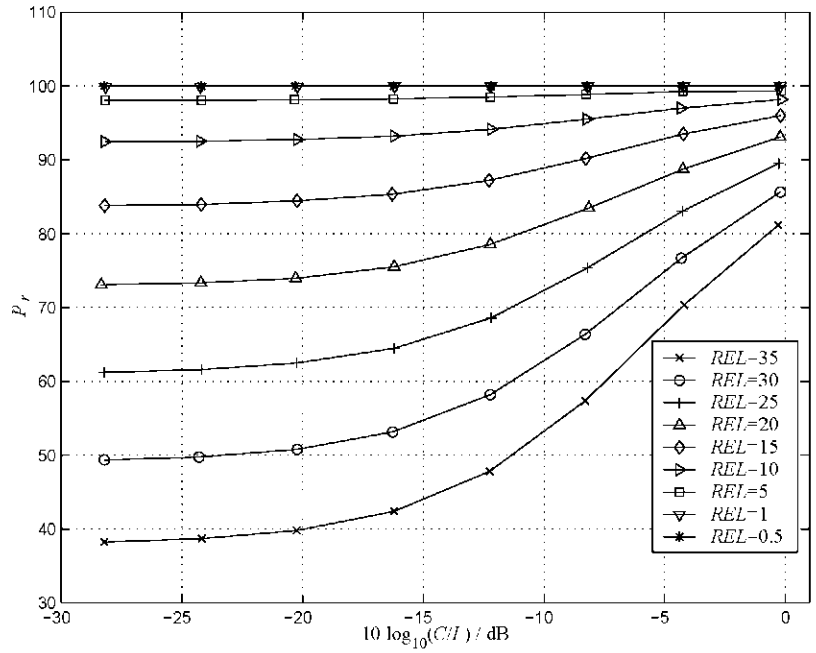

Figure 4.44. Four users, four antenna, URA 2 2, all the percentages of replacement as a function of C/I.

4.2.3 Simulation results considering eight users and one antenna

Compared to the previous section the results in this section are quite different. From the figures, it can be seen that for a high REL, in the range of 25-30, the uncoded BER $P_{\mathrm{b,u2}}$ is already lower than the uncoded BER $P_{\mathrm{b,u1}}$. In the both corresponding situations in the previous sections the uncoded BER $P_{\mathrm{b,u2}}$ always reaches 10^{-3}, however for this situation 10^{-3} never is reached. For a C/I ratio larger than -4 dB and a REL equal to 0.5, see Fig. 4.61, the uncoded BER $P_{\mathrm{b,u2}}$ increases and is almost equal to the uncoded BER $P_{\mathrm{b,u1}}$ for a C/I ratio of 0 dB. This is due to the influence of single errors in the convolutional code, see Subsection 2.4 and (2.45). In this range of C/I from -4 dB to 0 dB, the coded BER $P_{\mathrm{b,c1}}$ is low, which means that a few bit errors are present. So a single error in the input of the coder will generate 7 in the output. Therefore the signal $\underline{\hat{\mathbf{e}}}_{\mathrm{r}}$ will have more errors than the received signal $\underline{\mathbf{e}}$. For this value of REL, the percentage of replacement, see Fig. 4.62, is almost 100%, thus this result is clear. The last two figures 4.63 and 4.64 are the summary of all the other figures when considering eight users and one antenna.

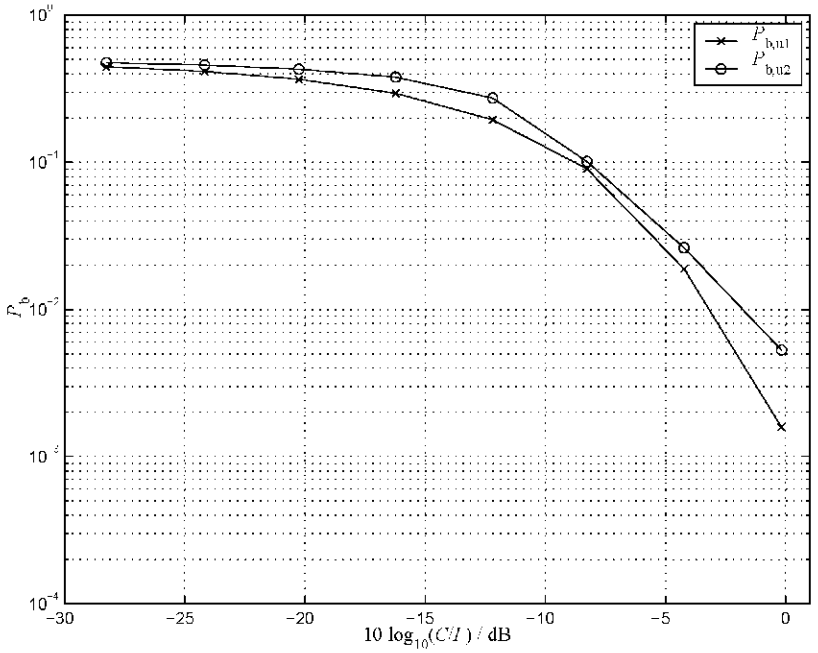

Figure 4.45. Eight users, one antenna, ULA 1, uncoded BER $P_{\mathrm{b,u1}}$ and $P_{\mathrm{b,u2}}$ as a function of C/I with $REL = 35$.

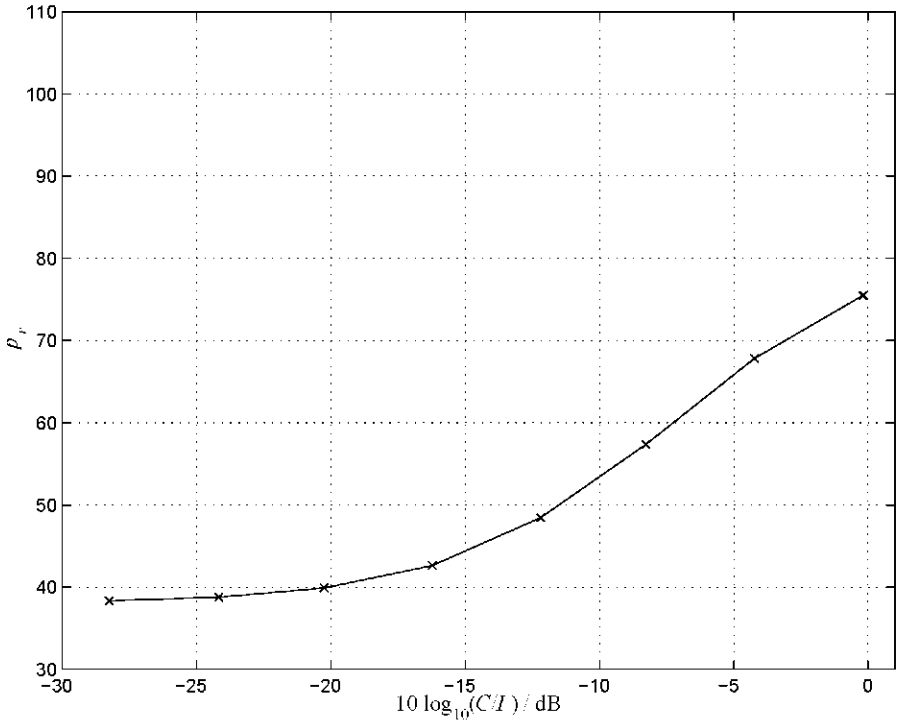

Figure 4.46. Eight users, one antenna, ULA 1, percentage of replacement, p_r, as a function of C/I with $REL = 35$.

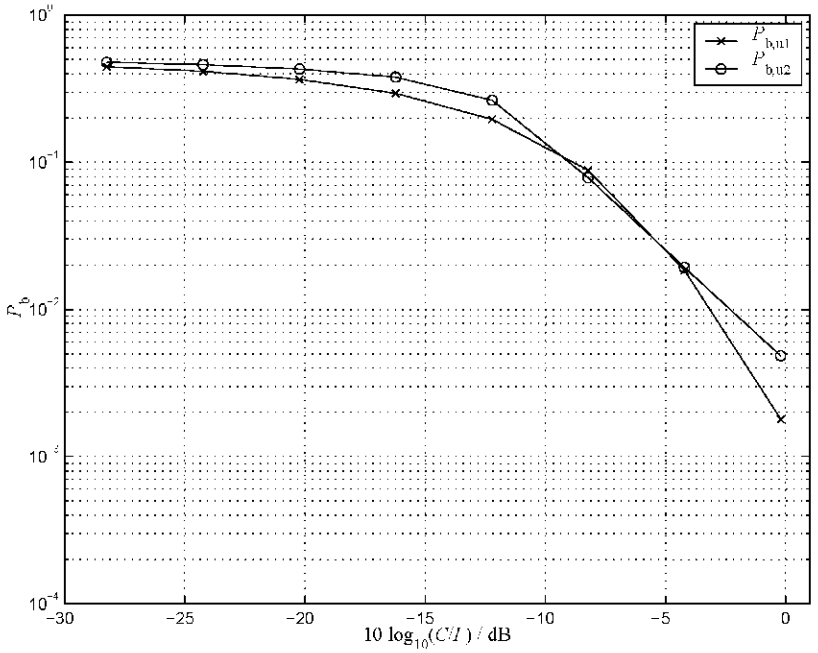

Figure 4.47. Eight users, one antenna, ULA 1, uncoded BER $P_{\mathrm{b,u1}}$ and $P_{\mathrm{b,u2}}$ as a function of C/I with $REL = 30$.

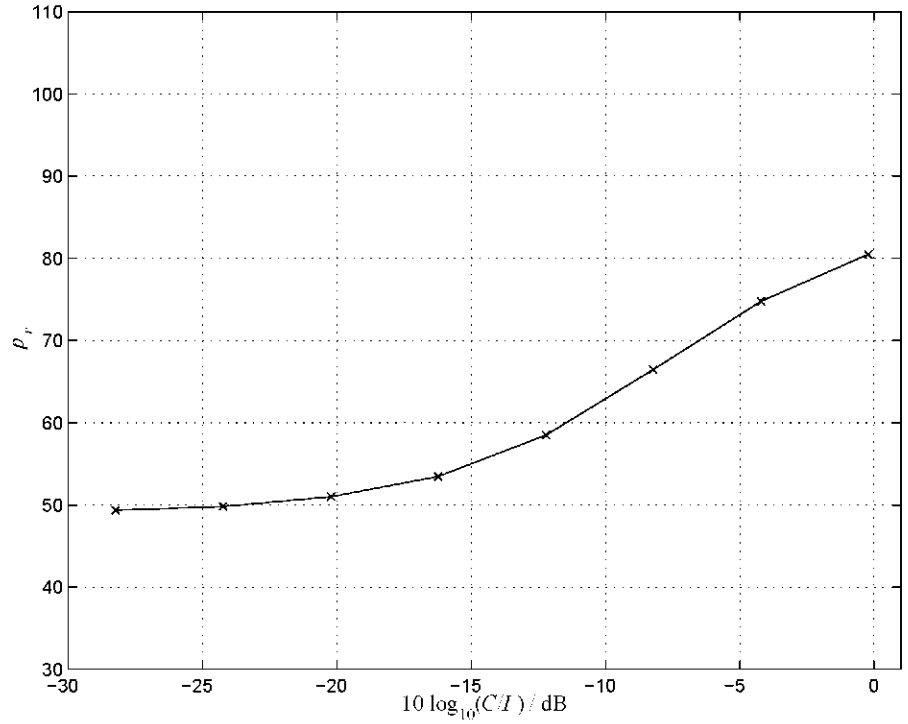

Figure 4.48. Eight users, one antenna, ULA 1, percentage of replacement, p_r, as a function of C/I with $REL = 30$.

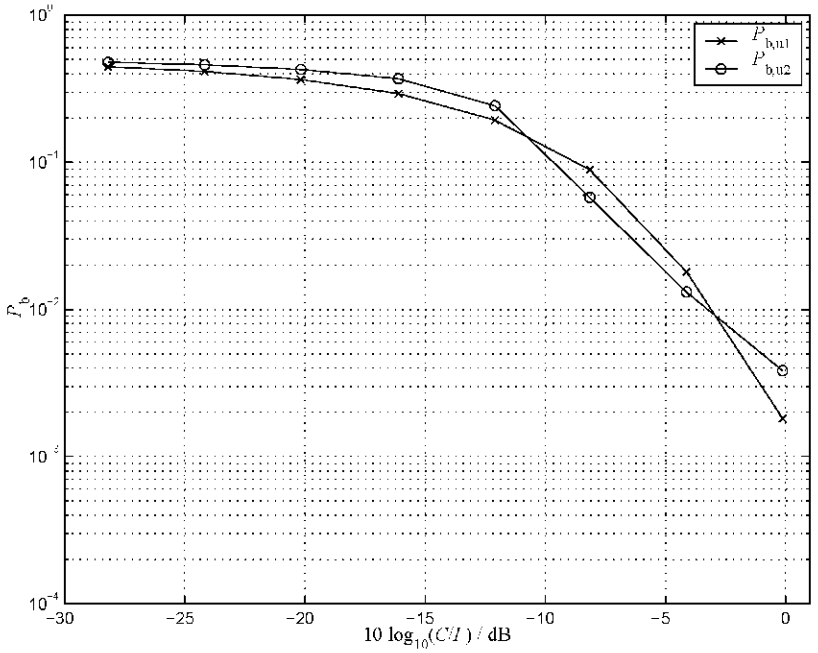

Figure 4.49. Eight users, one antenna, ULA 1, uncoded BER $P_{\mathrm{b,u1}}$ and $P_{\mathrm{b,u2}}$ as a function of C/I with $REL = 25$.

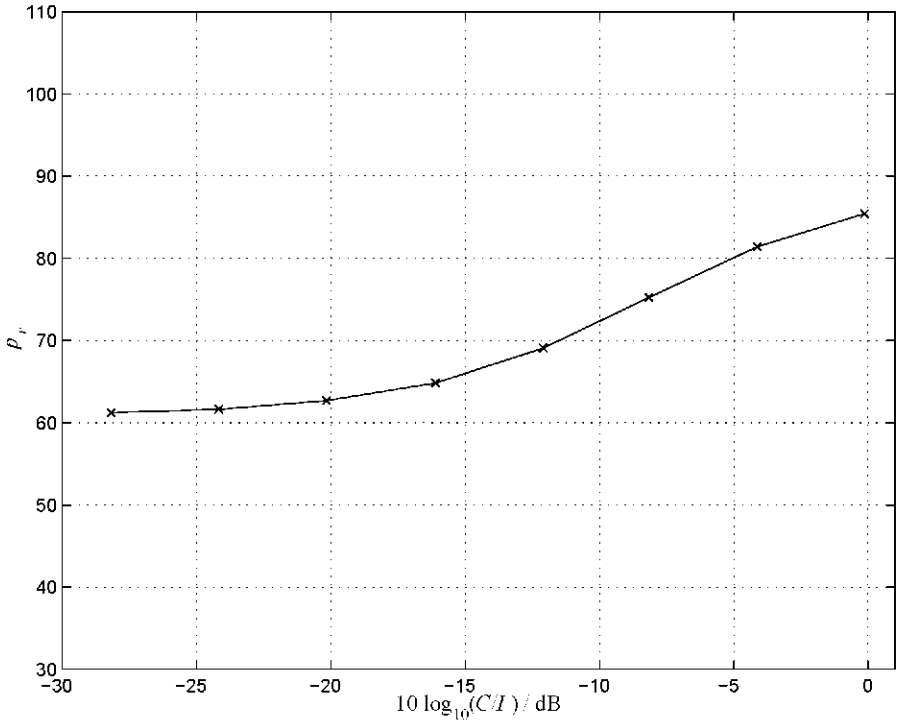

Figure 4.50. Eight users, one antenna, ULA 1, percentage of replacement, p_r, as a function of C/I with $REL = 25$.

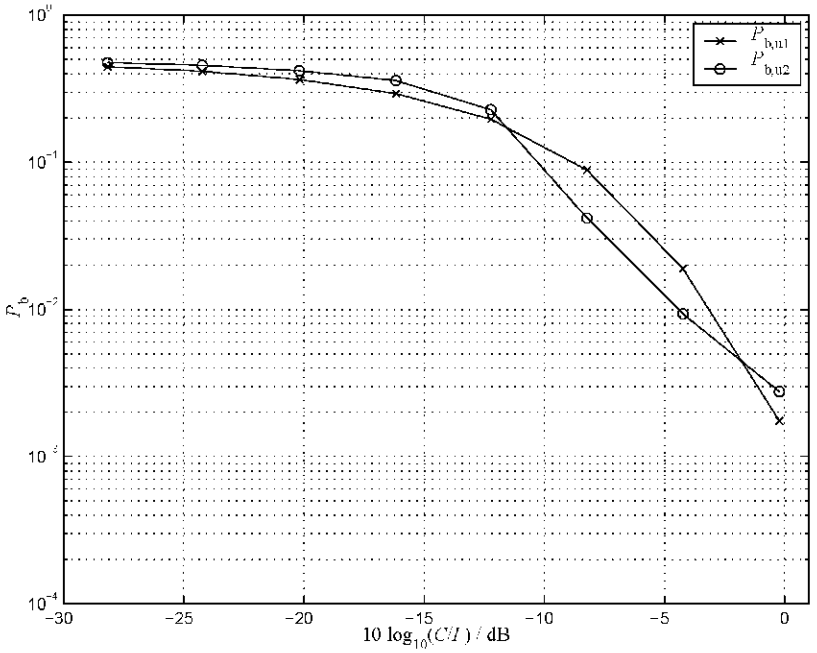

Figure 4.51. Eight users, one antenna, ULA 1, uncoded BER $P_{\mathrm{b,u1}}$ and $P_{\mathrm{b,u2}}$ as a function of C/I with $REL = 20$.

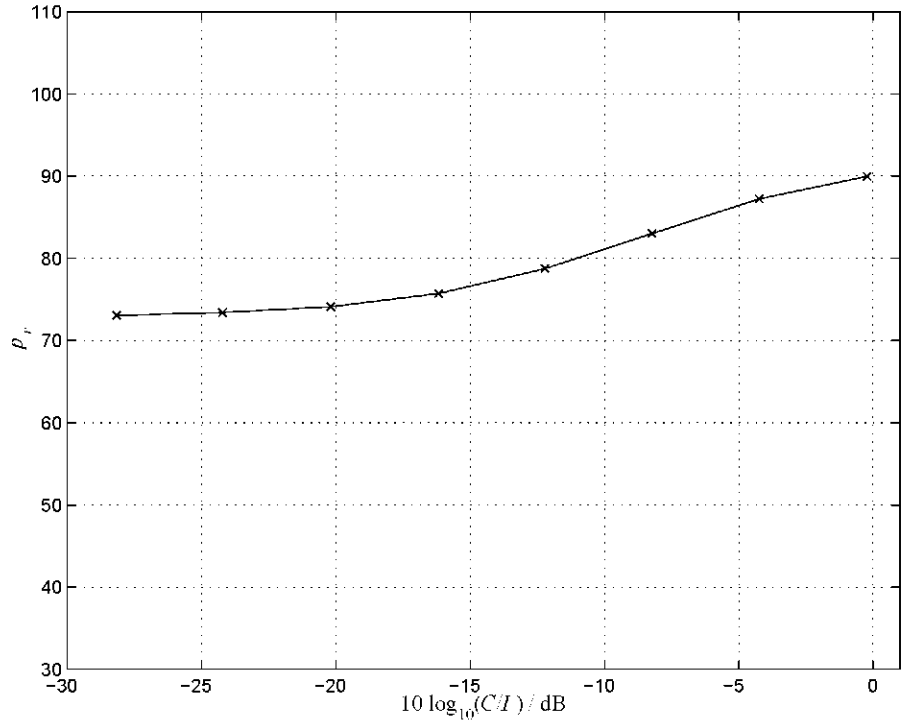

Figure 4.52. Eight users, one antenna, ULA 1, percentage of replacement, p_r, as a function of C/I with $REL = 20$.

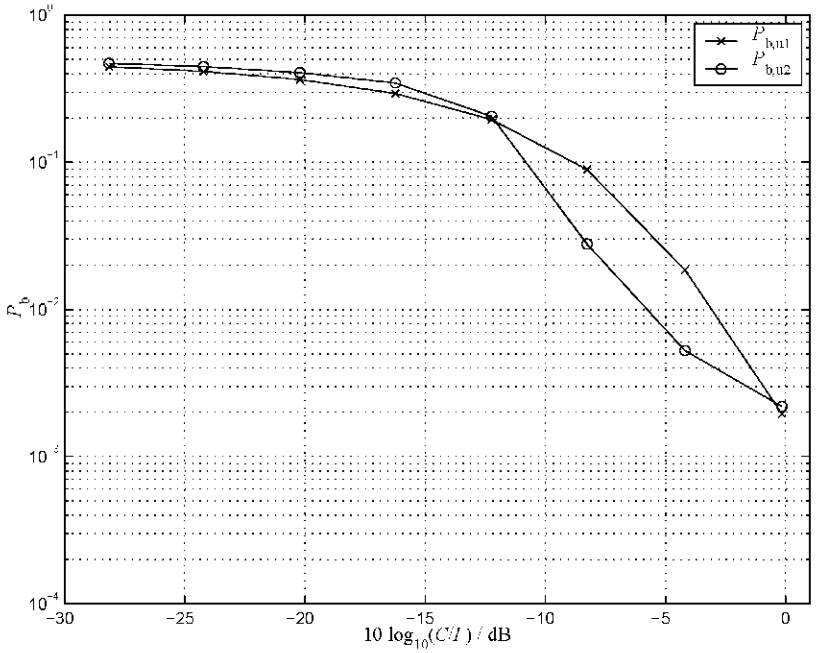

Figure 4.53. Eight users, one antenna, ULA 1, uncoded BER $P_{\mathrm{b,u1}}$ and $P_{\mathrm{b,u2}}$ as a function of C/I with $REL = 15$.

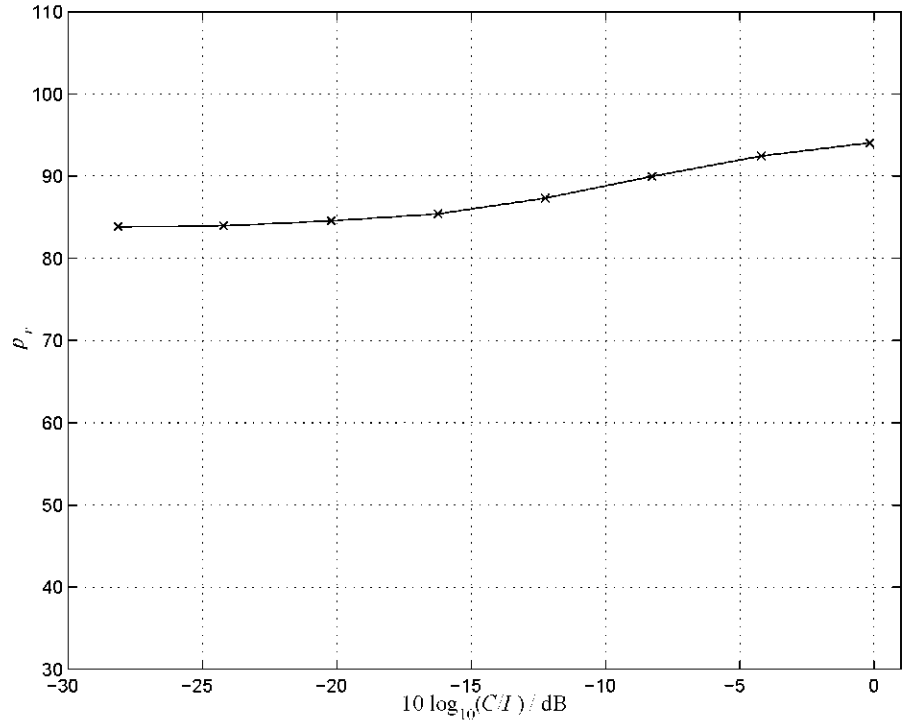

Figure 4.54. Eight users, one antenna, ULA 1, percentage of replacement, p_r, as a function of C/I with $REL = 15$.

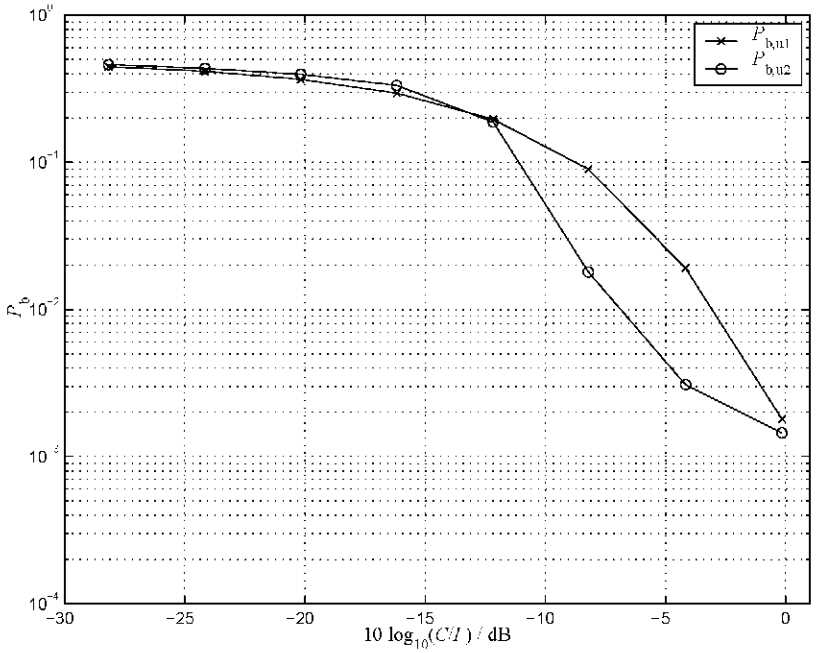

Figure 4.55. Eight users, one antenna, ULA 1, uncoded BER $P_{\mathrm{b,u1}}$ and $P_{\mathrm{b,u2}}$ as a function of C/I with $REL = 10$.

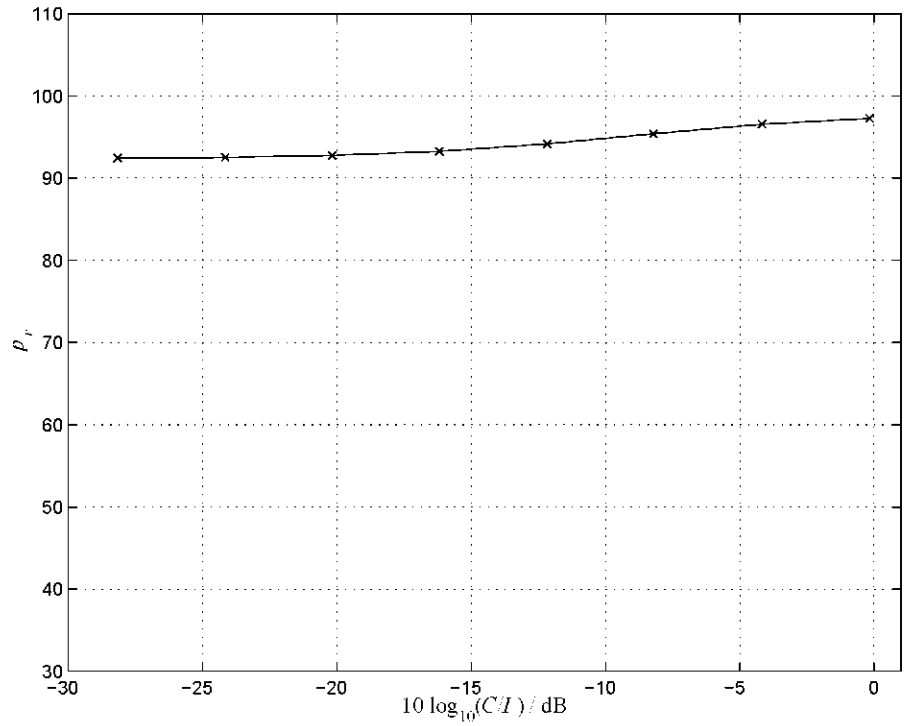

Figure 4.56. Eight users, one antenna, ULA 1, percentage of replacement, p_r, as a function of C/I with $REL = 10$.

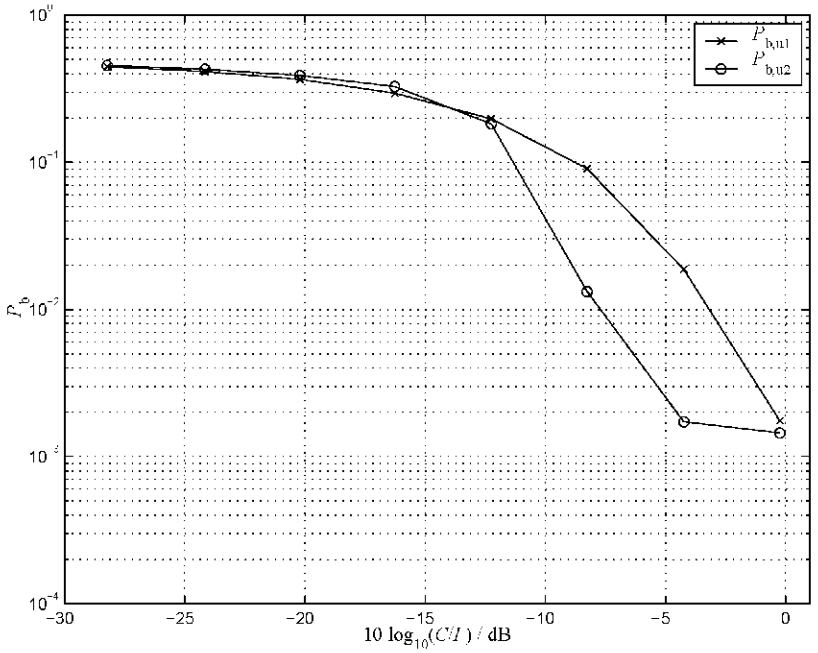

Figure 4.57. Eight users, one antenna, ULA 1, uncoded BER $P_{\mathrm{b,u1}}$ and $P_{\mathrm{b,u2}}$ as a function of C/I with $REL = 5$.

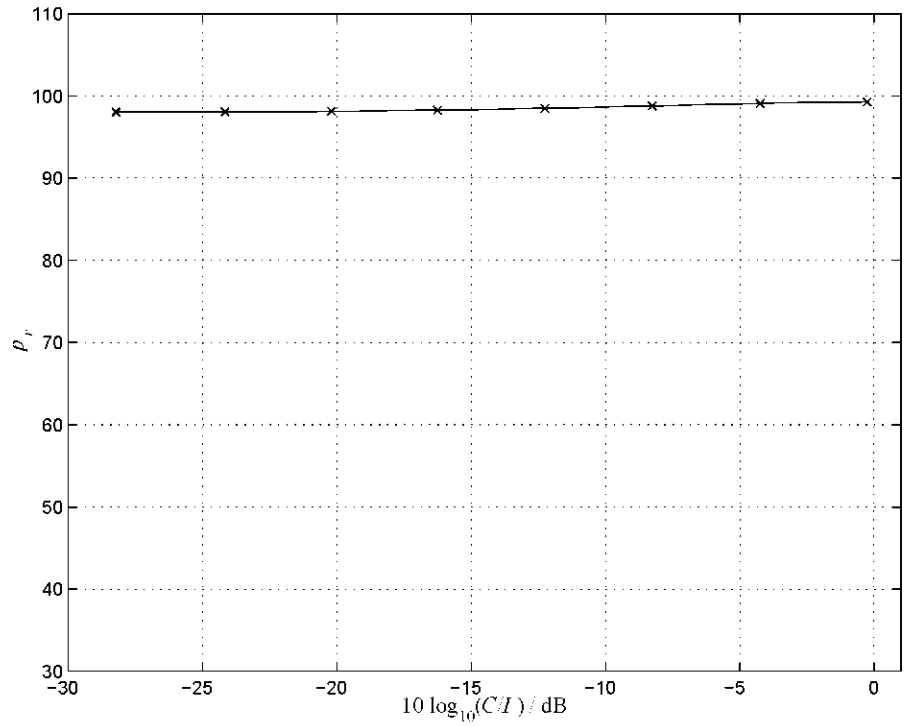

Figure 4.58. Eight users, one antenna, ULA 1, percentage of replacement, p_r, as a function of C/I with $REL = 5$.

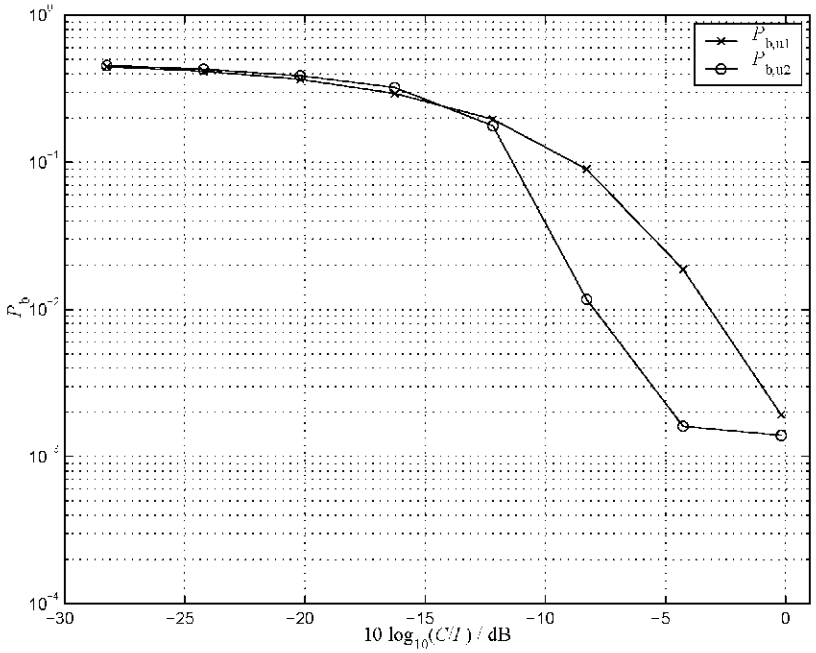

Figure 4.59. Eight users, one antenna, ULA 1, uncoded BER $P_{\mathrm{b,u1}}$ and $P_{\mathrm{b,u2}}$ as a function of C/I with $REL = 1$.

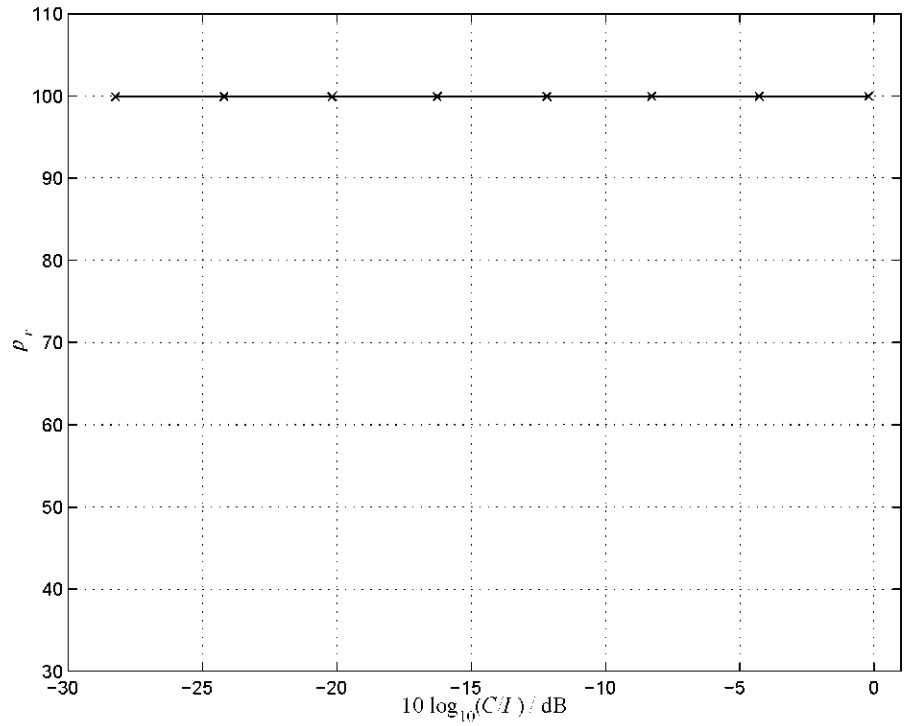

Figure 4.60. Eight users, one antenna, ULA 1, percentage of replacement, p_r, as a function of C/I with $REL = 1$.

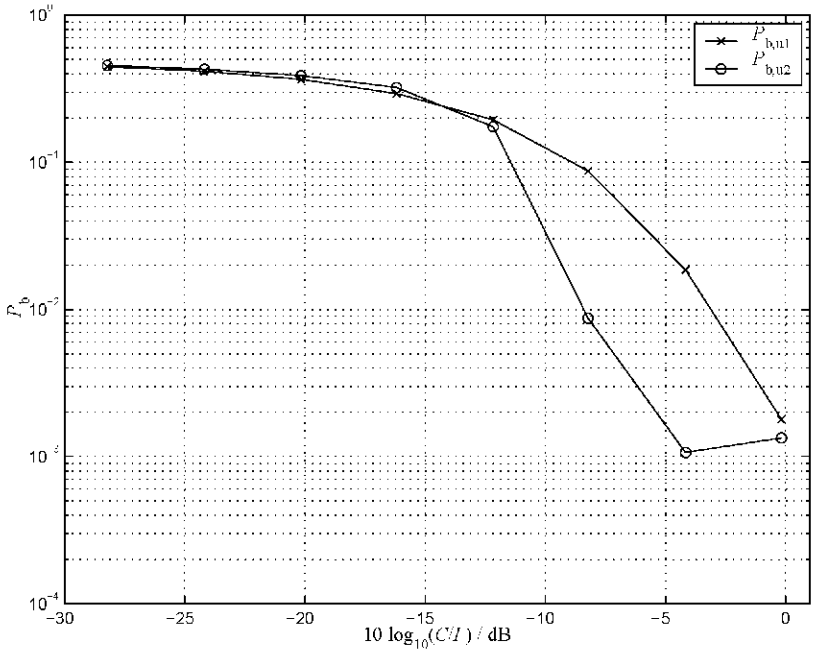

Figure 4.61. Eight users, one antenna, ULA 1, uncoded BER $P_{\mathrm{b,u1}}$ and $P_{\mathrm{b,u2}}$ as a function of C/I with $REL = 0, 5$.

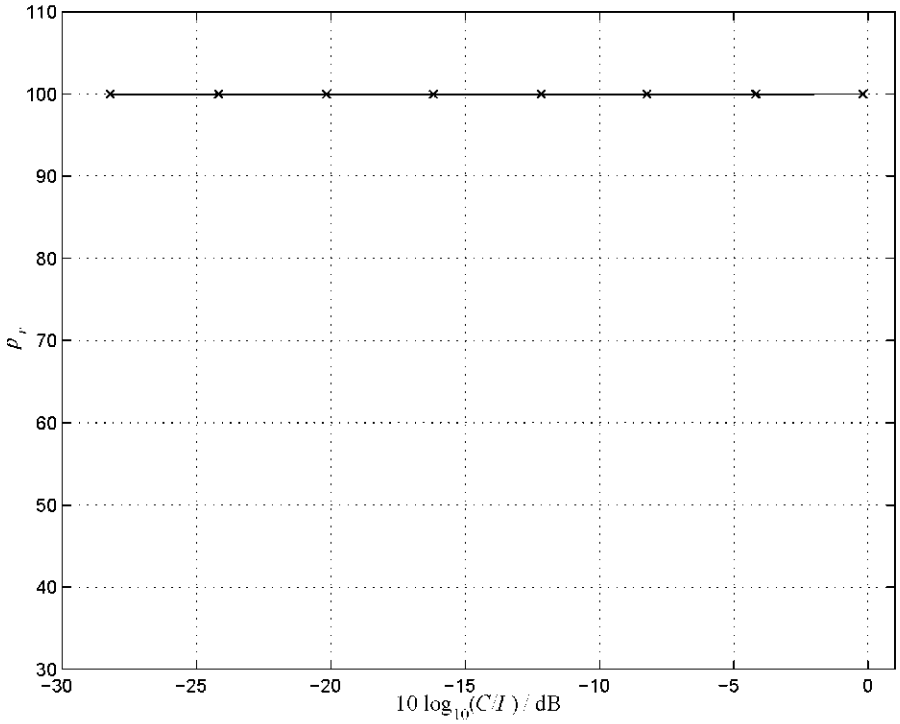

Figure 4.62. Eight users, one antenna, ULA 1, percentage of replacement, p_r, as a function of C/I with $REL = 0, 5$.

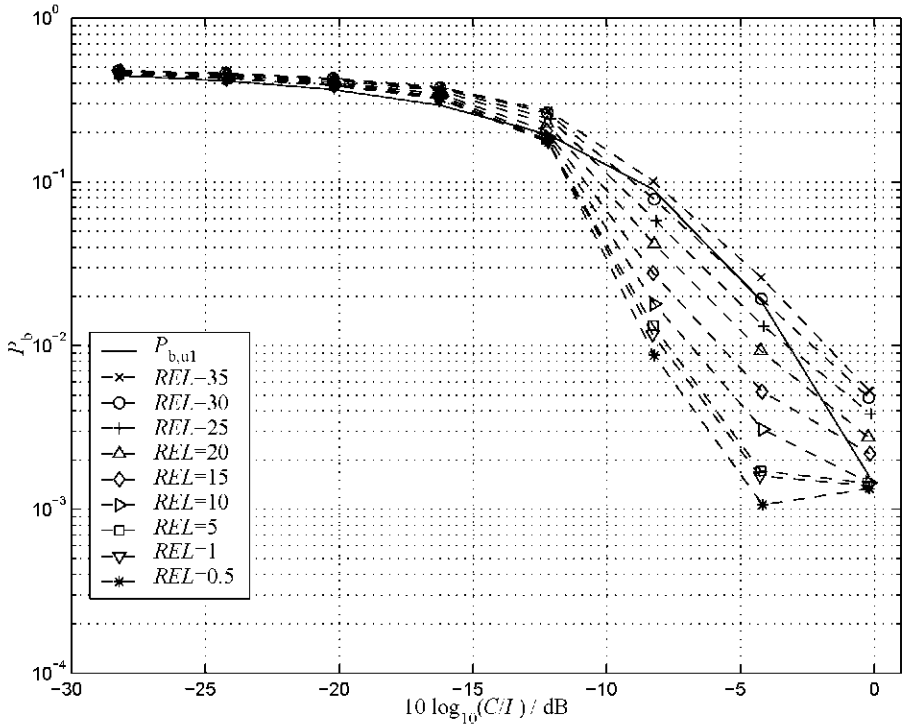

Figure 4.63. Eight users, one antenna, ULA 1, comparison with all the seconds estimations uncoded $P_{\mathrm{b,u2}}$ and a uncoded $P_{\mathrm{b,u1}}$ as a function of C/I.

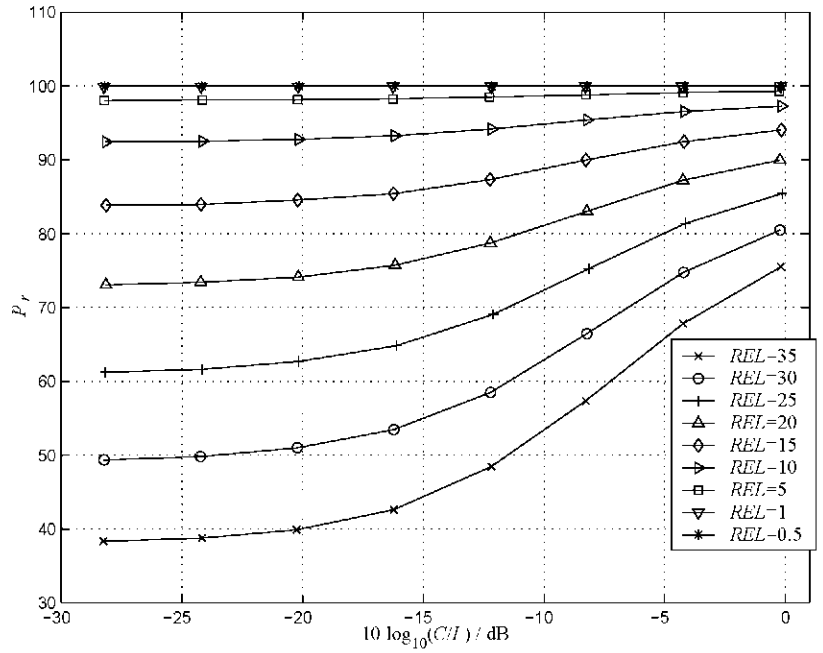

Figure 4.64. Eight users, one antenna, ULA 1, all the percentage of replacements as a function of C/I.

4.2.4 Comparison of the situations results

In this subsection, comparison of the results obtained with the direct interference cancellation receiver are shown. In the Fig. 4.65 the influence of the antennas on the results can be observed for REL equal to 1 and for the three simulated situations. For the situations with four antennas, a shifting to the left of the curves can be observed, due to the JD data estimation principle, that performs better with more than one antenna. By increasing the number K_{a} of antennas the differences of $P_{\mathrm{b,u1}}$ and $P_{\mathrm{b,u2}}$ also increases for the presented receiver. For REL equal to 1 the percentage of replacement is almost 100%, see Fig. 4.20, 4.40 and 4.60. Therefore for four antennas and JD, we obtain an uncoded BER $P_{\mathrm{b,u1}}$ better than for a single antenna, see Fig. 4.65 a) and b), which leads to a better signal $\underline{\hat{\mathbf{e}}}_{\mathrm{r}}$ and finally a lower uncoded BER $P_{\mathrm{b,u2}}$.

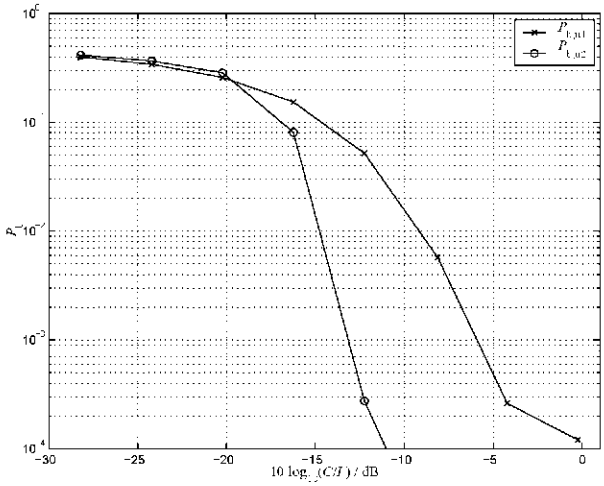

a)

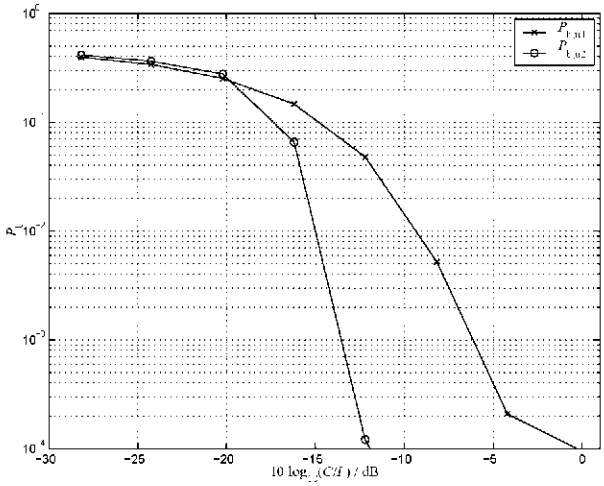

b)

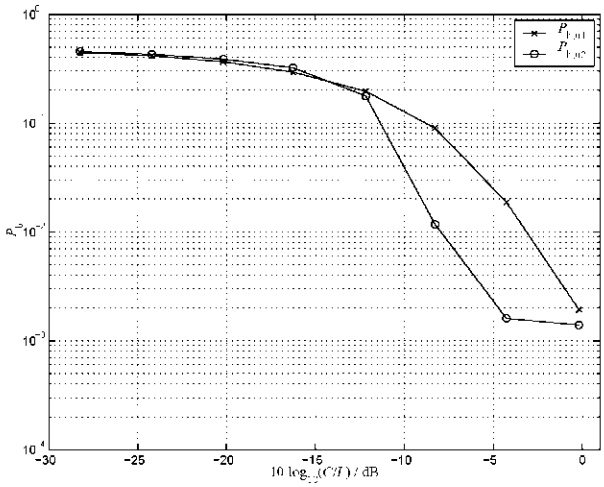

c)

Figure 4.65. a) Eight users four antenna. b) Four users four antenna. c) Eight users one antenna, the uncoded BER $P_{\mathrm{b,u1}}$ and $P_{\mathrm{b,u2}}$ as a function of C/I for REL=1.

4.3 Results with interference cancellation after matched filtering receiver

In this section, the results obtained with the second receiver, which performs interference cancellation after matched filtering, are showed. In the following simulations the initial conditions, like perfect channel estimation, speed and position of the users as well as the same intercell MAI scenario are the same as for the first receiver. The four BER, coded BER $P_{\mathrm{b,c1}}$ and $P_{\mathrm{b,c2}}$, the uncoded BER $P_{\mathrm{b,u1}}$ and $P_{\mathrm{b,u2}}$, will be taken into account in the following figures. Four situation namely, 4 users 8 antennas, 8 user 4 antennas, 4 users 4 antennas, 8 users one antenna, have been simulated. For each situation, a figure shows coded BER $P_{\mathrm{b,c1}}$ and $P_{\mathrm{b,c2}}$ and another figure shows the uncoded BER $P_{\mathrm{b,u1}}$ and $P_{\mathrm{b,u2}}$. At the end of this Section a comparison of all four situations will be presented.

4.3.1 Simulation results considering four users and eight antennas

In this section an improvement of coded BER can be observed, see Fig. 4.66. The coded BER $P_{\mathrm{b,c2}}$ is always lower than the coded BER $P_{\mathrm{b,c1}}$. The curves $P_{\mathrm{b,c1}}$ and $P_{\mathrm{b,c2}}$ are very similar but $P_{\mathrm{b,c2}}$ is shifted to the left, e.g., for P_{b} equal to 10^{-3} there is a improvement of 1 dB. For uncoded BER $P_{\mathrm{b,u1}}$ and $P_{\mathrm{b,u2}}$, see Fig. 4.67, also there is a improvement. The uncoded BER $P_{\mathrm{b,c2}}$ is lower than the uncoded BER $P_{\mathrm{b,c1}}$, for P_{b} equal 10^{-3} the gain of C/I is 1.7 dB.

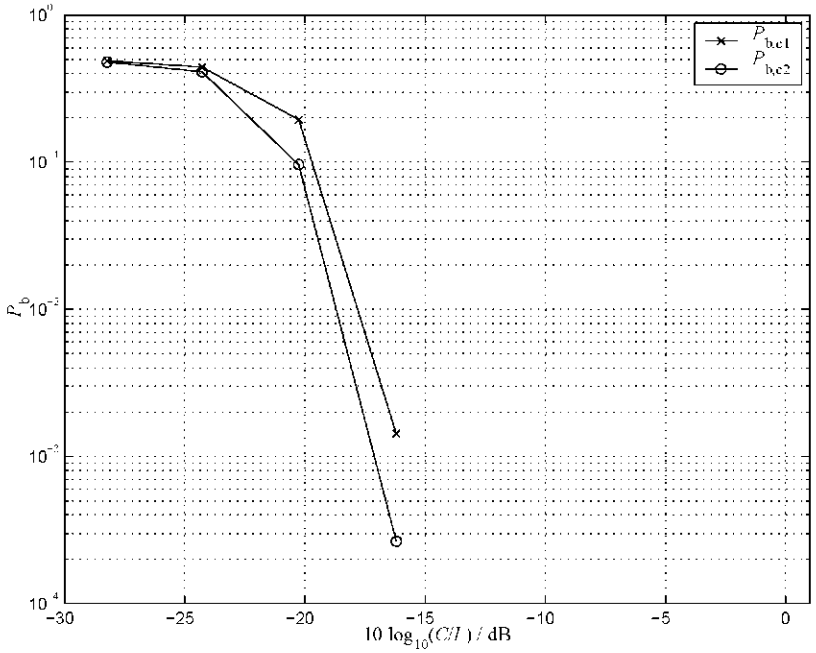

Figure 4.66. Four users, eight antenna, URA 2 2, coded BER $P_{\mathrm{b,c1}}$ and $P_{\mathrm{b,c2}}$ as a function of C/I.

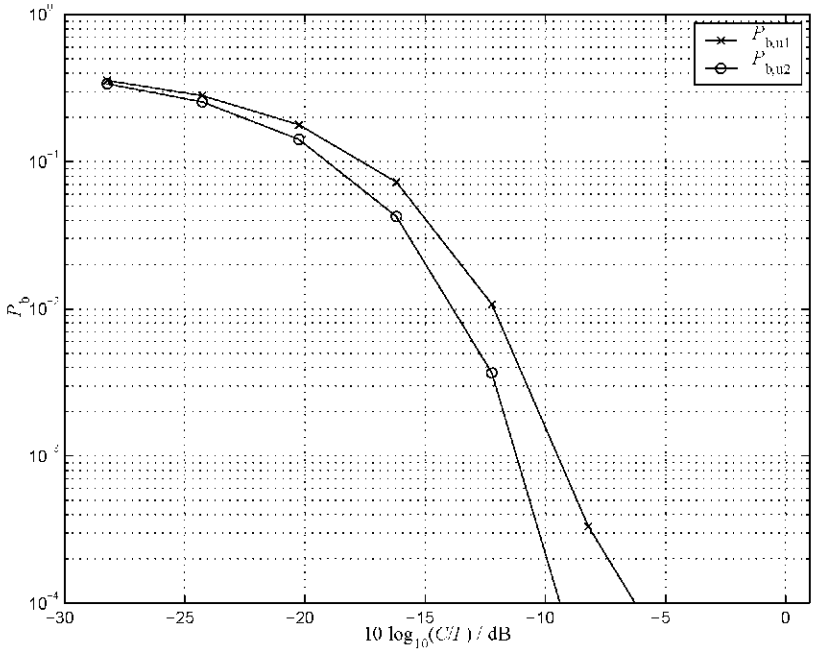

Figure 4.67. Four users, Eight antenna, URA 2 2, uncoded BER $P_{\mathrm{b,u1}}$ and $P_{\mathrm{b,u2}}$ as a function of C/I.

4.3.2 Simulation results considering eight users and four antennas

Performing simulation with eight users and four antennas one can see in Fig. 4.68 that the coded BER $P_{\mathrm{b,c1}}$ and the coded BER $P_{\mathrm{b,c2}}$, are very near to each other in the C/I range from -28 dB to -20 dB. Since C/I is equal to -20 dB, there is a improvement but the gain is smaller than in the previous situation with four users and eight antennas, e.g., for P_{b} equal to 10^{-3} the C/I gain is almost equal to 0.4 dB, which is smaller than in the previous situation. For the uncoded BER $P_{\mathrm{b,u1}}$ and $P_{\mathrm{b,u2}}$, see Fig. 4.69, the curves have a similar tendency compared to the previous situation, with four users and eight antennas, but with a smaller gain. For P_{b} equal to 10^{-3} there is a C/I gain of 1 dB.

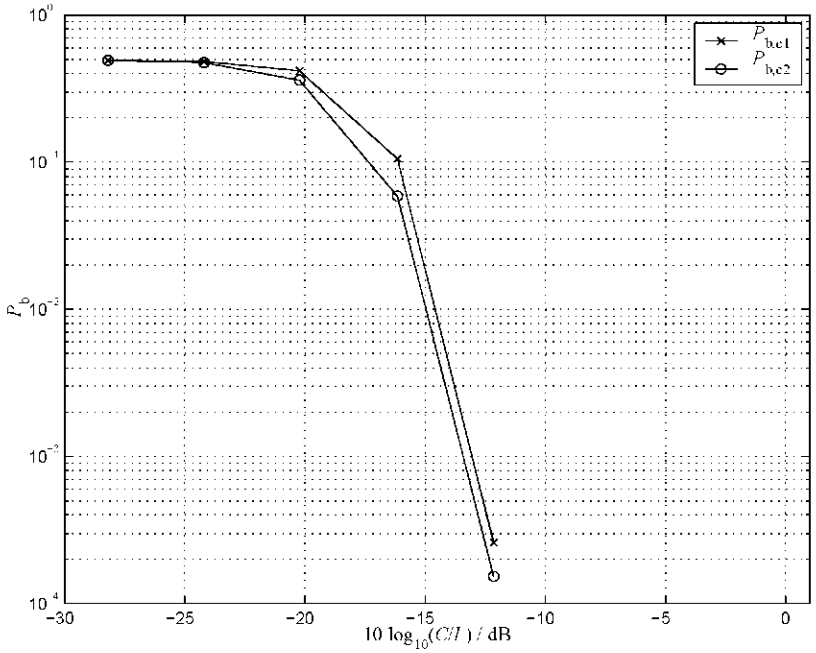

Figure 4.68. Eight users, four antenna, URA 2 2, coded BER $P_{\mathrm{b,c1}}$ and $P_{\mathrm{b,c2}}$ as a function of C/I.

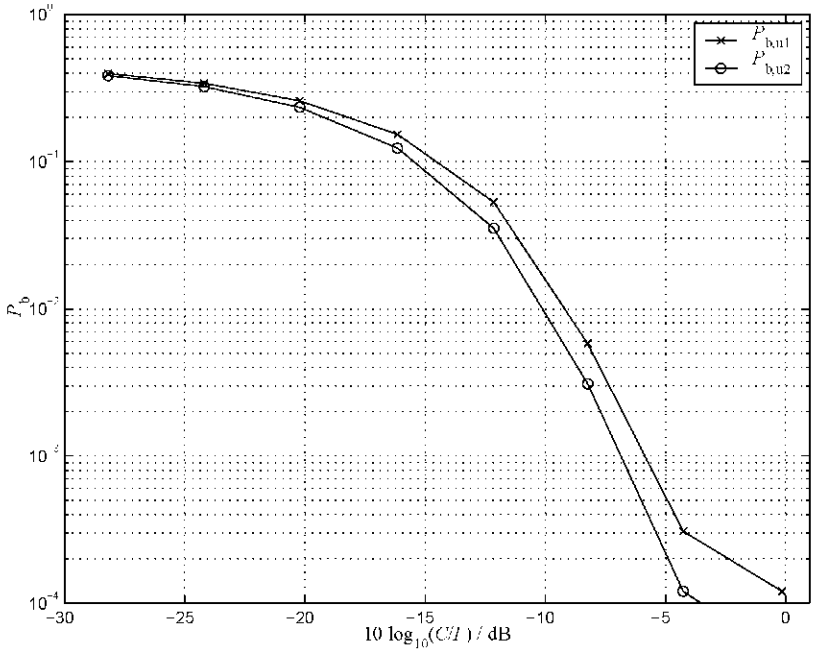

Figure 4.69. Eight users, four antenna, URA 2 2, uncoded BER $P_{\mathrm{b,u1}}$ and $P_{\mathrm{b,u2}}$ as a function of C/I.

4.3.3 Simulation results considering four users and four antennas

In the following figures, see Fig. 4.70 and Fig. 4.71, it can be seen that the curves are similar as in the previous section. From C/I equal to -20 dB there are improvements in both, coded and uncoded BER. For a C/I value less than -20 dB, both curves are almost superimposed. There is a improvement of 0.6 dB for the coded BER $P_{\mathrm{b,c1}}$ and $P_{\mathrm{b,c2}}$. For uncoded BER $P_{\mathrm{b,u1}}$ and $P_{\mathrm{b,u2}}$, the corresponding C/I improvement is almost 1 dB.

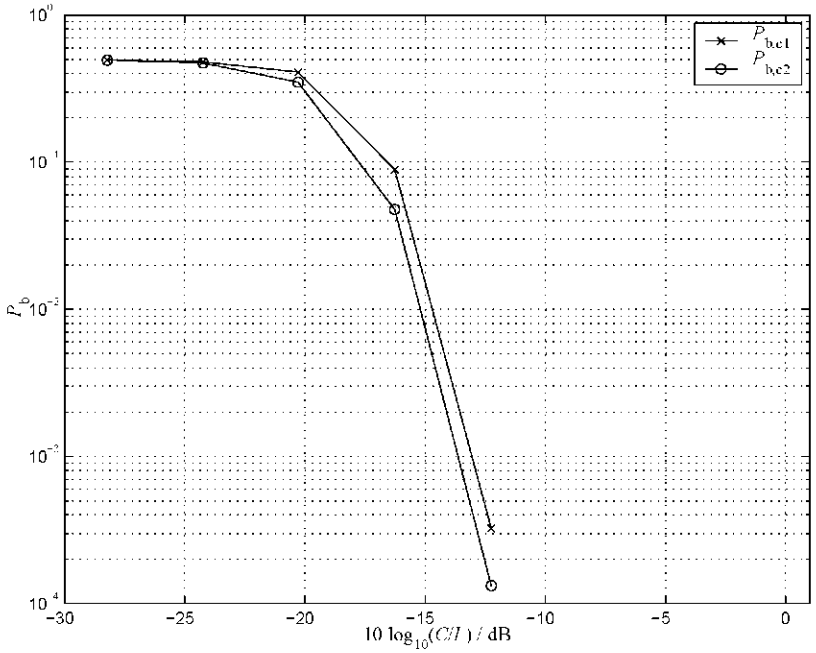

Figure 4.70. Four users, four antenna, URA 2 2, coded BER $P_{\mathrm{b,c1}}$ and $P_{\mathrm{b,c2}}$ as a function of C/I.

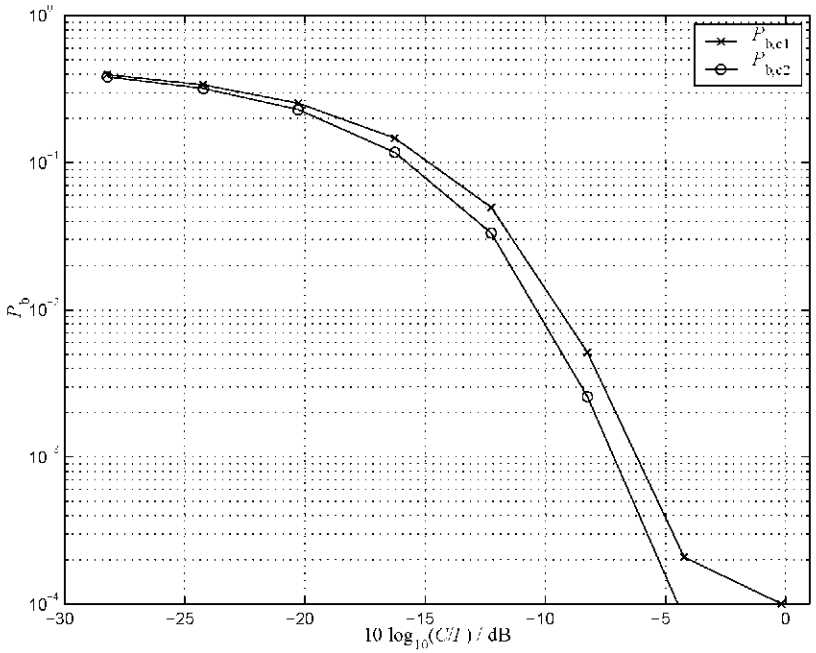

Figure 4.71. Four users, four antenna, URA 2 2, uncoded BER $P_{\mathrm{b,u1}}$ and $P_{\mathrm{b,u2}}$ as a function of C/I.

4.3.4 Simulation results considering eight users and one antenna

With only one antenna, there are no improvements for the coded and uncoded BER, see Fig. 4.72 and 4.73. This situation is the worst case because there is no gain of C/I ratio for any BER.

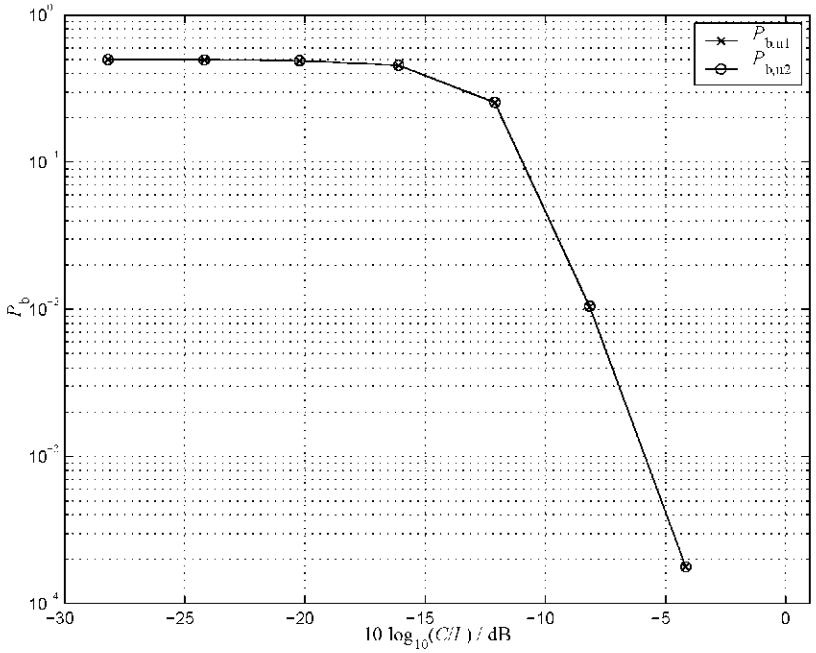

Figure 4.72. Eight users, one antenna, ULA 1, coded BER $P_{\mathrm{b,c1}}$ and $P_{\mathrm{b,c2}}$ as a function of C/I.

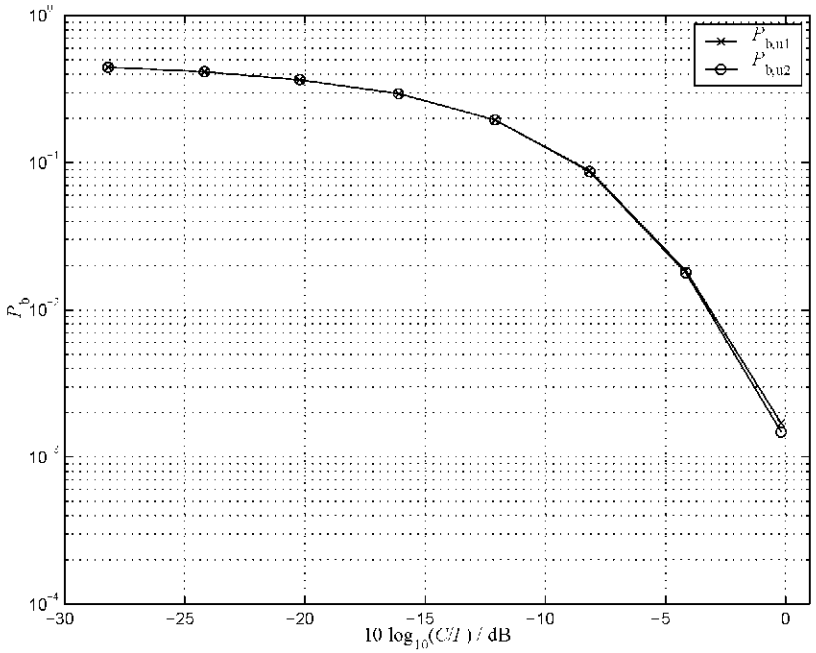

Figure 4.73. Eight users, one antenna, ULA 1, uncoded BER $P_{\mathrm{b,u1}}$ and $P_{\mathrm{b,u2}}$ as a function of C/I.

4.3.5 Comparison of all the results

From the Fig 4.74 and Fig. 4.75 one can observe the influence of the number of antennas on the BER performance. For a single antenna, see Fig. 4.74 d) and Fig. 4.75 d), the curves are less shifted to the left than for four and eight antennas, see Fig. 4.74 a), b), c) and Fig. 4.75 a), b) c). This is due to the data estimation principle JD, which performs better with more than one antenna. The differences of the uncoded BER $P_{\mathrm{b,u1}}$ and $P_{\mathrm{b,u2}}$ result from the principle of the interference cancellation after the matched filtering block. For more antennas, by JD, see Fig. 4.74, the coded BER $P_{\mathrm{b,c1}}$ is better, therefore the signal reconstruction have less errors. With the matched filter are obtained a data, that comparing with the estimated data after FEC-coding and interleaving $\underline{\hat{\mathbf{d}}}_{\mathrm{FEC}}$ leads to a modified signal $\underline{\mathbf{e}}_{\mathrm{mo}}$, with a better second data estimation and subsequently a lower uncoded BER $P_{\mathrm{b,u2}}$. In the second estimation we will take advantage of the estimated spatial interference covariance matrix $\underline{\mathbf{R}}_{\mathrm{s}}$ and together with JD we will obtain a better coded BER $P_{\mathrm{b,c2}}$ than in the first estimation. With only one single antenna, the coded BER $P_{\mathrm{b,c1}}$ is quite worst, see Fig. 4.74, which leads to a worst signal reconstruction, thus in the interference cancellation after matched filtering, errors are compared with errors which leads to obtain a modified signal $\underline{\mathbf{e}}_{\mathrm{mo}}$ very similar to the received signal $\underline{\mathbf{e}}$. Therefore we will have an uncoded BER $P_{\mathrm{b,c2}}$ very similar to the first one $P_{\mathrm{b,c1}}$. Using only one antenna, we can not use $\underline{\mathbf{R}}_{\mathrm{s}}$ and as in the first receiver with direct interference cancellation, the coded BER $P_{\mathrm{b,c2}}$ will be the same than the coded BER $P_{\mathrm{b,c1}}$ of the first data estimation.

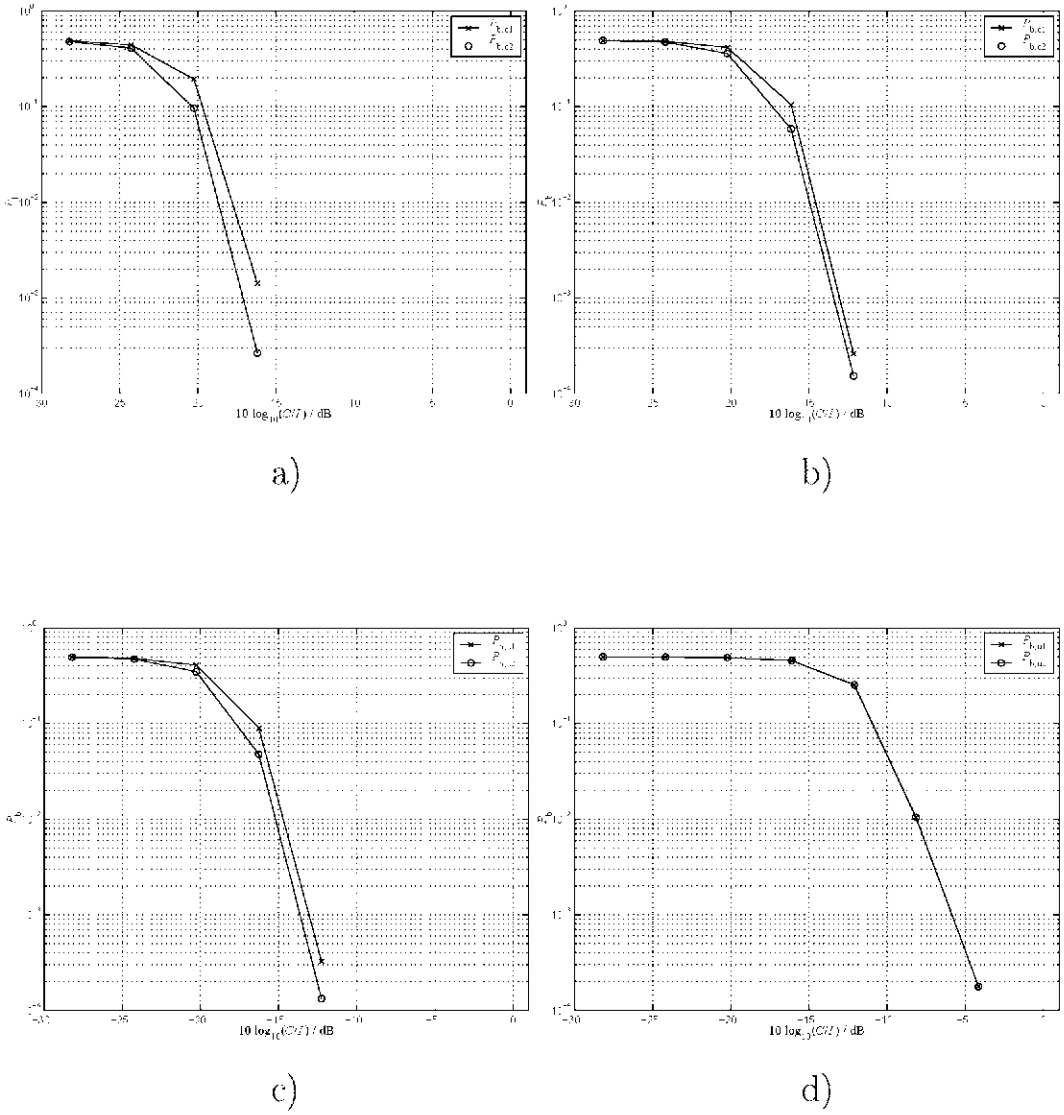

Figure 4.74. a) Four users eight antenna. b) Eight users four antenna. c) Four users four antenna. d) Eight users one antenna, uncoded BER $P_{\mathrm{b,c1}}$ and $P_{\mathrm{b,c2}}$ as function of C/I.

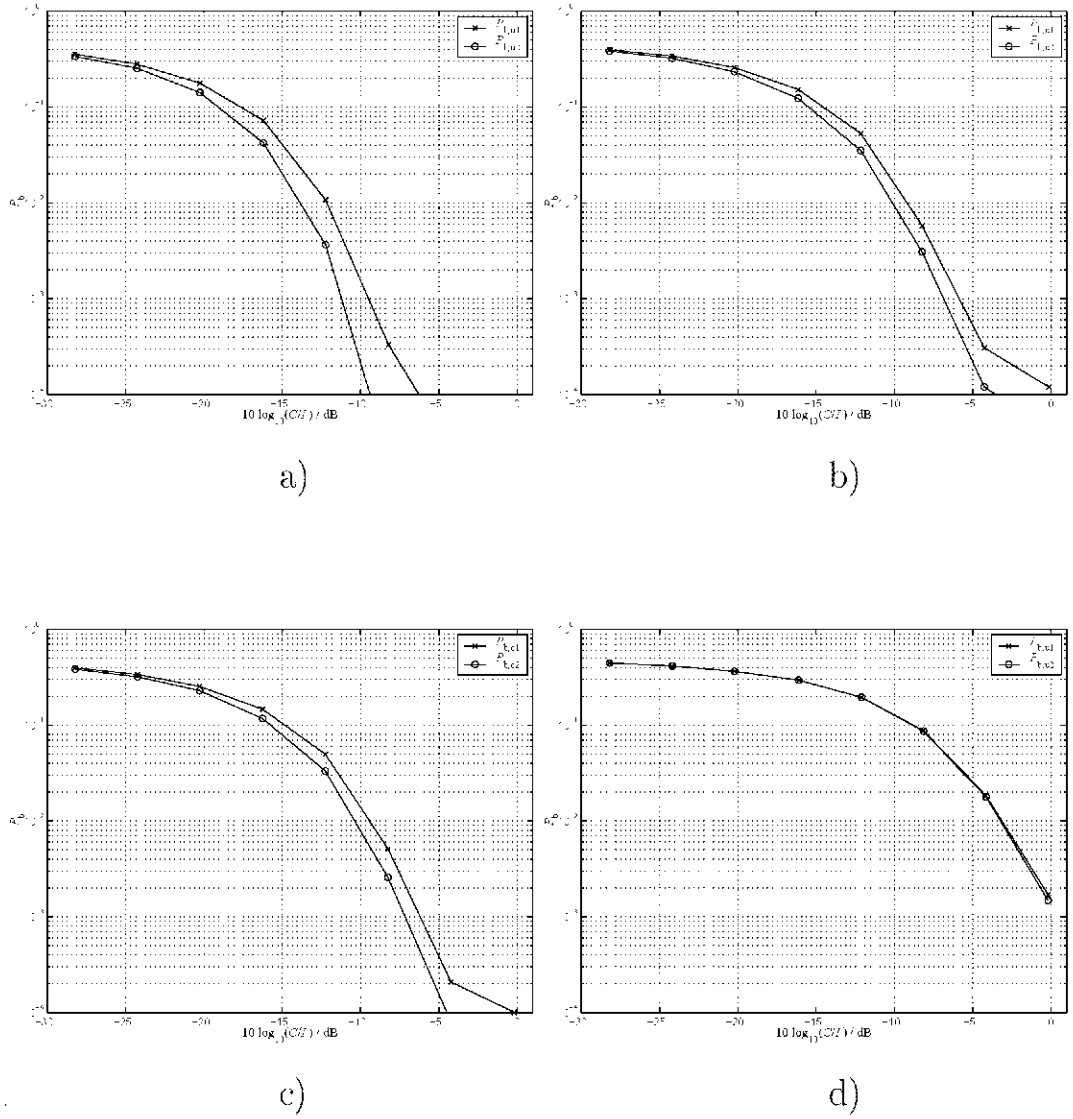

Figure 4.75. a) Four users eight antenna. b) Eight users four antenna. c) Four users four antenna. d) Eight users one antenna, uncoded BER $P_{\mathrm{b,u1}}$ and $P_{\mathrm{b,u2}}$ as function of C/I.

5 Conclusions

In this thesis, simulation results of the uplink of a TD-CDMA mobile system with JD and two novel receiver structures for the interference cancellation have been presented. The first interference cancellation principle, which is called direct interference cancellation, compares the received signal with a reconstructed signal based on a conventional joint data detection. High differences of received and reconstructed signal are supposed to indicate the presents of high noise levels. In this cases the received signal is replaced by the reconstructed signal to generate a modified signal, which is finally detected once again. The second interference cancellation principle is quite similar to the first one. Only the comparision of the received signal and the reconstructed one is not done chip by chip, but it is done symbol by symbol after matched filtering the received signal and comparing the matched filter signal with the detected data under consideration of FEC-coding. The benefits of using the interference cancellator after matched filtering the recived signals as well as the direct interference cancellation have been demostrated by evaluating the BER. The simulation results show that only improvement of the uncoded BER but not of the coded BER can be achieved. Both receivers performs better and shows further improvements of the uncoded BER, if the number of antennas is increased.

Since an improvement of uncoded BER is achieved with both interference cancellation principles, one would expect also an improvement of the coded BER, which can not be observed. The reason for this lies in the distribution of errors in the reconstruction of errors in the reconstructed signal. The error in the reconstructed signal appear often in burst. Therefore, the FEC-decoder can not eliminate these errors. Changing the error distribution in the transmitted signal, e.g. by addittional interleaving, could cope with this problem. But in this case a corresponding interleaving or deinterleaving must already be done on the transmitter side. Further simulation results show that the consideration of the estimated interference covarince matrix $\hat{\underline{\mathbf{R}}}_s$ in the second data detection improves even the coded BER, but this improvement is not achieved by the interference cancellation concepts.

Bibliography

[ARY95] J. B. Andersen, T. S. Rappaport and S. Yoshida, "Propagation measurements and models for wireless communications channels", IEEE Communications Magazine, vol. 33, pp. 42-49, Jan 1995.

[Bai94] P.W. Baier, "CDMA or TDMA? CDMA for GSM? ", Proc. IEEE International Symposium on Personal, Indoor and Mobile Radio Communications (PIMRC '94), Den Haag, 1994, S. 1280 - 1284.

[BKN94] J.J. Blanz, A. Klein, M.M. Nashan, A.Steil, "Performance of a Cellular hybrid C/TDMA mobile radio system applying joint detection and coherent receiver antenna diversity", IEEE Journal on Selected Areas in Communications, vol. 12, pp. 568 - 579 May 1994.

[BPH] J.J. Blanz, A. Papathanassiou, M. Haardt, I. Furió, P.W. Baier, "Smart antennas for combined DOA and joint channel estimation in time–slotted CDMA mobile radio systems with joint detection", submitted for publication in the IEEE Transactions on Vehicular Technology.

[COST99] "Digital mobile radio channels towards future generations systems", COST action 231, Final Report, Brussels, 1999.

[ECSR98] R.B. Ertel, P. Cardieri, K.W. Sowerby, T.S. Rappaport, J.H. Reed, "Overview of spatial channel models for antenna array communications systems", IEEE Personal Communications, 1998, pp. 10-21.

[ETSI97] ETSI SMG2#24, "WB TDMA/CDMA System description performance evaluation," Tdoc SMG2 368/97, Cork, 1997.

[FBK93] T. Felhauer, P.W. Baier, W. König, W. Mohr, "Optimized wideband system for unbiased mobile radio channel sounding with periodic spread spectrum signals," IEICE Transactions on Communications, vol. E76-B, 1993, pp. 1016–1029.

[ITU98] "TD-SCDMA Radio transmission technology for IMT-2000 ", Proposal to ITU for G3 RTT, 1998. http://www.itu.int/imt/2_rad_devt/proposals/chs/3gdoc04.pdf.

[JCN95] B. Jabbari, G. Colombo, A. Nakajima and J. Kulkarni, "Network issues for wireless communications", IEEE Communications Magazine, vol 33, pp 88-98, Jan 1995.

[JS95] P. Jung, B. Steiner, "A joint detection CDMA mobile radio system concept developed within COST 231", Proc. IEEE 45th International Vehicular Technology Conference (VTC'95), Chicago, 1995, pp. 469–473.

[KB93] A. Klein, P.W. Baier, "Linear unbiased data estimation in mobile radio systems applying CDMA", IEEE Journal on Selected Areas in Communications, vol. 11, 1993, pp. 1058–1066.

[Kit94] L. Kittel, "Bewertung von Mobilfunkvorhaben ", Proc. Aachener Kolloquium signaltheorie, Aachen, 1994.

[Kl96] A. Klein, "Multi-user detection of CDMA signals algorithms and their application to cellular mobile radio", Düsseldorf: VDI Verlag, Fortschrittberichte VDI, Reihe 10, Nr. 423, 1996.

[Koh94] R. Kohno, "Spatial and temporal filtering for co-channel interference in CDMA ", Proc. International Symposium on Spread Spectrum Techniques and Applications, Oulu, 1994.

[Lor93] R. W. Lorenz, "Vergleich der digitalen Mobilfunksysteme in Europa (GSM) und in Japan (JDC) unter besonderer Berücksichtigung der Wirtsschaftlichkeitsaspekte ", Der Fernmelde-Ingenieur, 1993.

[LP96] J.Liberti, T. Pappaport, "A geometrically based model for line-of-sight multipath radio channels", Proc. IEEE 46th International Vehicular Technology Conference (VTC'96), Atlanta, 1996, pp. 844-848.

[LR98] J. C. Liberti Jr., T. S. Rappaport, "Smart antennas for wireless communications IS-95 and third generation CDMA applications, ", Prentice Hall, 1998.

[MoP92] M. Mouly and M.-B. Paulet, "The GSM system for mobile communications ", Published by the authors, ISBN 2-9507190-0-7, 1992.

[MSW97] J. Mayer, J. Schlee, and T. Weber, "Realtime feasibility of joint detection CDMA", Proc. 2nd European Personal Mobile Communications Conference (EPMCC'97), Bonn, 1997, pp. 245 252.

[NB98] O. Norklit, J. Bach Andersen, "Diffuse channel model and experimental results for array antennas in mobile environments", IEEE Transactions on Antennas and Propagation, 1998, pp. 834-840.

[PGH95] J. E. Padgett, C. G. Günter and T. Hattori, "Overview of wireless personal comunications", IEEE Communications Magazine, vol.33, pp.28-41, Jan 1995.

[PHF97] A. Papathanassiou, M. Haardt, I. Furió, J.J. Blanz, "Multi-user direction of arrival and channel estimation for time-slotted CDMA with joint detection", Proc. IEEE International Conference on Digital Signal Processing (DSP'97), Santorini, 1997, pp. 375 378.

[PMF98] K.I. Pedersen, P.E. Mogensen, B.H. Fleury, "Spatial channel characteristics in outdoor environments and their impact on BS antenna system performance", Proc. IEEE 48th International Vehicular Technology Conference (VTC'98), Ottawa, 1998, pp. 719-724.

[Poh99] T. Pohlen, "Implementieren neuartiger realisierbarer Verfahren zum Ausnutzen räumlicher Inhomogenitäten von Nutz-und Störsignalen in picozellularer Umgebung", Diploma thesis, University of Kaiserslautern, 1999.

[Pro89] J. G. Proakis, "Digital communications ", New York, McGraw-Hill, 1989.

[Rap96] T. S. Rappaport, "Wireless comunications: Principles and Practice ", Prentice Hall, 1996.

[Rec88] CEPT/CCH/GSM Reccommendations, series 1-12, 1988.

[RK89] R. Roy, T. Kailath, "ESPRIT–Estimation of Signal Parameters via Rotational Invariance Techniques", IEEE Trans. Acoust., Speech, Signal Processing, vol. 37, 1989, pp. 984-995.

[SaG91] A. Salmasi and K. S. Gilhousen, "On the system design aspects of code division multiple access (CDMA) applied to digital cellular and personal communication networks", in Proc. Vehicular Technology Conference, St Louis, 1991.

[SB97] R. Schmalenberger, J. Blanz, "Multi antenna C/I balancing in the downlink of digital cellular mobile radio systems", Proc. IEEE 47th Vehicular Technology Conference (VTC'97), Phoenix, 1997, pp. 607–611.

[SJ94] B. Steiner and P.Jung, "Optimum and suboptimum channel estimation for the uplink of CDMA mobile radio systems with joint detection", European Transactions on Telecommunications and Related Techniques, vol. 5, 1994, pp.39-50.

[Wec99] M. Weckerle, "Adaptive Antennenkonzepte für TD-CDMA in kleinen Zellen", Research report, University of Kaiserslautern, Kaiserslautern, 1999.

[WP99] M. Weckerle, A. Papathanassiou "Performance analysis of multi-antenna TD-CDMA receivers with estimation and consideration of the interference covariance matrix", International Journal of Wireless Information Networks, vol 6, no. 3, 1999.

[WPE98] M. Weckerle, A. Papathanassiou, D. Emmer, "The benefits of intelligent antenna arrays in TD-CDMA a study based on measured channel impulse responses", Proc. IEEE 9th International Symposium on Personal, Indoor and Mobile Radio Communications (PIMRC'98), Boston, 1998, pp. 962-966.

[YL98] N. Yee, J.P. Linnartz, "Multicarrier CDMA in an Indoor Wireless radio channel", University of California, 1998.
http://diva.eecs.berkeley.edu/~linnatz/MCCDMA.html.

A Matched Filter

In this Apendix, the linear data detector based on the decorrelating MF is derived.In the following diag() and $\overline{\text{diag}()}$ belongs to a diagonal matrix containig only the diagonal elements of the matrix and matrix with zero diagonal elements containing all but the diagonal elements, respectively. The DMF consist of a prewhitening or decorrelating filter and a MF followed by symbol-rate samplers [KKB.JuB95].

The DMF maximizes the SNR of the data estimates $\hat{\underline{\mathbf{d}}}_n, n = 1...KN$, at its output while neglecting perturbation due to ISI and MAI, The data estimate of the combined data vector $\underline{\mathbf{d}}$ determined by the DMF is

$$\begin{aligned} \hat{\underline{\mathbf{d}}} &= (\text{diag}(\underline{\mathbf{A}}^{*\text{T}}\underline{\mathbf{R}}_{\text{n}}{}^{-1}\underline{\mathbf{A}}))^{-1}\underline{\mathbf{A}}^{*\text{T}}\underline{\mathbf{R}}_{\text{n}}{}^{-1}\underline{\mathbf{e}} \\ &= (\text{diag}(\underline{\mathbf{A}}^{*\text{T}}\underline{\mathbf{R}}_{\text{n}}{}^{-1}\underline{\mathbf{A}}))^{-1}(\underline{\mathbf{L}}\underline{\mathbf{A}})^{*\text{T}}\underline{\mathbf{L}}\underline{\mathbf{e}}, \end{aligned} \tag{A.1}$$

with the Cholesky descomposition [Mar87,ZuF84]

$$\underline{\mathbf{R}}_{\text{n}}{}^{-1} = \underline{\mathbf{L}}^{*\text{T}}\underline{\mathbf{L}} \tag{A.2}$$

of $\underline{\mathbf{R}}_{\text{n}}{}^{-1}$. $\underline{\mathbf{L}}$ is an upper triangular matrix [Mar87] of dimension $(NQ+W-1)\times(NQ+W-1)$ and $\underline{\mathbf{A}}$ is the system matrix. The operation $\underline{\mathbf{L}}\underline{\mathbf{e}}$ decorrelates, i.e., prewhitens the noise vector $\underline{\mathbf{n}}$ contained in $\underline{\mathbf{e}}$. The vector $\underline{\mathbf{L}}\underline{\mathbf{e}}$ is fed into a filter represented by $(\text{diag}(\underline{\mathbf{A}}^{*\text{T}}\underline{\mathbf{R}}_{\text{n}}{}^{-1}\underline{\mathbf{A}}))^{-1}(\underline{\mathbf{L}}\underline{\mathbf{A}})^{*\text{T}}$ which is matched to the concatenation of the K channels with combined channel impulse responses $\underline{\mathbf{b}}^{(k,k_{\text{a}})}, k = 1...K, k_{\text{a}} = 1...K_{\text{a}}$. The data estimate $\hat{\underline{\mathbf{d}}}$, consist of three contributions:

$$\hat{\underline{\mathbf{d}}} = \underline{\mathbf{d}} + (\text{diag}(\underline{\mathbf{A}}^{*\text{T}}\underline{\mathbf{R}}_{\text{n}}{}^{-1}\underline{\mathbf{A}}))^{-1}\overline{\text{diag}}(\underline{\mathbf{A}}^{*\text{T}}\underline{\mathbf{R}}_{\text{n}}{}^{-1}\underline{\mathbf{A}})\underline{\mathbf{d}} + (\text{diag}(\underline{\mathbf{A}}^{*\text{T}}\underline{\mathbf{R}}_{\text{n}}{}^{-1}\underline{\mathbf{A}}))^{-1}\underline{\mathbf{A}}^{*\text{T}}\underline{\mathbf{R}}_{\text{n}}{}^{-1}\underline{\mathbf{n}}. \tag{A.3}$$

Where $(\text{diag}(\underline{\mathbf{A}}^{*\text{T}}\underline{\mathbf{R}}_{\text{n}}{}^{-1}\underline{\mathbf{A}}))^{-1}\overline{\text{diag}}(\underline{\mathbf{A}}^{*\text{T}}\underline{\mathbf{R}}_{\text{n}}{}^{-1}\underline{\mathbf{A}})\underline{\mathbf{d}}$ is the ISI and MAI contribution and $(\text{diag}(\underline{\mathbf{A}}^{*\text{T}}\underline{\mathbf{R}}_{\text{n}}{}^{-1}\underline{\mathbf{A}}))^{-1}\underline{\mathbf{A}}^{*\text{T}}\underline{\mathbf{R}}_{\text{n}}{}^{-1}\underline{\mathbf{n}}$ is the noise.

The DMF maximizes the SNR of the data estimates $\hat{\underline{\mathbf{d}}}$ at the output while neglecting perturbation due to ISI and MAI. Thus, the DMF maximizes the SNR for one single transmitted data symbol $\hat{\underline{\mathbf{d}}}_n, n = 1...KN$.

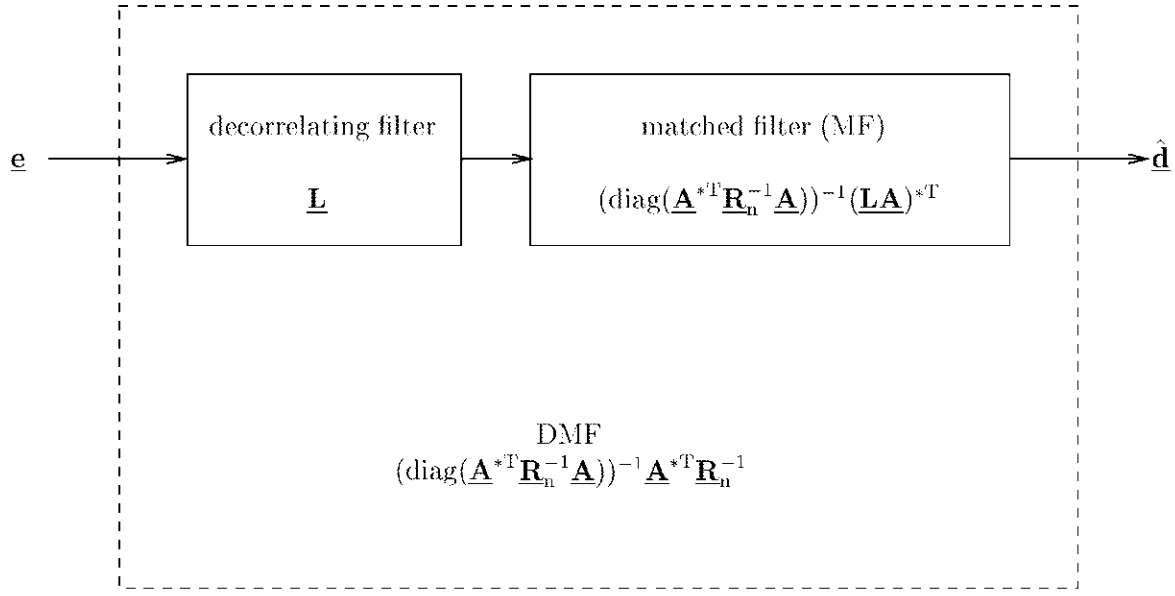

Figure A.1. Structure of the DMF

For the special case of uncorrelated noise characterized by $\underline{\mathbf{R}}_{\mathrm{n}}$ equal to $\sigma^2\mathbf{I}$, the data estimates determined by the DMF according to (A.1) becomes

$$\hat{\underline{\mathbf{d}}} = (\mathrm{diag}(\underline{\mathbf{A}}^{*\mathrm{T}}\underline{\mathbf{A}}))^{-1}\underline{\mathbf{A}}^{*\mathrm{T}}\underline{\mathbf{e}}. \tag{A.4}$$

In this case, the DMF is reduced to the conventional MF reciver consisting of a bank of K MFs, matched to the combined channel impulse responses $\underline{\mathbf{b}}^{(k,k_{\mathrm{a}})}, k = 1...K, k_{\mathrm{a}} = 1...K_{\mathrm{a}}$.

The computational complexity of the DMF defined by (A.1) is investigated. The computational complexity strongly depends on the effort required to determine $\underline{\mathbf{R}}_{\mathrm{n}}{}^{-1}$. Important special case $\underline{\mathbf{R}}_{\mathrm{n}}$ equal to $\sigma^2\mathbf{I}$ given by (B.1) shall be investigated in more detail. In this case, no effort is required to determine $\underline{\mathbf{R}}_{\mathrm{n}}{}^{-1}$. Firstly, the matrix $\underline{\mathbf{A}}^{*\mathrm{T}}$ or, equivalently, $\underline{\mathbf{A}}$ has to be determined, which requires the calculation of the KK_{a} combined channel impulse responses $\underline{\mathbf{b}}^{(k,k_{\mathrm{a}})}, k = 1...K, k_{\mathrm{a}} = 1...K_{\mathrm{a}}$, each of which is the convolution of the user-specific CDMA code $\underline{\mathbf{c}}^{(k)}$ and the channel impulse response $\underline{\mathbf{h}}^{(k,k_{\mathrm{a}})}$. Secondly, the matrix-vector multiplication $\underline{\mathbf{A}}^{*\mathrm{T}}\underline{\mathbf{e}}$, cf. (B.1), has to be carried out. The weighting by the diagonal matrix $(\mathrm{diag}(\underline{\mathbf{A}}^{*\mathrm{T}}\underline{\mathbf{A}}))^{-1}$ in (B.1) is arbitrary and can be omitted. The computational effort required is small, especially compared with

the computational effort required for the optimum Minimum Likelihoodean Sequence Estiamtor (MLSE) and Minimum Likelyhood Symbol-by-Symbol Estimator (MLSSE) which are not considered in this document. However, the DMF is only suitable if the perturbation due to ISI and MAI is negligible, which is the case for large spreading, i.e., Q much larger than W, and orthogonal CDMA codes $\underline{\mathbf{c}}^{(k)}, k = 1...K$. This entails low spectrum efficiency. For instance in mobile radio application, the perturbation due to ISI and MAI is usually considerably large and therefore leads to a subtantial performance degradation of the DMF.

B Zero forcing block linear equalization

In this section, the ZF-BLE performing JD, is derived starting from the general approach of linear data detection. This detector is based on the ZF-BLE performing linear equalization and is an extension of the ZF detector or decorrelating detector presented in [Sch79,KIH83b,LuV89,XSR90] for the single path channel to multipath channels. In contrast to other extensions of the ZF detector to multipath channels, this extension allows to exploit the multipath diversity. The ZF-BLE is furthermore a generalization of the block equalizer presented in [Kaw95] for the single user case to the multi-user case.

$$\begin{aligned}\hat{\underline{\mathbf{d}}} &= (\underline{\mathbf{A}}^{*\mathrm{T}}\underline{\mathbf{R}}_{\mathrm{n}}{}^{-1}\underline{\mathbf{A}})^{-1}\underline{\mathbf{A}}^{*\mathrm{T}}\underline{\mathbf{R}}_{\mathrm{n}}{}^{-1}\underline{\mathbf{e}} \\ &= \underline{\mathbf{H}}_{ZF}^{-1}(\underline{\mathbf{H}}_{ZF}^{*\mathrm{T}})^{-1}\mathrm{diag}(\underline{\mathbf{A}}^{*\mathrm{T}}\underline{\mathbf{R}}_{\mathrm{n}}{}^{-1}\underline{\mathbf{A}})(\mathrm{diag}(\underline{\mathbf{A}}^{*\mathrm{T}}\underline{\mathbf{R}}_{\mathrm{n}}{}^{-1}\underline{\mathbf{A}}))^{-1}\underline{\mathbf{A}}^{*\mathrm{T}}\underline{\mathbf{R}}_{\mathrm{n}}{}^{-1}\underline{\mathbf{e}}, \quad \text{(B.1)}\end{aligned}$$

where $\underline{\mathbf{H}}_{ZF}^{-1}$ is the ISI and MAI eliminator, $(\underline{\mathbf{H}}_{ZF}^{*\mathrm{T}})^{-1}$ is the whitening filter, $\mathrm{diag}(\underline{\mathbf{A}}^{*\mathrm{T}}\underline{\mathbf{R}}_{\mathrm{n}}{}^{-1}\underline{\mathbf{A}})$ is the normalization operator and $(\mathrm{diag}(\underline{\mathbf{A}}^{*\mathrm{T}}\underline{\mathbf{R}}_{\mathrm{n}}{}^{-1}\underline{\mathbf{A}}))^{-1}\underline{\mathbf{A}}^{*\mathrm{T}}\underline{\mathbf{R}}_{\mathrm{n}}{}^{-1}$ is the DMF. Furthermore $(\underline{\mathbf{H}}_{ZF}^{*\mathrm{T}})^{-1}$ is an upper triangular matrix [Mar87] of dimension $(KN)\times(KN)$ obtained by the Cholesky decomposition [Mar87,ZuF84]

$$\underline{\mathbf{A}}^{*\mathrm{T}}\underline{\mathbf{R}}_{\mathrm{n}}{}^{-1}\underline{\mathbf{A}} = \underline{\mathbf{H}}_{ZF}^{*\mathrm{T}}\underline{\mathbf{H}}_{ZF} \quad \text{(B.2)}$$

of $\underline{\mathbf{A}}^{*\mathrm{T}}\underline{\mathbf{R}}_{\mathrm{n}}{}^{-1}\underline{\mathbf{A}}$. The ZF-BLE contains a DMF, which is applied to the received vector $\underline{\mathbf{e}}$. After weighting or normalization, the output of the DMF is fed into the whitening filter (WF) represented by $(\underline{\mathbf{H}}_{ZF}^{*\mathrm{T}})^{-1}$. The output of the WF is fed into a filter represented by $(\underline{\mathbf{H}}_{ZF}^{*\mathrm{T}})^{-1}$ performing ISI and MAI elimination. The structure of the ZF-BLE is shown Figure B.1 The data estimes $\hat{\underline{\mathbf{d}}}$, can be displayed as

$$\hat{\underline{\mathbf{d}}} = \underline{\mathbf{d}} + (\underline{\mathbf{A}}^{*\mathrm{T}}\underline{\mathbf{R}}_{\mathrm{n}}{}^{-1}\underline{\mathbf{A}})^{-1}\underline{\mathbf{A}}^{*\mathrm{T}}\underline{\mathbf{R}}_{\mathrm{n}}{}^{-1}\underline{\mathbf{n}}. \quad \text{(B.3)}$$

Where $(\underline{\mathbf{A}}^{*\mathrm{T}}\underline{\mathbf{R}}_{\mathrm{n}}{}^{-1}\underline{\mathbf{A}})^{-1}\underline{\mathbf{A}}^{*\mathrm{T}}\underline{\mathbf{R}}_{\mathrm{n}}{}^{-1}\underline{\mathbf{n}}$ is the noise. From B.3 is evident that $\hat{\underline{\mathbf{d}}}$ contains no ISI and MAI pertubation term, but only the desired symbols and a noise term with covariance matrix $\underline{\mathbf{A}}^{*\mathrm{T}}\underline{\mathbf{R}}_{\mathrm{n}}{}^{-1}\underline{\mathbf{A}}$. Consequently, $\hat{\underline{\mathbf{d}}}$ is an unbiased [Wha71] estimate of $\underline{\mathbf{d}}$. The estimate $\hat{\underline{\mathbf{d}}}$ is the only linear unbiased estimated of minimum variance. The equalizer leading to $\hat{\underline{\mathbf{d}}}$ is termed zero forzing equalizer and the operation $(\underline{\mathbf{H}}_{ZF}^{*\mathrm{T}})^{-1}$ given in (B.1) is termed ISI and MAI elimination since ISI and MAI are totally eliminated.

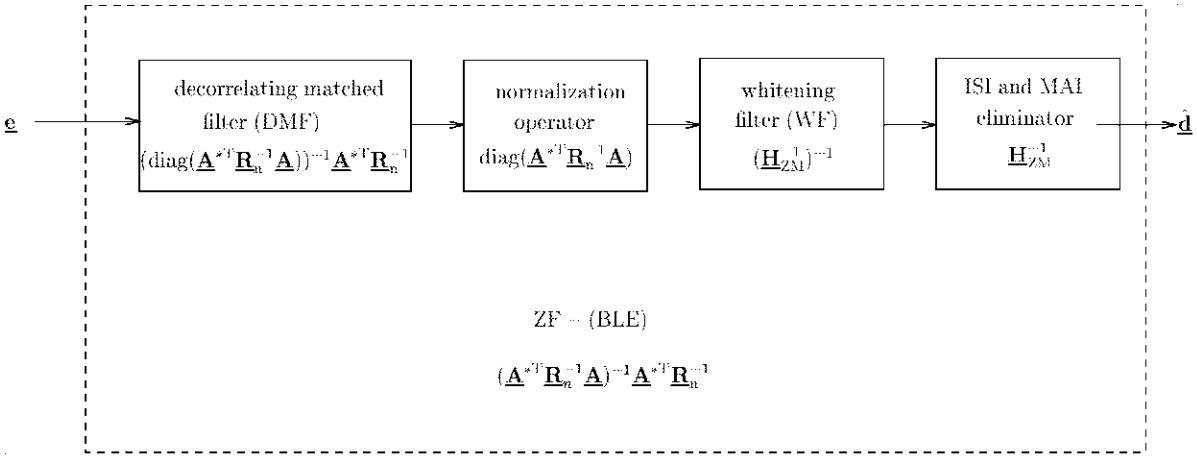

Figure B.1. Structure of the ZF-BLE

For special case $\underline{\mathbf{R}}_{\mathrm{n}}$ equal to $\sigma^2\mathbf{I}$ the data estimate determined by the ZF-BLE according to (B.1) becomes

$$\hat{\underline{\mathbf{d}}} = (\underline{\mathbf{A}}^{*\mathrm{T}}\underline{\mathbf{A}})^{-1}\underline{\mathbf{A}}^{*\mathrm{T}}\underline{\mathbf{e}}. \tag{B.4}$$

Most importantly, by the operation $\underline{\mathbf{A}}^{*\mathrm{T}}\underline{\mathbf{e}}$ which corresponds to filtering matched to the combined channel impulse responses $\underline{\mathbf{b}}^{(k,k_{\mathrm{a}})}, k = 1...K, k_{\mathrm{a}} = 1...K_{\mathrm{a}}$, the number of samples to be taken at the outputs of the MFs is reduced to KN samples at the symbol rate. The knowledge of the channel impulse response $\underline{\mathbf{h}}^{(k,k_{\mathrm{a}})}$, at the receiver is a prerequisite for filtering matched to the combined channel responses $\underline{\mathbf{b}}^{(k,k_{\mathrm{a}})}$. The computational effort required for the ZF-BLE, which perfectly eliminates ISI and MAI, is increased as compared with the DMF. However, it is still moderate, especially compared with the computational effort required for the optimum MLSE or MLSSE.

C Abbreviations

BER	Bit Error Rate
BS	Base station
CDMA	Code Division Multiple Access
DECT	Digital European Cordless Telephone
DOA	Direction of arrival
DS-CDMA	Direct Sequence Code Division Multiple Access
FDMA	Frequency Division Multiple Access
FEC	Forward error correction
GSM	Global System for Mobile Communications
ISI	InterSymbol Interference
JD	Joint Detection
LOS	Line Of Sight
MAI	Multiple Access Interference
MLSE	Maximum Likelyhood Sequence Estimator
MLSSE	Maximum Likelyhood Symbol-by-Symbol Estimator
PACS	Personal Access Communications System
PDC	Personal Digital Cellular system
PN	pseudo noise
TDMA	Time Division Multiple Access
RP	Reference Point
SNR	Signal-to-Noise Ratio
ZF-BLE	Zero Forcing Block Linear Equalization